RNF5 Regulation of RBBP4 Defines Acute Myeloid Leukemia Growth and Susceptibility to Histone Deacetylase Inhibitors

Ali Khateb[1,2], Anagha Deshpande[2], Yongmei Feng[2], Joo Sang Lee[3], Ikrame Lazar[1,2], Bertrand Fabre[1,2], Yan Li[2], Darren Finlay[2], Yu Fujita[2^], Tongwu Zhang[4], Jun Yin[2], Ian Pass[2], Ido Livneh[1], Carol Burian[5], James R. Mason[5], Ronit Almog[6], Nurit Horesh[7], Yishai Ofran[1,7], Kevin Brown[4], Kristiina Vuori[2], Michael Jackson[2], Eytan Ruppin[3], Aniruddha J. Deshpande[2], Ze'ev A. Ronai[2*]

[1]Technion Integrated Cancer Center, Faculty of Medicine, Technion Israel Institute of Technology, Haifa 31096, Israel; [2]Cancer Center, Sanford Burnham Prebys Medical Discovery Institute, La Jolla, CA 92037, USA; [3]Cancer Data Science Lab (CDSL), National Cancer Institute, National Institute of Health, Bethesda, MD 20892, USA; [4]Laboratory of Translational Genomics, Division of Cancer Epidemiology and Genetics, National Cancer Institute, Bethesda, MD 20892, USA; [5]Scripps MD Anderson Cancer Center, La Jolla, CA 92121, USA; [6]Rambam Health Care Campus, Epidemiology Department and Biobank, Haifa 31096, Israel; [7]Rambam Health Care Campus, Hematology and Bone marrow Transplantation Department, Haifa 31096, Israel

^Current Address: Division of Respiratory Medicine, Department of Internal Medicine, Jikei University School of Medicine, Tokyo, 105-8461, Japan.

Keywords: AML, HDAC, RBBP4, RNF5, ubiquitin ligase

*Corresponding Author: Ze'ev A. Ronai; SBP Discovery, 10901 N. Torrey Pines Road, La Jolla, CA 92037; Tel: +1 (858) 646-3185; zeev@ronailab.net

ABSTRACT

Acute myeloid leukemia (AML) remains incurable, largely due to its resistance to conventional treatments. Here, we found that increased expression and abundance of the ubiquitin ligase RNF5 contributes to AML development and survival. High RNF5 expression in AML patients correlated with poor prognosis. RNF5 inhibition decreased AML cell growth in culture and *in vivo*, and blocked development of MLL-AF9–driven leukemogenesis in mice, prolonging their survival. RNF5 inhibition led to transcriptional changes that overlapped with those seen upon HDAC1 inhibition. RNF5 induced the formation of K29 ubiquitin chains on the histone-binding protein RBBP4, promoting its recruitment and subsequent epigenetic regulation of genes involved in AML development and maintenance. Correspondingly, RNF5 or RBBP4 knockdown enhanced the sensitivity of AML cells to histone deacetylase (HDAC) inhibitors. Notably, low expression of *RNF5* and *HDAC* coincided with a favorable prognosis. Our studies identified ERAD-independent role for RNF5, demonstrating that its control of RBBP4 constitutes an epigenetic pathway that drives AML while highlighting RNF5/RBBP4 as markers to stratify patients for treatment with HDAC inhibitors.

INTRODUCTION

AML is a heterogeneous hematological cancer characterized by the accumulation of somatic mutations in immature myeloid progenitor cells. The mutations alter the self-renewal, proliferation, and differentiation capabilities of the progenitor cells [1,2]. The prognosis of AML patients is strongly influenced by the type of chromosomal or genetic alterations and by changes in gene expression [1,3]. Although numerous mutations and chromosomal aberrations that drive AML development have been identified [1,4], the molecular components and epigenetic modulators that contribute to the etiology and pathophysiology of AML are not well defined. Approximately one third of AML patients fail to achieve complete remission in response to chemotherapy, and 40 – 70% of those who do enter remission relapse within 5 years. Thus, there is an urgent need to better understand the molecular mechanisms underlying AML development and progression to facilitate the development of more effective therapies.

RING finger protein 5 (RNF5) is an ER-associated E3 ubiquitin ligase and a component of the UBC6e-p97 complex, which has been implicated in ER-associated degradation (ERAD) [5,6], a pathway involved in maintaining protein homeostasis. RNF5 recognizes misfolded proteins and promotes their ubiquitination and proteasome-dependent degradation [5,6]. *RNF5* expression is increased in several cancers, including breast cancer, hepatocellular carcinoma, and AML [7]. RNF5 regulates glutamine metabolism through degradation of misfolded glutamine carrier proteins, a function that is important in the response of cancer cells to ER stress-inducing chemotherapies such as paclitaxel [8]. RNF5 promoted the degradation of the protease ATG4B, which limits basal amounts of autophagy [9]. RNF5 also limits intestinal inflammation by its control of S100A8 protein stability [10]. Given the important pathophysiological roles of RNF5, the observation that it is upregulated in AML cells and patient samples prompted us to

investigate the possible contribution of RNF5 to the development and progression of this disease.

Histone modification by acetylation contributes to the dynamic regulation of chromatin structure and affects gene expression programs. Histone acetylation status is associated with the transcriptional regulation of leukemic fusion proteins, such as AML1-ETO, PML-RARα, and MLL-CBP [11,12]. Correspondingly, histone deacetylases (HDACs) are implicated in the etiology and progression of leukemia [13], and HDAC inhibitors affect the growth, differentiation, and apoptosis of leukemia cells [14]. The retinoblastoma binding protein 4 (RBBP4) is a component of multi-protein complexes involved in nucleosome assembly and histone modifications, which influences gene transcription and regulates cell cycle and proliferation [15]. Such complexes include nucleosome remodeling and deacetylase (NuRD) complex, polycomb repressor complex 2 (PRC2), and switch independent 3A (SIN3A) [15,16]. Overexpression of *RBBP4* and *HDAC1* correlates with clinicopathologic characteristics and prognosis in breast cancer [17], and *RBBP4* expression correlates with hepatic metastasis and poor prognosis in colon cancer patients [18]. RBBP4 was also implicated in the regulation of DNA repair genes and its suppression in glioblastoma enhanced the sensitivity to temozolomide chemotherapy [19]. However, the function of RBBP4 in AML has not been studied.

Here, we identified a central role for the RNF5-RBBP4 axis in AML maintenance and responsiveness to HDAC inhibitors. Our data suggest that targeting RNF5 and HDAC pathways represents a new therapeutic modality to inhibit AML and that expression of *RNF5* could serve as a prognostic marker and means to stratify patients for treatment with HDAC inhibitors.

RESULTS

Increased expression of RNF5 in AML patients correlates with poor prognosis

Analysis of RNA-seq datasets for various cancer cells from the Cancer Cell Line Encyclopedia database identified higher amounts of *RNF5* transcripts in AML, chronic myeloid leukemia (CML), and T-cell acute lymphoblastic leukemia (T-ALL), compared with other tumor types (Extended Data Fig. 1A). Higher amounts of RNF5 protein were confirmed in AML and CML, compared with other tumor types (Extended Data Fig. 1B). To assess the clinical relevance of RNF5 in AML, we analyzed the amount of RNF5 in peripheral blood mononuclear cells (PBMCs) from independent cohorts of AML patients. Similar to the AML cell lines, the average of RNF5 abundance was significantly higher in PBMCs from AML patients compared with PMBCs from healthy subjects (Fig. 1A,B). Stratification of the 50 patients into two groups based on high (N = 8, 15%) and low (n = 42, 85%) revealed that high level of RNF5 abundance coincided with poor overall survival (P = 0.05, Fig. 1C). An independent analysis of AML patients (n = 154) from The Cancer Genome Atlas (TCGA) dataset confirmed a significant correlation between high *RNF5* expression (10%) and poor survival (P = 0.009, Fig. 1D). Notably, AML patients with or without *FLT3* or *NPM1* mutations did not exhibit any difference in *RNF5* expression (Extended Data Fig. 1C,D), suggesting that the importance of RNF5 in AML depends on select oncogenic driver(s) and the activation of related signaling pathways.

Assessment of an independent AML patient cohort (Rambam Health Campus Center, Haifa, Israel) corroborated the higher level of RNF5 in AML patients (n = 18), compared with healthy donors (n = 5) (Fig. 1E,F). Because this cohort included multiple samples from the same patient, that were obtained prior to and following therapy, we could monitor changes in RNF5 abundance in AML patients that were subjected to therapy and at remission and relapse stages. Notably, RNF5 abundance markedly decreased following chemotherapy and during remission

(n = 8) (Fig. 1G,H and Extended Data Fig. 1E). Conversely, the amount of RNF5 was similar to that observed at diagnosis in patients that either relapsed or were refractory to treatment (n = 5) (Fig. 1I, J). These results suggested that the amount of RNF5 may serve as a prognostic marker for AML.

RNF5 is required for AML cell proliferation and survival

Discovering high amounts of RNF5 in AML, CML, and T-ALL cell lines, coupled with the link to AML progression, led us to explore the impact of RNF5 knockdown (RNF5-KD) on leukemia cell growth. Interestingly, RNF5-KD using RNF5-targeting short hairpin RNAs (shRNF5) reduced the viability and attenuated the growth of the AML cell lines MOLM-13 and U937 (Fig. 2A and Extended Data Fig. 2A) but not of CML cells (K-562) or T-ALL cells (Jurkat) (Extended Data Fig. 2B,C). RNF5-KD in MOLM-13 and U937 AML cells also caused the accumulation of cells in the G1 phase of the cell cycle (Fig. 2B), which was accompanied by an increase in the cell cycle regulatory proteins p27 and p21 (Fig. 2C). Moreover, RNF5-AML cells reduced colony formation in soft agar (Fig. 2D) and increased the abundance of proteins associated with apoptosis reflected in the level of cleaved forms of caspase-3 (Fig. 2E) and poly ADP ribose polymerase (PARP) (Extended Data Fig. 2D). The effects of RNF5-KD on U937 and MOLM-13 cells were corroborated in two additional AML cell lines, HL-60 and THP-1 (Extended Data Fig. 2E–H). Importantly, re-expression of RNF5 restored cell proliferation and reduced the apoptosis-associated proteins in RNF5-KD cells (Fig. 2F,G), substantiating the role of RNF5 in the control of cell cycle and death programs in AML cells.

To verify the role of RNF5 in AML cells, we used the CRISPR-Cas9 editing technology to deplete RNF5. Indeed, impaired growth of MOLM-13 AML cells stably expressing Cas9 and transduced with RNF5-targeting guide RNAs (sgRNAs) was seen, compared with control cells

transduced with *Renilla* luciferase-targeting sgRNAs (Fig. 2H,I). These data substantiated our observations with shRNA-mediated knockdown and supported a role for RNF5 in AML cell proliferation.

Despite detecting high amounts of the ubiquitin ligase RNF5 in many AML, CML, and T-ALL cell lines, our data suggested that RNF5 was specifically important for the survival and growth of AML cells. A cell- or tissue-specific role for RNF5 is supported by studies in breast cancer and melanoma, in which RNF5-KD or overexpression elicits distinct outcomes: RNF5 overexpression promotes the growth of melanoma by affecting the tumor microenvironment, whereas RNF5 overexpression inhibits breast cancer growth through tumor-intrinsic effects [7,20].

ER stress-induced apoptosis in AML cells is enhanced upon RNF5 inhibition and attenuated by RNF5 overexpression

Because RNF5 is part of ERAD and the ER stress response, we assessed whether modulation of RNF5 abundance alters the ER stress response in AML cells. We exposed MOLM-13 cells to thapsigargin or tunicamycin to inhibit the ER Ca^{2+}-ATPase (SERCA) or protein glycosylation, respectively [21], and induce ER stress. Both agents caused a greater increase in the abundance of apoptotic markers in RNF5-KD MOLM-13 cells than in control cells (Fig. 3A,B), and thapsigargin also decreased viability to a greater extent in RNF5-KD MOLM-13 cells (Fig. 3C). Tunicamycin also reduced viability of RNF5-KD HL-60 cells (Extended Data Fig. 3A). Consistent with a role in ER stress, RNF5-KD resulted in increased transcripts for key UPR components, including CHOP, ATF3, and sXBP1, in thapsigargin-treated MOLM-13 (Fig. 3D) and HL-60 cells (Extended Data Fig. 3B).

Given the close link between ER stress and proteasomal degradation, we assessed potential synergy between knockdown of RNF5 and inhibition of the proteasomes. Indeed,

RNF5-KD MOLM-13 cells treated with the proteasome inhibitor bortezomib (BTZ) exhibited increased amounts of apoptotic markers (Fig. 3E) and decreased viability (Fig. 3F), compared with control cells. Using annexin V and propidium iodide staining, which monitor degree of programmed cell death, we showed that RNF5-KD enhanced apoptosis of HL-60 cells exposed to BTZ (Fig. 3G), reducing the inhibitory concentration at which 50% of cells died (IC_{50}) from 9.6 nM in control cells to 5.4 nM in RNF5-KD cells. Overexpression of Flag-tagged RNF5 partially protected AML cells from tunicamycin or BTZ-induced activation of apoptosis (Fig. 3H,I , Extended Data Fig. 3C,D), confirming the role of RNF5 in protecting AML cells from proteotoxic stress.

RNF5 loss delays leukemia establishment and progression

Our findings with cultured AML cells prompted us to examine the role of RNF5 in leukemia growth *in vivo*. We used the human AML xenograft model in which the luciferase-expressing U937 cells (U937-pGFL) were transduced with doxycycline-inducible shRNF5 before the cells were injected intravenously into NOD/SCID mice (Extended Data Fig. 4). Following leukemia establishment, confirmed by bioluminescence, mice were fed a doxycycline-containing diet and monitored for disease progression and overall survival. RNF5-KD markedly decreased leukemia burden resulting in prolonged survival, compared with control mice (Fig. 4A,B). These data indicated that RNF5 is also required for proliferation of AML cells *in vivo*.

We also assessed whether RNF5 has a role in AML initiation using the MLL-AF9 model [22] for *in vitro* and *in vivo* studies. Hematopoietic stem and progenitor (Lin- depleted) cells (HSPCs) were purified from the bone marrow of wild-type (WT) or *Rnf5*$^{-/-}$ C57/BL6 mice and retrovirally transduced with a bicistronic construct harboring MLL-AF9 and a green fluorescent protein (GFP) marker. We then assessed the colony-forming ability of these pre-leukemic cells

in vitro. Compared with WT GFP-MLL-AF9 cells, *Rnf5*$^{-/-}$ GFP-MLL-AF9 cells exhibited markedly reduced colony-forming capacity in methylcellulose after 7, 14, and 21 days in culture, with a striking reduction in the number of blast-like colonies (Fig. 4C). The reduced size and number of cells in these colonies was consistent with terminal differentiation of *Rnf5*$^{-/-}$ cells, reflected by a greater cytoplasm/nuclei ratio and more vacuolated cytoplasm (Fig. 4D,E).

To assess leukemogenesis *in vivo*, sublethally irradiated WT C57/BL6 recipient mice were injected with GFP-MLL-AF9–transduced *Rnf5*^{WT} or *Rnf5*$^{-/-}$ cells, and cell engraftment was monitored by flow cytometry of GFP-positive (GFP+) cells in peripheral blood (Fig. 4F). Analysis on days 15 and 28 post-injection identified fewer GFP+ cells in mice injected with GFP-MLL-AF9 *Rnf5*$^{-/-}$ cells, compared with mice injected with GFP-MLL-AF9 *Rnf5*^{WT} cells, indicating a delay in leukemia development (Fig. 4G). Moreover, mice harboring GFP-MLL-AF9 *Rnf5*$^{-/-}$ cells exhibited prolonged survival compared with mice injected with GFP-MLL-AF9 *Rnf5*^{WT} cells (Fig. 4H). Collectively, these data showed that RNF5 loss promotes terminal differentiation and decreases the colony-forming ability of MLL-AF9–transformed pre-leukemic cells *in vitro* and delays leukemia progression *in vivo*.

RNF5 affects gene transcription in AML cells.

To assess possible pathways affected by RNF5 in AML cells, we first monitored transcriptional changes in MOLM-13, U937, and HL-60 AML cell lines expressing RNF5-WT or subjected to RNF5-KD. RNA sequencing (RNA-seq) analysis identified a differentially expressed gene set in RNF5 KD AML, compared with control (RNF5 WT) cells (Fig. 5A, Extended Data Fig. 5A and Supplemental Table 1). Ingenuity Pathway Analysis identified selective enrichment of genes implicated in myeloid cell function, such as NF-κB signaling, IL-8 signaling, reactive oxygen species, and several pathways related to cell migration such as Rho GTPases and Tec

kinase signaling (Fig. 5B). Among the genes upregulated by RNF5-KD in all three AML cell lines were *CDKN1A* and *CDKN2D* encoding cell cycle inhibitors, *LIMK1* encoding a kinase involved in regulation of the actin cytoskeleton, *ANXA1* encoding a calcium-binding protein involved in metabolism, EGFR and cell death programs, and *NCF1* encoding a subunit of NADPH oxidase (Fig. 5C and Extended Data Fig. 5B). These regulatory pathways and the transcriptional changes are consistent with the phenotypic changes of reduced proliferation, increased apoptosis, and increased differentiation that we observed in RNF5-KD AML cell lines. Interestingly, analysis of the Library of Integrated Network-Based Cellular Signatures (LINCS) drug screening database identified a notable overlap between the transcriptomic changes induced by the HDAC1 inhibitor mocetinostat in different cancer cells, to those seen in shRNF5 treated MOLM-13 and HL-60 cells (Fig. 5D). Five out of top ten transcriptional changes identified in LINCS following HDAC inhibition overlapped with those seen following shRNF5 in MOLM-13 cells (Fig. 5D and Extended Data Fig. 5C). Among the commonly affected pathways were activation of GP6 and Rho GTPase signaling, and repression of the nucleotide excision repair (NER) pathway (Fig. 5E). These observations point to the possibility that HDAC may underlie RNF5 role in AML.

RNF5 interacts with and ubiquitinates retinoblastoma binding protein 4

We hypothesized that RNF5 elicited transcriptional changes through intermediate regulatory component(s). Therefore, we performed liquid chromatography–tandem mass spectrometry (LC-MS/MS) to identify RNF5-interacting proteins, which may also include RNF5 substrates that mediate the transcriptional and phenotypic changes seen upon RNF5-KD. We compared the proteins isolated from MOLM-13 cells expressing inducible Flag-tagged RNF5 or empty vector by immunoprecipitation with an antibody recognizing Flag-RNF5 (Extended Data Fig.

5D,E). Among the 65 RNF5-interacting proteins that we identified were previously reported substrates, such as 26S proteasome components, VCP and S100A8 [5,10], as well as proteins implicated in AML development, such as DHX15 [23] and gelsolin [24,25] (Supplemental Table 2). Among the more abundant RNF5-bound proteins were components of the ERAD, translation initiation, proteolysis, and mRNA catabolic processes (Fig. 5F , Extended Data Fig. 5D,E and Supplemental Table 2).

Although none of the interacting proteins were transcription factors, epigenetic modification upon altered RNF5 expression may underlie changes observed in gene expression. Thus, we assessed whether RNF5-interacting proteins include epigenetic regulators, identifying the histone binding protein RBBP4 (Fig. 5F and Supplemental Table 2). Analysis of transcriptome data from TCGA revealed that expression of *RBBP4* was inversely correlated with the expression of genes that were increased in RNF5-KD cells (Fig. 5G and Extended Data Fig. 5F), which implies that RNF5 positively controls the transcriptional regulatory function of RBBP4. RBBP4 is a component of chromatin assembly, remodeling, and nucleosome modification complexes, including PRC2 [26] and the corepressor NuRD complex which contains HDAC1 and HDAC2 [27]. Indeed, such correlation between *RBBP4* and RNF5-upregulated genes was also seen for *HDAC1*, *HDAC2* and *EZH2* (Fig. 5H and Extended Data Fig. 5G-I). Increased *RBBP4* expression is correlated with the malignant phenotypes in human tumors including AML [28]. Analysis of tumor data in TCGA revealed high expression of *RBBP4* in AML compared with other tumor types (Extended Data Fig. 5J). Assessment of AML patient cohort confirmed higher RBBP4 expression in AML patients, compared with healthy donors (Fig. 5I). Stratifying AML patients by *RBBP4* expression showed that high expression correlated with poor overall survival (Fig. 5J).

If RNF5 is a positive regulator of RBBP4, we expected that RBBP4-KD would result in similar phenotypic changes to AML cells subjected to RNF5-KD. Indeed, knock down of RBBP4 in MOLM-13 and U937 cells with shRNAs impaired their growth (Fig. 5K and Extended Data Fig. 5K), exhibited PARP cleavage indicating apoptosis (Fig. 5L and Extended Data Fig. 5L) and showed induction of genes induced by RNF5-KD (Fig. 5M). These observations further substantiate a possible link between RNF5 and RBBP4 .

RNF5 is a transmembrane protein primarily associated with the ER with the ubiquitin ligase domain in the cytosol [6,29]. We assessed a possible interaction between RNF5 and RBBP4 in HEK293T and MOLM-13 cell lines by coimmunoprecipitation of ectopically expressed WT, catalytically inactive RING mutant (RNF5 RM), or C-terminal transmembrane domain deletion mutant (RNF5 ΔCT) (Figure 6A). Endogenous RBBP4 coimmunoprecipitated with all RNF5 constructs, suggesting that both the RING and transmembrane domain are dispensable for this interaction (Fig. 6B,C). Next, we assessed potential effects of RNF5 on RBBP4 ubiquitination. Co-expression of HA-tagged ubiquitin, Myc-tagged RBBP4, and Flag-tagged RNF5 constructs, revealed that RBBP4 was ubiquitinated by WT RNF5, but not by RNF5 RM nor by RNF5 ΔCT (Fig. 6D), indicating that ubiquitin ligase activity (RING domain-dependent) and membrane association are required for RNF5-mediated increase in RBBP4 ubiquitination. Correspondingly, RNF5-KD in HEK293T or MOLM-13 cells decreased RBBP4 ubiquitination (Extended Data Fig, 6A,B).

Notably, neither RNF5 overexpression nor RNF5-KD altered the abundance of RBBP4, suggesting that ubiquitination of RBBP4 by RNF5 is not through the formation of proteasome-targeting K48 ubiquitin chains and does not affect RBBP4 stability (Fig. 6E,F and Extended Data Fig. 6C). To assess the type of RBBP4 ubiquitination induced by RNF5, we used mutant HA-ubiquitin constructs, which disable ubiquitin chain formation on specific lysines (K48, K63,

or K29), and monitored changes in Myc-tagged RBBP4 ubiquitination in cells expressing Flag-tagged RNF5. Only ubiquitin with the K29R mutation impaired RNF5-induced RBBP4 ubiquitination (Fig. 6G), suggesting that RNF5 induces K29-topology polyubiquitination of RBBP4.

RNF5 promotes recruitment of RBBP4 to gene promoters

Because RBBP4 stability was not altered by RNF5, we evaluated whether RNF5 affects RBBP4 localization or interactions with other proteins. Subcellular fractionation and immunofluorescent analyses of nuclear and chromatin bound RBBP4 did not identify changes in RBBP4 localization following RNF5 inhibition (Extended Data Fig. 6E,F).

RBBP4 is a component of PRC2 and complexes containing HDACs [30,31], thus, we assessed whether RNF5 affects the formation of these complexes or their recruitment to promoters of target genes. Neither overexpression nor KD of RNF5 affected the interaction of RBBP4 with HDAC1, HDAC2, or EZH2 (Fig. 6H,I and Extended Data Fig. 6G), suggesting that ubiquitination of RBBP4 by RNF5 is not required for the assembly of RBBP4-containing complexes.

Chromatin immunoprecipitation (ChIP) and quantitative PCR (qPCR) assays were next used to evaluate the recruitment of RBBP4 to the promoters of genes that were regulated by either RNF5 or RBBP4. RNF5-KD reduced the recruitment of RPPB4 to the *ANXA1*, *NCF1*, and *CDKN1A* promotors (Fig. 6J). Examination of histone modifications in the promoters of these genes identified that RNF5-KD increased H3K9 and H3K27 acetylation (Fig. 6K and L) and reduced H3K27 methylation (Fig. 6M), changes that are indicative of increased gene expression [32,33]. These changes are consistent with their increased expression upon RNF5-KD (Fig. 5C). These results suggested that RNF5 control of gene expression in AML cells is mediated by RBBP4.

RNF5 inhibition sensitizes AML cells to HDAC inhibitors

To provide independent support for the importance of the RNF5-RBBP4 regulatory axis in promoting AML cell growth, we screened for synergistic interactions between RNF5 and epigenetic modulators. We assessed the effect of 261 epigenetic inhibitors at two concentrations (Supplemental Table 3) on the growth of AML cells that stably express inducible shRNF5 (Fig. 7A,B). Of the epigenetic inhibitors, 49 reduced viability of shRNF5-expressing cells compared with that of control AML cells (Fig. 7B). Among the inhibitors were several hypomethylation agents, including several histone methyltransferases (such as G9a), histone demethylases (such as Jumonji histone demethylases) and HDAC inhibitors (for example, TMP269, pimelic diphenylamide 106, and *N*-acetyldinaline [CI-994]). Because RBBP4 is a key component of the HDAC complex, and given that RNF5 KD induces transcriptional changes that resemble those seen upon HDAC1 inhibition (Fig. 5D,E), we further assessed possible synergy between RNF5 inhibition and HDAC inhibitors. CI-994, which is in clinical trials for several cancers (https://www.drugbank.ca/drugs/DB12291), was thus selected for additional validation. Indeed, U937 and HL-60 cells that were subjected to RNF5-KD exhibited a lower IC_{50} for cell viability by CI-994, compared with control cells (Fig. 7C and Extended Data Fig. 7A). These observations suggested that RNF5-KD sensitizes AML cells to HDAC inhibition.

We noted that the HDAC inhibitor (romidepsin, also known as FK228) did not score positively in our screen. This was due to the relatively high concentrations tested, which were lethal to both RNF5-KD and control U937 cells. FK228 is approved by the Food and Drug Administration (FDA) for treatment of peripheral T-cell lymphoma [34] and was investigated in preclinical studies as a potential treatment for AML [24,35]. Therefore, we re-assessed FK228 at non-lethal concentrations (up to 6 nM for 24 h) in multiple AML cell lines. Notably, FK228 synergized with RNF5-KD in reducing cell viability (Fig. 7D,E and Extended Data Fig. 7B-D)

and inducing apoptosis (Fig. 7F). We further confirmed the synergistic effect of HDACi in MOLM-13 cells in which *RNF5* was deleted using the CRISPR/Cas9 system (Extended Data Fig. 7E). The synergistic effect of RNF5-KD and FK228 on AML cell death was lost upon RNF5 re-expression (Fig. 7G), substantiating the role of RNF5 in sensitization of AML cells for HDAC inhibition.

Of the AML cell lines tested, we determined that the AML cell line MV-4-11 has a low amount of RNF5 (Extended Data Fig. 1B). MV-4-11 cells were the most sensitive to FK228 (Extended Data Fig. 7F), and RNF5-KD did not increase their sensitivity (Extended Data Fig. 7G). These observations further support the importance of RNF5 abundance in the response of AML cells to HDAC inhibitors. Moreover, RBBP4 KD sensitized AML cells to FK228 treatment (Fig. 7H and Extended Data Fig. 7H), consistent with our findings that RNF5 is a positive regulator of RBBP4. Notably, H3K9 acetylation on the promotors of RNF5 or RBBP4 regulated genes, *ANXA1* and *CDKN1A*, was elevated following FK228 treatment and further increased upon RNF5 KD (Fig. 7I). The latter is consistent with increased *ANXA1* and *CDKN1A* expression upon treatment with FK228 alone, or in combination with RNF5 KD (Fig. 7J and Extended Data Fig. 7I). To verify the relevance of the combination of RNF5 and HDAC in patients, we analyzed data from a bioinformatic pipeline that identifies clinically relevant synthetic lethal interactions [36]. This analysis revealed a more favorable prognosis in patients with a concomitant downregulation of *HDAC* and *RNF5* (Fig. 7K). Collectively, these findings suggested that RNF5 signaling is central to the sensitivity of AML to HDAC inhibitors.

CONCLUSIONS

High mortality of patients with AML predominantly results from failure to achieve complete remission following chemotherapy coupled with a high relapse rate. We identified the

role that the ubiquitin ligase RNF5 plays in AML, and mechanisms underlying RNF5 contribution to this form of leukemia. Our studies highlighted a function for RNF5 beyond its established functions in ERAD and proteostasis [6,29], demonstrating its impact on gene expression programs governing AML development and therapy response. RNF5 effect on gene expression is mediated via its interaction with and non-canonical ubiquitination of RBBP4, which enhanced the recruitment of RBBP4 to genes implicated in AML initiation and maintenance. The clinical relevance and the importance of RNF5 for AML was supported by our studies in genetic mouse models where RNF5 depletion inhibited the progression of AML and prolonged survival of mice. Furthermore, analysis of human AML samples revealed that high *RNF5* RNA and protein abundance, commonly seen in AML patient samples, correlated with poor prognosis.

RNF5-KD affected the expression of genes beyond those involved in proteostasis, in particular genes implicated in AML development and progression. We determined that RNF5 mediated these transcriptional changes, through a K29-toplogy ubiquitination of RBBP4. Limited reports on K29-linked protein ubiquitination highlights proteasome-independent functions, including changes in Wnt signaling [37], antiviral innate immune response [38], or protein aggregation in Parkinson disease [39]. RNF5 was shown to affect cholesterol biosynthesis through induction of K29-linked polyubiquitination of the sterol regulatory element-binding protein 2 (SREBP2) chaperone SCAP [40]. Notably, the importance of RNF5 control of RBBP4 for altered expression of genes seen in AML was substantiated by finding an inverse correlation between gene expression associated with RNF5- vs. RBBP4- expression. The implications of RNF5 effect on RBBP4 recruitment to transcriptional regulatory complexes were illustrated by the finding that RNF5 abundance affects the sensitivity of AML cells to HDAC inhibitors. Correspondingly, the transcriptional changes induced by RNF5 overlapped with those seen

following HDAC1 inhibitor treatment. Further, synthetic lethal (ISLE) analysis identified a favorable prognosis in a cohort of AML patients with low *HDAC* and *RNF5* expression, substantiating the importance of RNF5 in the regulation of histone modification that control gene expression programs. Our results also indicated that *RNF5* expression may serve as a marker for stratification of patients for HDAC or proteasome inhibitors treatment. Lastly, our data suggested that pharmacological inhibitors that phenocopy RNF5-KD potentially represent a novel therapeutic modality for AML.

METHODS

Animal studies

All animal experiments were approved by the Sanford Burnham Prebys Medical Discovery Institute's Institutional Animal Care and Use Committee (approval AUF 16-028). Animal care followed institutional guidelines. *Rnf5*$^{-/-}$ mice were generated on a C57BL/6 background as described [41]. C57BL/6 WT mice were obtained by crossing *Rnf5*$^{+/-}$ mice. Female mice were maintained under controlled temperature (22.5°C) and illumination (12 h dark/light cycle) conditions and were used in experiments at 6 – 10 weeks of age.

The xenograft model was established using U937 expressing the p-GreenFire1 Lenti-Reporter Vector (pGFL). NOD/SCID (NOD.CB17-Prkdcscid/J) mice were obtained from SBP Animal Facility. Mice were irradiated (2.5 Gy), and U937-pGFL cells (2×10^4 per mouse) expressing inducible shRNF5 or empty vector were then injected intravenously. Leukemia burden was serially assessed using noninvasive bioluminescence imaging by injecting mice intraperitoneally (i.p.) with 150 mg/kg D-Luciferin (PerkinElmer, 122799) in phosphate-buffered saline (PBS, pH 7.4), anesthetizing them with 2 – 3% isoflurane, and imaging them on an IVIS Spectrum (PerkinElmer). Upon disease onset (day 15), as measured by bioluminescent imaging, mice were fed with rodent chow containing 200 mg/kg doxycycline (Dox diet, Bio-Serv) to induce RNF5-KD. Mice were sacrificed upon signs of morbidity resulting from leukemic engraftment (> 10% weight loss, lethargy, and ruffled fur).

Cell culture

Human HEK293T cells were obtained from the American Type Culture Collection (ATCC). U937 and K562 cells were kindly provided by Prof. Yuval Shaked; Kasumi-1 cells were from Prof. Tsila Zuckerman; and MV4-11, GRANTA, THP-1, and MEC-1 cells were from Dr.

Netanel Horowitz. MOLM-13, U937, THP-1, Kasumi, Jurkat, and RPMI-8226 cells were cultured in RPMI medium; HL-60, MV-4-11, K-562, MEC-1, HAP-1, and KG-1α cells were cultured in IMDM; and GRANTA, A375 and HEK293T cells were cultured in DMEM. All media were supplemented with 10% fetal bovine serum (FBS), 1% L-glutamine, penicillin (83 U/mL), and streptomycin (83 µg/mL) (Gibco). Cells were regularly checked for mycoplasma contamination using a luminescence-based kit (Lonza).

Primary AML cells

AML patient samples were obtained from Scripps MD Anderson, La Jolla, CA (IRB-approved protocol 13-6180) and written informed consent was obtained from each participant, and Rambam Health Campus Center, Haifa, Israel (IRB-approved protocol 0372-17). Fresh blood samples were obtained by peripheral blood draw, PICC line, or central catheter. Filgrastim-mobilized peripheral blood cells were collected from healthy donors and cryopreserved with DMSO. PBMCs were isolated by centrifugation through Ficoll-Paque™ PLUS (17-1440-02, GE Healthcare). Residual red blood cells were removed using RBC Lysis Buffer for Human (Alfa Aesar, cat. # J62990) according to the manufacturer's instructions. The final PBMC pellets were resuspended in Bambanker serum-free freezing medium (Wako Pure Chemical Industries, Ltd.) and stored under liquid N_2.

Antibodies and reagents

The RNF5 antibody was described previously [7,41]. Other antibodies were obtained as follows: rabbit anti-cleaved caspase 3 (#9661, Cell Signaling Technology), rabbit anti-PARP (#9532, Cell Signaling Technology), mouse anti-RBBP4 (NBP1-41201, Novus Biologicals), mouse anti-glyceraldehyde 3-phosphate dehydrogenase (GAPDH; ab8245, Abcam), mouse anti-

Tubulin (T9026, Sigma), mouse anti-Flag (F1804, Sigma), mouse anti-Myc-Tag (#2276, Cell Signaling Technology), mouse anti-HA (901501, Biolegend), rabbit anti-HDAC1 (#2062, Cell Signaling Technology), rabbit anti-HDAC2 (57156, Cell Signaling Technology), rabbit anti-Ezh2 (5246, Cell Signaling Technology), mouse anti-HSP90 (sc-13119, Santa Cruz Biotechnology), rabbit anti-p27, (#3688, Cell Signaling Technology), rabbit anti-p21 (#2947, Cell Signaling Technology), mouse anti-Ubiquitin (#3939, Cell Signaling Technology), rabbit anti-K63-linkage Specific Polyubiquitin (#5621, Cell Signaling Technology), rabbit anti-Actin (#4970, Cell Signaling Technology), rabbit anti-Histone H3 (#9717, Cell Signaling Technology), mouse anti-Caspase 3 (sc-56053, Santa Cruz Biotechnology), and mouse anti-Calregulin (sc-166837, Santa Cruz Biotechnology).

Romidepsin, and *N*-acetyldinaline were purchased from Cayman Chemicals. Thapsigargin and tunicamycin were purchased from Sigma-Aldrich. MG132 was obtained from Selleckchem. Puromycin was purchased from Merck. Annexin V-FITC and propidium iodide were from BioLegend.

Plasmids and constructs

Plasmids expressing Flag-RNF5-WT, Flag-RNF5-RM, and Flag-RNF5-ΔCT were described previously [5,7]. To generate doxycycline-inducible RNF5-WT, RNF5-RM, and RNF5-ΔCT overexpression vectors, coding sequences were amplified from pCDNA3.1-RNF5-WT, pCDNA3.1-RNF5-RM, and pCDNA3.1-RNF5-ΔCT, respectively. The amplified PCR product was inserted into EcoRI-linearized pLVX TetOne-puro plasmid (Clontech) using the NEBuilder HiFi Assembly kit (New England BioLabs). RBBP4 expression vector was obtained from Addgene (Plasmid #20715).

Gene silencing

Lentiviral pLKO.1 vectors expressing RNF5 or RBBP4-specific shRNAs were obtained from the La Jolla Institute for Allergy and Immunology RNAi Center (La Jolla, CA, USA). Sequences were: shRNF5 #1 (TRCN0000004785) GAGTGTCCAGTATGTAAAGCT, shRNF5 #2 (TRCN0000004788) CGGCAAGAGTGTCCAGTATGT, shRNF5 #3 GAGGATGGATTGAGAGAAT, inducible shRNF5 has same sequence as shRNF5#1. shRBBP4#1 (TRCN0000286103) GCCTTTCTTTCAATCCTTATA, shRBBP4#2 (TRCN0000293556) TGGTCATACTGCCAAGATATC, shRBBP4#3 (TRCN0000293554) ATGCGTCACACTACGACAGTG.

Transfections and infections

Transient transfections were carried out using CalFectin (SignaGen) according to the manufacturer's recommendations. Lentiviral particles were prepared using standard protocols. In brief, HEK293T cells were transfected with the relevant vectors and the second-generation packaging plasmids ΔR8.2 and Vsv-G (Addgene). Virus-containing supernatants were collected 48 h later and added with Polybrene to AML cells pre-seeded at ~5 × 10^5/well in 24-well plates (Sigma-Aldrich). After 8 h, cells were transferred to 10-cm culture dishes for an additional 24 h prior to experiments.

Western blotting

Cells were washed twice with cold PBS and lysed by addition of Tris-buffered saline (TBS)-lysis buffer (TBS [50 mM Tris-HCl pH 7.5, 150 mM NaCl], 0.5% Nonidet P-40, 1× protease inhibitor cocktail [Merck], and 1× phosphatase inhibitor cocktail [42]) followed by incubation on ice for 20 min. Cells from healthy control subjects and AML patients were lysed using hot lysis

buffer [100 mM Tris-HCl pH 7.5, 5% sodium dodecyl sulfate (SDS)] followed by incubation 5 min at 95ºC and sonication. Some samples were subjected to fractionation using a subcellular protein fractionation kit (Thermo Scientific Pierce), as indicated. Samples were resolved by SDS-PAGE and transferred to nitrocellulose membranes. Membranes were incubated for 1 h at room temperature with blocking solution (0.1% Tween 20/5% non-fat milk in TBS) and then overnight at 4°C with the primary antibodies. Membranes were washed with TBS and incubated 1 h at room temperature with appropriate secondary antibodies (Jackson ImmunoResearch). Finally, proteins were visualized using a chemiluminescence method (Image-Quant LAS400, GE Healthcare).

Immunoprecipitation

Cells were lysed in TBS-lysis buffer as described above, centrifuged for 10 min at 17,000*g*, and incubated overnight at 4°C with appropriate antibodies. Protein A/G agarose beads (Santa Cruz Biotechnology) were then added for 2 h at 4°C. Beads were pelleted by centrifugation, washed five times with TBS-lysis buffer, and boiled in Laemmli buffer to elute proteins. Finally, proteins were resolved by SDS-PAGE and subjected to Western blotting as described above.

LC-MS/MS

MOLM-13 cells were infected with doxycycline-inducible Flag-tagged RNF5-encoding or empty plasmids and expression was induced by addition of doxycycline (1 µg/mL) for 48 h. The proteasome inhibitor MG132 (10 µM) was added for 4 h prior to harvest. Cells were lysed in TBS-lysis buffer, and lysates were incubated with anti-Flag-M2-agarose beads (Sigma-Aldrich) overnight at 4°C. Beads were washed with TBS-lysis buffer and proteins were eluted from beads

by addition of 3×Flag peptides (150 μg/mL, Sigma) for 1 h at 4°C and then subjected to tryptic digestion followed by LC-MS/MS, as described [43].

Raw data were analyzed using MaxQuant (v1.5.5.0) [44] with default settings. Protein intensities were normalized using the median centering method. Fold changes were calculated by dividing protein intensity of the Flag immunoprecipitates from RNF5-overexpressing cells by the protein intensity of the Flag immunoprecipitates from control cells. Thresholds were set at two for fold-change and 0.05 for p value obtained using Student's *t*-test. Proteins identified in all RNF5 immunoprecipitation replicates but in one or no control IP replicates were considered potential interactors with RNF5 if their corresponding fold-change was at least two. Data from the Crapome [42] repository were downloaded to filter potential contaminants. Cytoscape [45] was used to generate the RNF5 interaction network and the pathway enrichment analysis. Raw MS data were deposited in the MassIVE repository with the reference number MSV000083160.

Immunofluorescence microscopy

Cells were placed on coverslips on glass slides using a StatSpin cytofuge and fixed with 4% paraformaldehyde for 20 min at room temperature. Slides were then rinsed three times in PBS, and the cells were permeabilized in 0.2% Triton X-100 in PBS for 5 min and blocked with 0.2% TX-100/10% FBS in PBS for 30 min. Primary antibodies were diluted in staining buffer (0.2% Triton X-100/2% FBS in PBS), added to the cells, and the slides were incubated overnight at 4°C in a humidified chamber. Slides were then washed three times in staining buffer, and secondary antibodies (Life Technologies) were diluted in staining buffer and added to slides for 1 h at room temperature in a humidified chamber shielded from light. Finally, slides were washed three times in staining buffer and mounted with Fluoroshield Mounting Medium

containing 4′, 6-diamidino-2-phenylindole (DAPI; Sigma-Aldrich). Cells were analyzed using a fluorescence microscope (DMi8; Leica) with a 60× oil immersion objective. Images were processed using the 3D deconvolution tool from LASX software (Leica), and the same parameters were used to analyze all images.

Cell viability assay

Cell viability and growth were assayed using CellTiter Glo kit (Promega) according to the manufacturer's recommendations. Cell lines were plated in white 96-well clear-bottomed plates (Corning) at a density of 7×10^3 cells/well and growth was monitored every 24 h using CellTiter Glo reagent. Viability was quantified by measuring luminescence intensity with an Infinite 2000 Pro reader (Tecan).

Cell cycle analysis

Distribution of cells in each phase of the cell cycle was analyzed by staining with propidium iodide (Merck). Briefly, 1×10^6 cells were washed twice with cold PBS and fixed in 70% ethanol in PBS at 4°C overnight. Cells were washed, pelleted by centrifugation, and treated with RNase A (100 µg/mL) and propidium iodide (40 µg/mL) at room temperature for 30 min. Cell cycle distribution was assessed by flow cytometry (BD LSRFortessa™, BD Biosciences), and data was analyzed using FlowJo software.

Annexin V and propidium iodide staining

Cells were collected in FACS tubes, washed twice with ice-cold PBS, and resuspended in 100 µL PBS. Annexin V-APC (1.4 µg/mL) was added for 15 min at room temperature in the dark. Then, cells were washed in PBS and resuspended in 200 µL PBS and propidium iodide

(50 µg/mL) was added. Samples were then analyzed by flow cytometry (BD LSRFortessa™, BD Biosciences).

Colony-forming assays

For the soft agar assay, a base layer was formed by mixing 1.5% soft agar (low-melting point agarose, Bio-Rad) and culture medium at a 1:1 ratio and placing the mixture in 6-well plates. Cells were resuspended in medium containing 0.3% soft agar and added to the base layer at 1×10^4 (MOLM-13) or 5×10^3 (U937) cells/well. Agar was solidified by incubation at 4°C for 10 mins before incubation at 37°C. Plates were incubated at 37°C in a humidified atmosphere for 12–18 days. The cells were then fixed overnight with 4% paraformaldehyde, washed with PBS, and stained with 0.05% crystal violet (Merck) for 20 min at room temperature and washed again with PBS. Plates were photographed and colonies were counted on the captured images.

For the methylcellulose assay, WT or *Rnf5*$^{-/-}$ Lin$^-$Sca1$^+$c-Kit$^+$ cells transformed with GFP-MLL-AF9 were resuspended in methylcellulose M3234 (Stem Cell Technologies) supplemented with 6 ng/mL IL-3, 10 ng/mL IL-6, and 20 ng/mL stem cell factor (PeproTech). Cells were then added to 35-mm dishes at 10^3 cells/well and incubated for 6 – 7 days. Colonies were classified as compact and hypercellular (blast-like) or small and diffuse (differentiated). Virtually all colonies fell into one of these two categories.

RT-qPCR analysis

RNA was extracted using a GenElute Mammalian Total RNA Purification Kit (Sigma) according to standard protocols. RNA concentration was measured using a NanoDrop spectrophotometer (ThermoFisher). cDNA was synthesized from aliquots of 1 µg of total RNA using a qScript cDNA Synthesis Kit (Quanta). Quantitative PCR was performed with SYBR

Green I dye master mix (Roche) and a CFX connect Real-Time PCR System (Bio-Rad). Primer sequences are listed in Supplemental Table 4. Primer efficiency was measured in preliminary experiments, and amplification specificity was confirmed by dissociation curve analysis.

Gene targeting using CRISPR/Cas9

RNF5 sgRNAs were cloned into the pKLV2-U6gRNA-(BbsI)-PGKpuro2ABFP-W lentiviral expression vector and transduced into Cas9-expressing cell lines. All gRNAs were cloned into the BbsI site of the gRNA expression vector as previously described [46]. Briefly, HEK293T cells were co-transfected with pKLV2-U6gRNA-(BbsI)-PGKpuro2ABFP-W and ectopic packaging plasmids using CalFectin transfection reagent (SignaGen). Virus-containing supernatants were collected 48 h later. MOLM-13 cells were infected by addition of supernatants for 48 h. Cells were then selected with puromycin (0.5 µg/mL) for 48 h and viability was measured. The RNF5-targeting sgRNA sequences were: sgRNF5 #3 F-GCACCTGTACCCCGGCGGAA, R-TTCCGCCGGGGTACAGGTGC. sgRNF5 #4 F-GTTCCGCCGGGGTACAGGTG, R-CACCTGTACCCCGGCGGAAC.

RNA-seq analysis

PolyA RNA was isolated using the NEBNext Poly(A) mRNA Magnetic Isolation Module, and bar-coded libraries were constructed using the NEBNext Ultra™ Directional RNA Library Prep Kit for Illumina (NEB, Ipswich, MA). Libraries were pooled and single end-sequenced (1×75) on the Illumina NextSeq 500 using the High output V2 kit (Illumina, San Diego, CA). Quality control was performed using Fastqc (v0.11.5, Andrews S. 2010), reads were trimmed for adapters, low quality 5′ bases, and minimum length of 20 using CUTADAPT (v1.1). The number of reads per sample and the number of aligned reads suggested that read quality and

number were good and that the data were valid for analysis. High-quality data were then mapped to human reference genome (hg19) using STAR mapping algorithm (version 2.5.2a) [47]. FeatureCounts implemented in Subread (v1.50) [48] was used to count the sequencing reads from mapped BAM files. Analyses of differentially expressed genes was subsequently performed using a negative binomial test method (edgeR) [49] implemented using SARTools R Package [50]. A list of the differentially expressed genes was exported into Excel (Supplemental Table S1) and pathway analysis was performed by uploading the lists of differentially expressed genes to IPA (http://www.ingenuity.com) using the following criteria: |log2(fold change)| >0.4 and p value < 0.05 , and compared to public data sets processed by IPA using Analysis Match function. The top matched experiments in LINCS [51] were selected by ranking the overall z-scores.

Chromatin immunoprecipitation (ChIP)

ChIP assay was performed using ChIP Assay Kit (Millipore) following the manufacturer's instructions. Cells were fixed in 1% formaldehyde in PBS for 10 minutes at 37ºC. Briefly, 1×10^6 cells were used for each reaction. Cells were fixed in 1% formaldehyde at 37ºC for10 minutes, and nuclei were isolated with nuclear lysis buffer (Millipore) supplemented with protease inhibitor cocktail (Millipore). Chromatin DNA was sonicated and sheared to a length between 200 bp and 1000 bp. The sheared chromatin was immunoprecipitated at 4°C overnight with anti-H3K9ac (9649, Cell Signaling Technology), anti-H3K27ac (ab3594, Abcam), anti-H3K27me3 (9733, Cell Signaling Technology), anti-RBBP4 (NBP1-41201, Novus). IgG was used as a negative control and anti-RNA polII (Millipore) was used as a positive control antibody. Protein A/G bead-antibody/chromatin complexes were washed with low salt buffer, high salt buffer, LiCl buffer, and TE buffer to remove nonspecific binding. Protein/DNA complex was reverse cross-linked, and DNA was purified using NucleoSpin®. Levels of ChIP-purified DNA were

determined with qPCR (see Supplemental Table 5 for primer sequences). The relative enrichments of the indicated DNA regions were calculated using the Percent Input Method according to the manufacturer's instructions and are presented as % input.

Small molecule epigenetic regulators screen

Aliquots of compounds (10 mM in DMSO) from a library of 261 epigenetic regulators were dispensed at final concentrations of 0.5 µM or 5 µM into the wells of a Greiner (Monroe, NC, Cat #781080) 384-well TC-treated black plate using a Labcyte Echo 555 acoustic pipetter (Labcyte, San Jose, CA). U937 cells expressing an inducible shRNF5 vector were induced with doxycycline for 72 h and dispensed into the prepared plates at a density of 5×10^2/well in 50 µL RPMI-based culture medium (described above) using a Multidrop Combi (Thermo Fisher Scientific, Pittsburgh, PA). The plates were briefly centrifuged at 1000 rpm and incubated at 37°C with 5% CO_2 for an additional 6 days using MicroClime Environmental lids (Labcyte, San Jose, CA). Plates were placed at room temperature for 30 min to equilibrate, 20 µL/well CellTiter-Glo Luminescent Cell Viability Assay reagent (Promega, Madison, WI) was added using a Multidrop Combi, and the plates were analyzed with an EnVision multimode plate reader (PerkinElmer, Waltham, MA).

For the analysis, the intensity of induced shRNF5-expressing cells was divided by the intensity of uninduced cells. Ratios were $\log_2$ transformed and the thresholds were calculated based on the distribution of the $\log_2$ ratios. The upper threshold was calculated as the Q3 + 1.5xQ, where Q3 is the third quartile and IQ is the interquartile. The lower threshold was calculated as the Q1 − 1.5xIQ, where Q1 is the first quartile. Ratios outside these thresholds were considered outliers from the global ratio distribution and thus were potential candidates for having a differential effect on RNF5-KD or control cells.

MLL-AF9–mediated transformation of bone marrow cells and generation of MLL-AF9–leukemic mice

HEK293T cells were co-transfected with Murine Stem Cell Virus (MSCV)-based MLL-AF9 IRES-GFP [22] and ectopic packaging plasmids. Viral supernatants were collected 48 h later and added to $Lin^{-}Sca\text{-}1^{+}c\text{-}Kit^{+}$ cells isolated from the bone marrow of WT or *Rnf5*$^{-/-}$ C57BL/6 mice. Transduced cells were maintained in DMEM supplemented with 15% FBS, 6 ng/mL IL-3, 10 ng/mL IL-6, and 20 ng/mL stem cell factor, and transformed cells were selected by sorting for GFP^{+} cells. To generate "primary AML mice," GFP-MLL-AF9–transduced cells were resuspended in PBS at 1×10^{6} cells/200 µL and injected intravenously into sublethally irradiated (650 Rad) 6- to 8-week-old C57BL/6 female mice.

Statistical analysis

Differences between two groups were assessed using two-tailed unpaired or paired *t*-tests or Wilcoxon rank-sum test, and differences between group means were evaluated using *t*-tests or ANOVA. Two-way ANOVA with Tukey's multiple comparison test was used to evaluate experiments involving multiple groups. Survival was analyzed by the Kaplan–Meier method and evaluated with a log-rank test. All analyses were performed using Prism software (GraphPad, La Jolla, CA, USA). $P < 0.05$ was considered significant.

DATA AVAILABILITY

MS data is available on MSV online (MSV000083160). RNAseq data is available at the Gene Expression Omnibus under accession code GSE155929. Source files for original data (qPCR – excel files; Westerns raw data in PDF format are available online.

ACKNOWLEDGEMENTS

We thank Drs. Yuval Shaked, Tsila Zuckerman, and Netanel Horowitz (Faculty of Medicine, Technion) for providing leukemic cell lines, and members of the Deshpande and Ronai labs for technical support and discussions. We thank SBP and Technion Core facilities for help along different phases of this study. We thank Nancy R. Gough (BioSerendipity, LLC) for editorial assistance. Z.A.R. gratefully acknowledges support from the National Cancer Institute grant (R35CA197465) and the Technion. A.K. was supported by a Faculty of Medicine fellowship at the Technion. Sanford Burnham Prebys Shared Resources are supported by the NCI Cancer Center Support Grant (P30 CA030199).

AUTHOR CONTRIBUTIONS

A.K. and Z.A.R. designed the experiments; A.K., A.D., Yo.F., I.L., Y.L., and I.L., performed the experiments; A.K., J.S.L., B.F., D.F., Y.F., T.Z., J.Y., E.R., A.J.D and Z.A.R. analyzed the data; I.P., and M.J., performed the epigenetic screen; D.F., R.A., N.H., Y.O., C.B., J.R.M., and K.V. provided access to patient samples and data; and A.K. and Z.A.R. wrote the manuscript.

COMPETING INTERESTS STATEMENT

ZAR is co-founder and serves as scientific advisor to Pangea Therapeutics. All other authors declare no competing interests.

TABLES – This manuscript contains 5 supplemental tables

FIGURES – This manuscript contains 7 figures and 7 extended data figures

REFERENCES

1 Cancer Genome Atlas Research, N. *et al.* Genomic and epigenomic landscapes of adult de novo acute myeloid leukemia. *N Engl J Med* **368**, 2059-2074, doi:10.1056/NEJMoa1301689 (2013).

2 Mrozek, K., Heerema, N. A. & Bloomfield, C. D. Cytogenetics in acute leukemia. *Blood Rev* **18**, 115-136, doi:10.1016/S0268-960X(03)00040-7 (2004).

3 Shen, Y. *et al.* Gene mutation patterns and their prognostic impact in a cohort of 1185 patients with acute myeloid leukemia. *Blood* **118**, 5593-5603, doi:10.1182/blood-2011-03-343988 (2011).

4 Dohner, H. *et al.* Diagnosis and management of acute myeloid leukemia in adults: recommendations from an international expert panel, on behalf of the European LeukemiaNet. *Blood* **115**, 453-474, doi:10.1182/blood-2009-07-235358 (2010).

5 Tcherpakov, M. *et al.* Regulation of endoplasmic reticulum-associated degradation by RNF5-dependent ubiquitination of JNK-associated membrane protein (JAMP). *J Biol Chem* **284**, 12099-12109, doi:10.1074/jbc.M808222200 (2009).

6 Younger, J. M. *et al.* Sequential quality-control checkpoints triage misfolded cystic fibrosis transmembrane conductance regulator. *Cell* **126**, 571-582, doi:10.1016/j.cell.2006.06.041 (2006).

7 Bromberg, K. D. *et al.* Increased expression of the E3 ubiquitin ligase RNF5 is associated with decreased survival in breast cancer. *Cancer Res* **67**, 8172-8179, doi:10.1158/0008-5472.CAN-07-0045 (2007).

8 Jeon, Y. J. *et al.* Regulation of glutamine carrier proteins by RNF5 determines breast cancer response to ER stress-inducing chemotherapies. *Cancer Cell* **27**, 354-369, doi:10.1016/j.ccell.2015.02.006 (2015).

9 Kuang, E. *et al.* Regulation of ATG4B stability by RNF5 limits basal levels of autophagy and influences susceptibility to bacterial infection. *PLoS Genet* **8**, e1003007, doi:10.1371/journal.pgen.1003007 (2012).

10 Fujita, Y. *et al.* Regulation of S100A8 Stability by RNF5 in Intestinal Epithelial Cells Determines Intestinal Inflammation and Severity of Colitis. *Cell Rep* **24**, 3296-3311 e3296, doi:10.1016/j.celrep.2018.08.057 (2018).

11 Garcia-Manero, G. *et al.* Phase 1 study of the oral isotype specific histone deacetylase inhibitor MGCD0103 in leukemia. *Blood* **112**, 981-989, doi:10.1182/blood-2007-10-115873 (2008).

12 Masetti, R., Serravalle, S., Biagi, C. & Pession, A. The role of HDACs inhibitors in childhood and adolescence acute leukemias. *J Biomed Biotechnol* **2011**, 148046, doi:10.1155/2011/148046 (2011).

13 Redner, R. L., Wang, J. & Liu, J. M. Chromatin remodeling and leukemia: new therapeutic paradigms. *Blood* **94**, 417-428 (1999).

14 Bhalla, K. N. Epigenetic and chromatin modifiers as targeted therapy of hematologic malignancies. *J Clin Oncol* **23**, 3971-3993, doi:10.1200/JCO.2005.16.600 (2005).

15 Millard, C. J. *et al.* The structure of the core NuRD repression complex provides insights into its interaction with chromatin. *Elife* **5**, e13941, doi:10.7554/eLife.13941 (2016).

16 Zhang, Y., Iratni, R., Erdjument-Bromage, H., Tempst, P. & Reinberg, D. Histone deacetylases and SAP18, a novel polypeptide, are components of a human Sin3 complex. *Cell* **89**, 357-364, doi:10.1016/s0092-8674(00)80216-0 (1997).

17 Guo, Q. *et al.* Expression of HDAC1 and RBBP4 correlate with clinicopathologic characteristics and prognosis in breast cancer. *Int J Clin Exp Pathol* **13**, 563-572 (2020).

18 Li, Y. D., Lv, Z., Xie, H. Y. & Zheng, S. S. Retinoblastoma binding protein 4 up-regulation is correlated with hepatic metastasis and poor prognosis in colon cancer patients. *Hepatobiliary Pancreat Dis Int* **18**, 446-451, doi:10.1016/j.hbpd.2019.08.006 (2019).

19 Kitange, G. J. *et al.* Retinoblastoma Binding Protein 4 Modulates Temozolomide Sensitivity in Glioblastoma by Regulating DNA Repair Proteins. *Cell Rep* **14**, 2587-2598, doi:10.1016/j.celrep.2016.02.045 (2016).

20 Li, Y. *et al.* Gut microbiota dependent anti-tumor immunity restricts melanoma growth in Rnf5(-/-) mice. *Nat Commun* **10**, 1492, doi:10.1038/s41467-019-09525-y (2019).

21 Breckenridge, D. G., Germain, M., Mathai, J. P., Nguyen, M. & Shore, G. C. Regulation of apoptosis by endoplasmic reticulum pathways. *Oncogene* **22**, 8608-8618, doi:10.1038/sj.onc.1207108 (2003).

22 Krivtsov, A. V. *et al.* Transformation from committed progenitor to leukaemia stem cell initiated by MLL-AF9. *Nature* **442**, 818-822, doi:10.1038/nature04980 (2006).

23 Pan, L. *et al.* DHX15 is associated with poor prognosis in acute myeloid leukemia (AML) and regulates cell apoptosis via the NF-kB signaling pathway. *Oncotarget* **8**, 89643-89654, doi:10.18632/oncotarget.20288 (2017).

24 Tabe, Y. *et al.* Novel role of HDAC inhibitors in AML1/ETO AML cells: activation of apoptosis and phagocytosis through induction of annexin A1. *Cell Death Differ* **14**, 1443-1456, doi:10.1038/sj.cdd.4402139 (2007).

25 Watek, M. *et al.* Hypogelsolinemia in Patients Diagnosed with Acute Myeloid Leukemia at Initial Stage of Sepsis. *Med Sci Monit* **25**, 1452-1458, doi:10.12659/MSM.911904 (2019).

26 Kuzmichev, A., Nishioka, K., Erdjument-Bromage, H., Tempst, P. & Reinberg, D. Histone methyltransferase activity associated with a human multiprotein complex containing the Enhancer of Zeste protein. *Genes Dev* **16**, 2893-2905, doi:10.1101/gad.1035902 (2002).

27 Allen, H. F., Wade, P. A. & Kutateladze, T. G. The NuRD architecture. *Cell Mol Life Sci* **70**, 3513-3524, doi:10.1007/s00018-012-1256-2 (2013).

28 Casas, S. *et al.* Changes in apoptosis-related pathways in acute myelocytic leukemia. *Cancer Genet Cytogenet* **146**, 89-101, doi:10.1016/s0165-4608(03)00102-x (2003).

29 Morito, D. *et al.* Gp78 cooperates with RMA1 in endoplasmic reticulum-associated degradation of CFTRDeltaF508. *Mol Biol Cell* **19**, 1328-1336, doi:10.1091/mbc.E07-06-0601 (2008).

30 Xu, C. *et al.* Binding of different histone marks differentially regulates the activity and specificity of polycomb repressive complex 2 (PRC2). *Proc Natl Acad Sci U S A* **107**, 19266-19271, doi:10.1073/pnas.1008937107 (2010).

31 Liu, Z. *et al.* Structural basis of plant homeodomain finger 6 (PHF6) recognition by the retinoblastoma binding protein 4 (RBBP4) component of the nucleosome remodeling and deacetylase (NuRD) complex. *J Biol Chem* **290**, 6630-6638, doi:10.1074/jbc.M114.610196 (2015).

32 Duque-Afonso, J. *et al.* The HDAC class I-specific inhibitor entinostat (MS-275) effectively relieves epigenetic silencing of the LAT2 gene mediated by AML1/ETO. *Oncogene* **30**, 3062-3072, doi:10.1038/onc.2011.32 (2011).

33 Clarke, K. *et al.* The histone deacetylase inhibitor Romidepsin induces as a cascade of differential gene expression and altered histone H3K9 marks in myeloid leukaemia cells. *Oncotarget* **10**, 3462-3471, doi:10.18632/oncotarget.26877 (2019).

34 Argnani, L., Broccoli, A. & Zinzani, P. L. Cutaneous T-cell lymphomas: Focusing on novel agents in relapsed and refractory disease. *Cancer Treat Rev* **61**, 61-69, doi:10.1016/j.ctrv.2017.10.007 (2017).

35 Byrd, J. C. *et al.* A phase 1 and pharmacodynamic study of depsipeptide (FK228) in chronic lymphocytic leukemia and acute myeloid leukemia. *Blood* **105**, 959-967, doi:10.1182/blood-2004-05-1693 (2005).

36 Lee, J. S. *et al.* Harnessing synthetic lethality to predict the response to cancer treatment. *Nat Commun* **9**, 2546, doi:10.1038/s41467-018-04647-1 (2018).

37 Fei, C. *et al.* Smurf1-mediated Lys29-linked nonproteolytic polyubiquitination of axin negatively regulates Wnt/beta-catenin signaling. *Mol Cell Biol* **33**, 4095-4105, doi:10.1128/MCB.00418-13 (2013).

38 Yu, Z. *et al.* Lys29-linkage of ASK1 by Skp1-Cullin 1-Fbxo21 ubiquitin ligase complex is required for antiviral innate response. *Elife* **5**, doi:10.7554/eLife.14087 (2016).

39 Nucifora, F. C., Jr. *et al.* Ubiqutination via K27 and K29 chains signals aggregation and neuronal protection of LRRK2 by WSB1. *Nat Commun* **7**, 11792, doi:10.1038/ncomms11792 (2016).

40 Kuan, Y. C. *et al.* Ring finger protein 5 activates sterol regulatory element-binding protein 2 (SREBP2) to promote cholesterol biosynthesis via inducing polyubiquitination of SREBP chaperone SCAP. *J Biol Chem* **295**, 3918-3928, doi:10.1074/jbc.RA119.011849 (2020).

41 Delaunay, A. *et al.* The ER-bound RING finger protein 5 (RNF5/RMA1) causes degenerative myopathy in transgenic mice and is deregulated in inclusion body myositis. *PLoS One* **3**, e1609, doi:10.1371/journal.pone.0001609 (2008).

42 Mellacheruvu, D. *et al.* The CRAPome: a contaminant repository for affinity purification-mass spectrometry data. *Nat Methods* **10**, 730-736, doi:10.1038/nmeth.2557 (2013).

43 Braten, O. *et al.* Numerous proteins with unique characteristics are degraded by the 26S proteasome following monoubiquitination. *Proc Natl Acad Sci U S A* **113**, E4639-4647, doi:10.1073/pnas.1608644113 (2016).

44 Cox, J. & Mann, M. MaxQuant enables high peptide identification rates, individualized p.p.b.-range mass accuracies and proteome-wide protein quantification. *Nat Biotechnol* **26**, 1367-1372, doi:10.1038/nbt.1511 (2008).

45 Shannon, P. *et al.* Cytoscape: a software environment for integrated models of biomolecular interaction networks. *Genome Res* **13**, 2498-2504, doi:10.1101/gr.1239303 (2003).

46 Tzelepis, K. *et al.* A CRISPR Dropout Screen Identifies Genetic Vulnerabilities and Therapeutic Targets in Acute Myeloid Leukemia. *Cell Rep* **17**, 1193-1205, doi:10.1016/j.celrep.2016.09.079 (2016).

47 Dobin, A. *et al.* STAR: ultrafast universal RNA-seq aligner. *Bioinformatics* **29**, 15-21, doi:10.1093/bioinformatics/bts635 (2013).

48 Liao, Y., Smyth, G. K. & Shi, W. featureCounts: an efficient general purpose program for assigning sequence reads to genomic features. *Bioinformatics* **30**, 923-930, doi:10.1093/bioinformatics/btt656 (2014).

49 Robinson, M. D. & Oshlack, A. A scaling normalization method for differential expression analysis of RNA-seq data. *Genome Biol* **11**, R25, doi:10.1186/gb-2010-11-3-r25 (2010).

50 Varet, H., Brillet-Gueguen, L., Coppee, J. Y. & Dillies, M. A. SARTools: A DESeq2- and EdgeR-Based R Pipeline for Comprehensive Differential Analysis of RNA-Seq Data. *PLoS One* **11**, e0157022, doi:10.1371/journal.pone.0157022 (2016).

51 Subramanian, A. *et al.* A Next Generation Connectivity Map: L1000 Platform and the First 1,000,000 Profiles. *Cell* **171**, 1437-1452 e1417, doi:10.1016/j.cell.2017.10.049 (2017).

FIGURE LEGENDS

Fig. 1: RNF5 expression in AML patient samples.

(A) Representative western blot analysis of RNF5 in peripheral blood mononuclear cells (PBMCs) from 3 healthy control subjects and 10 AML patients (Scripps Health cohort). **(B)** Relative RNF5 abundance in AML samples (n = 50) compared with healthy control subjects (n = 6) from the Scripps Health Center. Data were quantified relative to RNF5 abundance in U937 cells that was used as a reference. Quantified data are presented as the mean ± SEM. $P = 0.008$ by unpaired two-tailed *t*-test. **(C)** Kaplan–Meier survival curve of AML patients stratified by top high (n = 8) versus low (n = 42) RNF5 abundance (Scripps Health cohort). $P = 0.05$ by Mantel–Cox log-rank test. **(D)** Kaplan–Meier survival curve of AML patients stratified by top high (n = 14) versus low (n = 150) *RNF5* transcript levels (TCGA dataset). $P = 0.009$ by Mantel–Cox log-rank test. **(E-G)** Abundance of RNF5 and control proteins in PBMCs from healthy control subjects and AML patients from the Rambam Health Campus Center cohort. Quantified data are presented as the mean ± SEM. $P = 0.006$ by unpaired two-tailed *t*-test. **(H, I)** Relative abundance of RNF5 protein in AML patient samples collected before and after induction treatment (H) or before and after relapse (I). Lines connect values for the same patient. $^{**}P = 0.0066$, $^{*}P = 0.054$, $^{**}P = 0.0074$ by unpaired (B and F) or paired (H and I) two-tailed *t*-test.

Fig. 2: RNF5 is required for AML cell proliferation and survival.

(A) Growth assay of MOLM-13 and U937 cells after transduction with empty vector (pLKO) or two different shRNF5 constructs. **(B)** Cell cycle analysis of MOLM-13 and U937 cell lines 5 days after transduction. **(C)** Western blot analysis of cell cycle regulatory proteins in MOLM-13 and U937 AML cells 5 days after transduction. **(D)** Representative images (left) and quantification (right) of MOLM-13 and U937 colonies in soft agar assessed after 15 days in

culture. **(E)** Western blot analysis of apoptosis-related proteins in MOLM-13 and U937 AML cells 5 days after transduction (C.casp.3 = cleaved caspase-3). (**F**) Growth assay of U937 cells expressing doxycycline-inducible Flag-tagged RNF5 or empty vector (EV). Cells were induced with doxycycline (1 µg/ml) for 48 h and then transduced with empty vector (pLKO) or shRNF5 for 5 days. **(G)** Western blot analysis of the indicated proteins in U937 infected as described in (F). **(H)** Growth assay of MOLM-13 cells stably expressing Cas9 and transduced with control *Renilla*-targeting sgRNA or two RNF5-targeting sgRNAs. CRIPSR was performed based on CRIPSR knockout cell pool. **(I)** Western blot analysis of the indicated proteins in MOLM-13 cells as described in (H). Quantified data are presented as the mean ± SD of three independent experiments. Western blot data are representative of three experiments. *$P < 0.05$, **$P < 0.01$, and ****$P < 0.0001$ by two-way ANOVA followed by Tukey's multiple comparison test (A, F, and H) or two-tailed *t*-test (B, and D).

Fig. 3: RNF5 inhibition sensitizes AML cells to ER stress-induced apoptosis.

(A, B) Western blot analysis of the indicated proteins in MOLM-13 cells expressing empty vector (pLKO) or shRNF5 #1 and treated with thapsigargin (TG, 1 µM) (A) or tunicamycin (TM, 2 µg/ml) (B) for the indicated times. **(C)** Luminescence viability assay of MOLM-13 cells expressing inducible shRNF5 treated with or without doxycycline (DOX, 1 µg/ml) for 3 days before treatment with TG (100 nM) for the indicated times. **(D)** RT-qPCR analysis of *CHOP* and *ATF3* mRNA in MOLM-13 cells expressing empty vector (pLKO) or shRNF5 #1 and treated with TG (100 nM) for the indicated times. **(E)** Western blot analysis of cleaved caspase-3 (C. casp.3) and PARP in MOLM-13 cells expressing empty vector (pLKO) or shRNF5 #1 and treated with bortezomib (BTZ, 5 nM) for the indicated times. **(F)** Fluorescence viability assay of HL-60 cells expressing empty vector (pLKO) or shRNF5 and treated with BTZ (5 nM) for

the indicated times. Cell viability was determined by flow cytometry of cells stained with annexin V conjugated to fluorescein isothiocyanate and propidium iodide. **(G)** Luminescence viability assay of HL-60 cells expressing empty vector (pLKO) or shRNF5 and treated with the indicated concentrations of BTZ for 48 h. **(H)** Western blot analysis of MOLM-13 cells expressing inducible empty vector (EV) or an RNF5 overexpression vector. Cells were first induced with DOX (1 µg/ml) for 24 h and then treated with BTZ (5 nM) for the indicated times. **(I)** Luminescence viability assay of MOLM-13 cells expressing DOX-inducible Flag-tagged RNF5 or empty vector (EV). Cells were treated with DOX (1 µg/ml) for 2 days and then treated with the indicated concentrations of BTZ for 12 h. Data are presented as the mean ± SD of three independent experiments. **P* < 0.05 and ***P* < 0.01 by two-tailed *t*-test (C, D, and F) or by two-way ANOVA (G). ns: not significant.

Fig. 4: RNF5 suppression impairs leukemia establishment and progression *in vivo*.

(A) Graph depicting growth in mice of U937-pGFL expressing empty vector (pLKO) or inducible shRNF5. Bioluminescence was quantified as measure of disease burden. Data are presented as the mean ± SD of 7 mice per group. **P* < 0.05 by unpaired two-tailed *t*-test. **(B)** Kaplan–Meier survival curves of mice injected with U937-pGFL cells expressing empty vector (pLKO) (n = 7 mice/group) or inducible shRNF5 (n = 7 mice/group). *P* < 0.001 by Mantel–Cox log-rank test. **(C)** Schematic representation of the experiment. $Lin^{-}Sca1^{+}c\text{-}Kit^{+}$ (LSK) cells were purified from the bone marrow of WT or *Rnf5*$^{-/-}$ mice, transduced *in vitro* with a GFP-tagged MLL-AF9 fusion gene, and then either analyzed in colony-forming assays *in vitro* or intravenously injected into sub lethally irradiated WT C57BL/6 mice. **(D)** Quantification of total colonies (left) or blast-like and differentiated colonies (right) of GFP-MLL-AF9–transformed WT or *Rnf5*$^{-/-}$cells after 7 days, 14, or 21 days in culture. Data are presented as the mean ± SD

of three independent experiments. $^{**}P < 0.01$ by paired two-tailed *t*-test. **(E)** Representative pictures of colonies of GFP-MLL-AF9–transformed WT or *Rnf5*$^{-/-}$cells after 7 days in culture. Scale bar 200 µm. **(F)** Wright–Giemsa-staining of GFP-MLL-AF9–transformed WT or *Rnf5*$^{-/-}$ cells after 7 days in culture. **(G)** Flow cytometric quantification of GFP+ cells in the peripheral blood of mice intravenously injected with GFP-MLL-AF9–transformed WT (n = 4) or *Rnf5*$^{-/-}$ (n = 4) cells at days 15 and 28 post-injection. Data are presented as the mean ± SD. $^{**}P < 0.01$ by unpaired two-tailed *t*-test. **(H)** Kaplan–Meier survival curves of mice injected with GFP-MLL-AF9–transformed WT or *Rnf5*$^{-/-}$ cells. Data are from two independent experiments (n = 4 mice/group per experiment). $P < 0.001$ by Mantel–Cox log-rank test.

Fig. 5: Transcriptional and survival outcome overlap for RNF5 and RBBP4 in AML.

(A) Heatmap of RNA-seq data performed on control (pLKO) or RNF5-KD (shRNF5) AML cell lines. Genes with Benjamini-Hochberg (BH) corrected p value< 0.05 and Log2 transformed fold change >=0.4 or <=-0.4 were selected as significantly differentially expressed genes. **(B)** Top canonical pathways identified by Ingenuity Pathway Analysis comparing the differentially expressed genes in AML cell lines (HL-60, U937, and MOLM-13) upon RNF5-KD**. (C)** RT-qPCR validation of indicated genes identified as deregulated by RNF5-KD. Data are presented as the mean ± SD of three independent experiments. **(D)** Top ten drug screening results from the Library of Integrated Network-Based Cellular Signatures (LINCS) matched by shRNF5 in MOLM-13 cell line. Values are overall z-scores from IPA Analysis Match database. HDAC1 inhibitor results are shown in red. **(E)** shRNF5 in MOLM-13 and HL-60 cell lines induced similar IPA Canonical Pathway changes compared with NPC, HEPG2, A549 and PC3 cancer cell lines treated with the HDAC1 inhibitor mocetinostat. Z-score was calculated by IPA, with positive z-score predicting activation of the pathway, and negative z-score predicting inhibition

of the pathway. **(F)** Log_2-transformed ratio of proteins in anti-Flag immunoprecipitates of RNF5-overexpressing versus control cells determined by MS intensity. Green indicates proteins significantly enriched in RNF5-overexpressing cells; blue indicates proteins in the ERAD pathway enriched in RNF5-overexpressing cells. RNF5 and RBBP4 are indicated in red. **(G, H**) Co-expression of *RBBP4* (G) or *HDAC2* (H) and the indicated RNF5 target genes in AML analyzed in cBioPortal using the TCGA database. **(I**) Western blot analysis of RBBP4 in PBMCs from healthy control subjects and AML patients from Scripps Health and Rambam Health Campus Center cohorts. RMS stands for remission. **(J**) Overall survival rate of AML patients expressing high (30%) or low (70%) *RBBP4* transcripts. Survival analysis was performed by the bioinformatics database GEPIA using TCGA tumor samples. TPM: Transcripts Per Million. HR: hazard ratio. **(K)** Growth assay of MOLM-13 cells after transduction with empty vector (pLKO) or the indicated shRBBP4 constructs. **(L)** Western blot analysis of the indicated proteins in MOLM-13 cells expressing empty vector (pLKO) or two different shRBBP4 constructs. **(M)** RT-qPCR analysis of indicated genes identified as deregulated by RNF5-KD in MOLM-13 cells expressing the indicated constructs. Data are presented as the mean ± SD of three independent experiments. $*P < 0.05$, $**P < 0.01$, $***P < 0.001$, and $****P < 0.0001$ by two-tailed *t*-test (C and M) or by two-way ANOVA followed by Tukey's multiple comparison test (K).

Fig. 6: RBBP4 is RNF5 substrate, mediates epigenetic regulation of RNF5 target genes.

(A) A schematic presentation of full-length RNF5 and its mutants. **(B)** Immunoprecipitation (IP) and Western blot analysis of HEK293T cells transfected with Flag-tagged full-length RNF5 (WT), a mutant with a catalytically inactive RING domain (RM), or a C-terminal transmembrane domain deletion mutant (ΔCT) and then treated with MG132 (10 μm 4 h) before

lysis. **(C)** Immunoprecipitation and Western blot analysis of ectopically expressed RNF5 and endogenous RBBP4 in MOLM-13 cells expressing doxycycline-inducible Flag-tagged RNF5. Cells were incubated with or without doxycycline (1 µg/ml) for 2 days and with MG132 (10 µm 4 h) before lysis. **(D)** Western blot analysis of anti-Myc immunoprecipitates and lysates of HEK293T cells co-expressing Myc-RBBP4, hemagglutinin-tagged ubiquitin (HA-Ub), and the indicated Flag-tagged RNF5 constructs. Cells were treated with MG132 (10 µm 4 h) before lysis. **(E)** Western blot analysis of the indicated proteins in MOLM-13 cells expressing empty vector (pLKO) or the indicated shRNF5 construct. **(F)** Western blot analysis of the indicated proteins in MOLM-13 cells expressing empty vector or doxycycline-inducible Flag-tagged RNF5. **(G)** Western blot analysis of anti-Myc immunoprecipitates and lysates of HEK293T cells co-expressing Myc-RBBP4, Flag-tagged RNF5, and different HA-tagged ubiquitin constructs. WT, wild-type ubiquitin; K48R, K63R, K29R are lysine-to-arginine ubiquitin mutants at the indicated positions. Cells were treated with MG132 (10 µm 4 h) before lysis. **(H)** Immunoprecipitation and Western blot analysis of the interaction of RBBP4 with HDAC1, HDAC2, or EZH2 in MOLM-13 cells expressing doxycycline-inducible Flag-tagged RNF5. **(I)** Immunoprecipitation and Western blot analysis of the interaction of RBBP4 with HDAC1, HDAC2, or EZH2 in MOLM-13 cells expressing empty vector or the indicated shRNF5 construct. Cells were treated with MG132 (10 µm 4 h) before lysis. **(J-M)** ChIP and qPCR indicating the enrichment of RBBP4, H3K9ac, H3K27ac, or H3K27me3 (normalized to input) at the indicated gene promoters in MOLM-13 cells expressing empty vector or two shRNF5 constructs. Data in L and M are presented as the mean ± SD of two independent experiments. $*P < 0.05$ and $***P < 0.001$ by two-tailed *t*-test (J and K).

Fig. 7: RNF5 inhibition sensitizes AML cells to HDAC inhibitors.

(A) Experimental design of the epigenetic screen. U937 cells expressing inducible shRNF5 were treated with doxycycline (Dox) for 72 h, incubated with library compounds at two concentrations for 6 days, and analyzed for viability using the luminescence assay. (**B**) Log_2-transformed ratios of the relative viability of doxycycline-induced (+Dox) versus uninduced (-Dox) U937 cells treated with compounds (0.5 μM or 5 μM) for 6 days. Grey dots represent all compounds tested, red dots represent candidate compounds that affected the viability of RNF5-KD more than of uninduced cells, and blue dots represent select HDAC inhibitors as potential candidates. **(C)** Viability of U937 cells expressing pLKO or shRNF5 after treatment for 24 h with the indicated concentrations of CI-994. **(D)** Viability of U937 cells after treatment for 24 h or 48 h with 3.5 nM FK228. (**E**) Viability of U937 cells or MOLM-13 cells expressing the indicated constructs after treatment for 24 h with the indicated FK228 concentrations. (**F**) Detection of apoptotic markers by Western blot analysis of MOLM-13 and U937 cells expressing pLKO or shRNF5#1. Cells were incubated with or without FK228 (4 nM 24 h) before lysis. **(G)** Viability of U937 cells expressing pLKO or shRNF5 and co-infected with control or RNF5 overexpression vectors. Cells were treated for 24 h with the indicated FK228 concentrations before analysis. EV-pLKO, control cells; EV-shRNF5, cells expressing empty vector and shRNF5; RNF5-pLKO, cells overexpressing RNF5 and empty pLKO vector; RNF5-shRNF5, cells overexpressing RNF5 and shRNF5. (**H**) Viability of MOLM-13 cells expressing the indicated constructs after treatment for 24 h with the indicated FK228 concentrations. (**I**) ChIP and qPCR indicating the enrichment of H3K9ac (normalized to input) at the indicated gene promoters in MOLM-13 cells expressing empty vector or shRNF5 constructs. Data are presented as the mean ± SD of two independent experiments. (**J**) RT-qPCR analysis of *ANXA1* and *CDKN1A* mRNA in MOLM-13 cells expressing empty vector (pLKO) or shRNF5 #1 and

treated with 4nM FK228 for 15 h. (**K**) Kaplan-Meier plot showing the AML patients whose tumor exhibit lower HDAC and RNF5 transcription show better prognosis than the rest of patients (yellow lines) with hazard ratio of 0.42 (N^{hi}=76, N^{lo}=79). The patients were segregated into two groups based on median synthetic lethality (SL) score, which counts the occurrence of co-inactivation of SL partners in each sample. Logrank *P*-values are denoted in the figure, and the median survival differences are 488 days.

Data are presented as the mean ± SD of three independent experiments. **P* < 0.05, ***P* < 0.01, ****P* < 0.001, and *****P* < 0.0001 by two-tailed *t*-test (D and J) or by two-way ANOVA followed by Tukey's multiple comparison test (C, E, G and H).

EXTENEDED DATA FIGURE LEGENDS

Extended Data Fig. 1: Level of RNF5 protein and transcripts inversely correlates with AML patient outcome.

(A) *RNF5* expression data obtained from RNA-seq datasets in the Cancer Cell Line Encyclopedia. Transcript per million (TPM) gene expression data for protein-coding genes using RSEM. Log2 transformed, using a pseudo-count of 1w. The box plot is sorted and colored by the average distribution of *RN5* expression in a lineage. Lineages are composed of a number of cell lines from the same area or system of the body. The number next to the lineage name indicates how many cell lines are in the lineage. The highest average distribution is on the left and is colored red. The dashed line within a box is the mean. **(B)** Western blot analysis of RNF5 in lysates of a panel of cancer cell lines: AML, acute myeloid leukemia; CML, chronic myeloid leukemia; ALL, acute lymphoblastic leukemia; CLL, chronic lymphoblastic leukemia; MM, multiple myeloma; MCL, mantle cell lymphoma; and melanoma. **(C, D)** Relative *RNF5* expression in AML samples positive or negative for NPM1 or FLT3 mutations. Samples were obtained from Scripps Health Center (C) or Rambam Health Care Campus Center (D). **(E)** Western blot analysis of RNF5 abundance in PBMCs from healthy donors and AML patients in the Rambam Health Campus Center cohort. The position of RNF5 is indicated. The upper band is unspecific.

Extended Data Fig. 2: RNF5 is required for AML cell growth

(A) Luminescence growth assay of U937 cells expressing empty vector (pLKO) or shRNF5 #3. **(B)** Luminescence growth assay of Jurkat cells expressing pLKO or shRNF5 #1. Western blot shows knockdown efficiency. (C. casp.3 = cleaved caspase 3). **(C)** Luminescence growth assay

of K562 cells expressing pLKO or shRNF5 #1. Western blot shows knockdown efficiency. **(D)** Western blot analysis of MOLM-13 and U937 cells 5 days after transduction with pLKO or the shRNF5 #3. Data are representative of three experiments. **(E, F)** Luminescence growth assays of HL-60 or THP-1 cells transduced with pLKO or shRNF5 #1. **(G)** Plate images (left) and quantification (right) of HL-60 colonies in soft agar. Colonies were assessed after 14 days in culture. **(H)** Western blot analysis of the indicated proteins in HL-60 and THP-1 cells 5 days after transduction with pLKO, shRNF5 #1, or shRNF5 #2. Data are representative of three experiments. Quantified data are presented as the mean ± SD and are representative of three independent experiments. *$P < 0.05$ and **$P < 0.01$ by two-tailed *t*-test.

Extended Data Fig. 3: ER Stress synergizes with RNF5 inhibition in AML cells

(**A**) Luminescence growth assay of HL-60 cells expressing pLKO or shRNF5 after treatment with tunicamycin (2 µg/mL) for the indicated times. **(B)** RT-qPCR analysis of UPR-related genes in HL-60 cells treated with thapsigargin (1 µM) for the indicated times. **(C)** Luminescence growth assay of MOLM-13 cells induced to express Flag-tagged RNF5 for 2 days with doxycycline 1 µg/mL and then treated with the indicated concentrations of bortezomib (BTZ) for 24 h. **(D)** Luminescence growth assay of MV-4-11 cells induced to express Flag-tagged RNF5 for 2 days with doxycycline 1 µg/mL and then treated with the indicated concentrations of tunicamycin for 24 h. Data are presented from two independent experiments. *$P < 0.05$, **$P < 0.01$, and ***$P < 0.001$ by two-tailed *t*-test. ns: not significant.

Extended Data Fig. 4: Validation of inducible RNF5 knockdown in U937 cells used for *in vivo* leukemia evaluation. U937-pGFL cells expressing pLKO or inducible shRNF5 were

treated with Dox (1 µg/mL) for three days. Western blot analysis was performed to detect RNF5. GADPH served as a loading control.

Extended Data Fig. 5: RNF5 affects gene transcription in AML cells

(A) Volcano plots highlight differentially expressed genes in WT compared with RNF5 KD AML cells. Each dot represents a gene. Genes with Benjamini-Hochberg (BH) corrected p value< 0.05 and Log2 transformed fold change >= 0.4 or <= -0.4 were selected as significantly differentially expressed genes and are highlighted in red. A list of differentially expressed genes is available in Supplementary Table 1. **(B)** qPCR validation of a select subset of genes identified as deregulated upon RNF5-KD by RNA-seq analysis. *$P < 0.05$, **$P < 0.01$, and ****$P < 0.0001$ by two-tailed *t*-test. **(C)** Top ten drug screening results from LINCS database matched by shRNF5 in HL-60 cell line. Values are overall z-scores from IPA Analysis Match database. HDAC1 inhibitor results are shown in red. **(D)** RNF5 interaction network generated from the immunoprecipitation data and Cytoscape. The colors associated with the different pathways are displayed. **(E)** Pathway enrichment analysis displaying the genes count (log2 transformed) and the corresponding false discovery rate (-log10 transformed) for each pathway**.** **(F-I)** Co-expression of *RBBP4* (F), *HDAC2* (G), *EZH2* (H) or *HDAC1* (I) RNA and the indicated RNF5 target genes in AML analyzed in cBioPortal using data from TCGA. **(J)** Analysis of RBBP4 expression in different human cancers from the cBioPortal using data from TCGA. **(K)** Growth assay of U937 cells after transduction with empty vector (pLKO) or the indicated shRBBP4 constructs. Data are presented as the mean ± SD of two independent experiments. **(L)** Western blot analysis of the indicated proteins in U937 cells expressing empty vector (pLKO) or two different shRBBP4 constructs.

Quantified data are presented as the mean ± SD and are representative of three independent experiments. *$P < 0.05$, **$P < 0.01$, ****$P < 0.0001$ by two-tailed *t*-test.

Extended Data Fig. 6: RNF5 interacts with- and ubiquitinates RBBP4

(A) Western blot analysis of anti-Myc immunoprecipitates and lysates of HEK293T cells co-expressing Myc-RBBP4, HA-Ub, and shRNF5. Cells were treated with MG132 (10 μm 4 h) before lysis. **(B)** Western blot analysis of anti-RBBP4 immunoprecipitates and lysates of MOLM-13 cells expressing the indicated shRNF5 constructs. Cells were treated with MG132 (10 μm 4 h) before lysis. Quantification of the ubiquitination smear relative to the amount of RBBP4 pull down is shown. **(C)** Western blot analysis of anti-Myc immunoprecipitates and lysates of HEK293T cells co-expressing Myc-RBBP4, HA-Ub, and the indicated Flag-tagged RNF5 constructs. Cells were treated with MG132 (10 μm 4 h) before lysis. **(D)** Western blot analysis of the indicated proteins in HEK293T cells transfected with Myc tagged RBBP4 (Myc-RBBP4) and Flag-tagged full-length RNF5 (Flag-RNF5). **(E)** Western blot analysis of RBBP4 and RNF5 in indicated cellular fractions in MOLM-13 cells expressing empty vector (pLKO) or shRNF5 #1. Histone H3, HSP90, and calreticulin serve as controls for chromatin, cytosol, and membrane fractions, respectively. **(F)** Immunofluorescence staining of RBBP4 (red) in control or shRNF5-expressing MOLM-13 cells. Nuclei were stained with DAPI (blue). Scale bar 60μM. Western blot shows RNF5-KD efficiency. **(G)** Immunoprecipitation and Western blot analysis of the interaction of RBBP4 with HDAC1, HDAC2, or EZH2 in U937 cells expressing empty vector or the indicated shRNF5 construct. Cells were treated with MG132 (10 μm 4 h) before lysis.

Extended Data Fig. 7: RNF5 KD sensitized AML cells to HDAC inhibition

(A) Viability of HL-60 cells expressing pLKO or two shRNF5 constructs after treatment for 24 h with the indicated concentrations of CI-994. Western blots show confirmation of RNF5-KD **(B)** Viability of MOLM-13 cells after treatment for 24 h with 3.5 nM FK228. **(C, D)** Viability of HL-60 (C) or THP-1(D) cells expressing pLKO or shRNF5 constructs after treatment for 24 h with the indicated concentrations of FK228. Western blots show confirmation of RNF5-KD. **(E)** Viability of MOLM-13 cells stably expressing Cas9 and transduced with control Renilla-targeting sgRNA or RNF5-targeting sgRNAs and treated for 24 h with indicated concentrations of FK228. Western blot shows reduction in RNF5. **(F)** Viability of MOLM-13, U937, MV-4-11, THP-1, and HL-60 cells after treatment for 24 h with the indicated concentrations of FK228. **(G)** Viability of MV-4-11 cells expressing pLKO or shRNF5 constructs and treated for 24 h with the indicated concentrations of FK228. Data are presented as the mean ± SD of two independent experiments. **(H)** Viability of U937 cells expressing pLKO or shRBBP4 and treated for 24 h with the indicated concentrations of FK228. **(I)** RT-qPCR analysis of *LIMK1* mRNA in MOLM-13 cells expressing empty vector (pLKO) or shRNF5 #1 and treated with 4nM FK228 for 15 h. Data are presented as the mean ± SD of two independent experiments.

**P* < 0.05, ****P* < 0.001, and *****P* < 0.0001 by two-tailed *t*-test (B) or by two-way ANOVA (H) followed by Tukey's multiple comparison test (A, C, E and F).

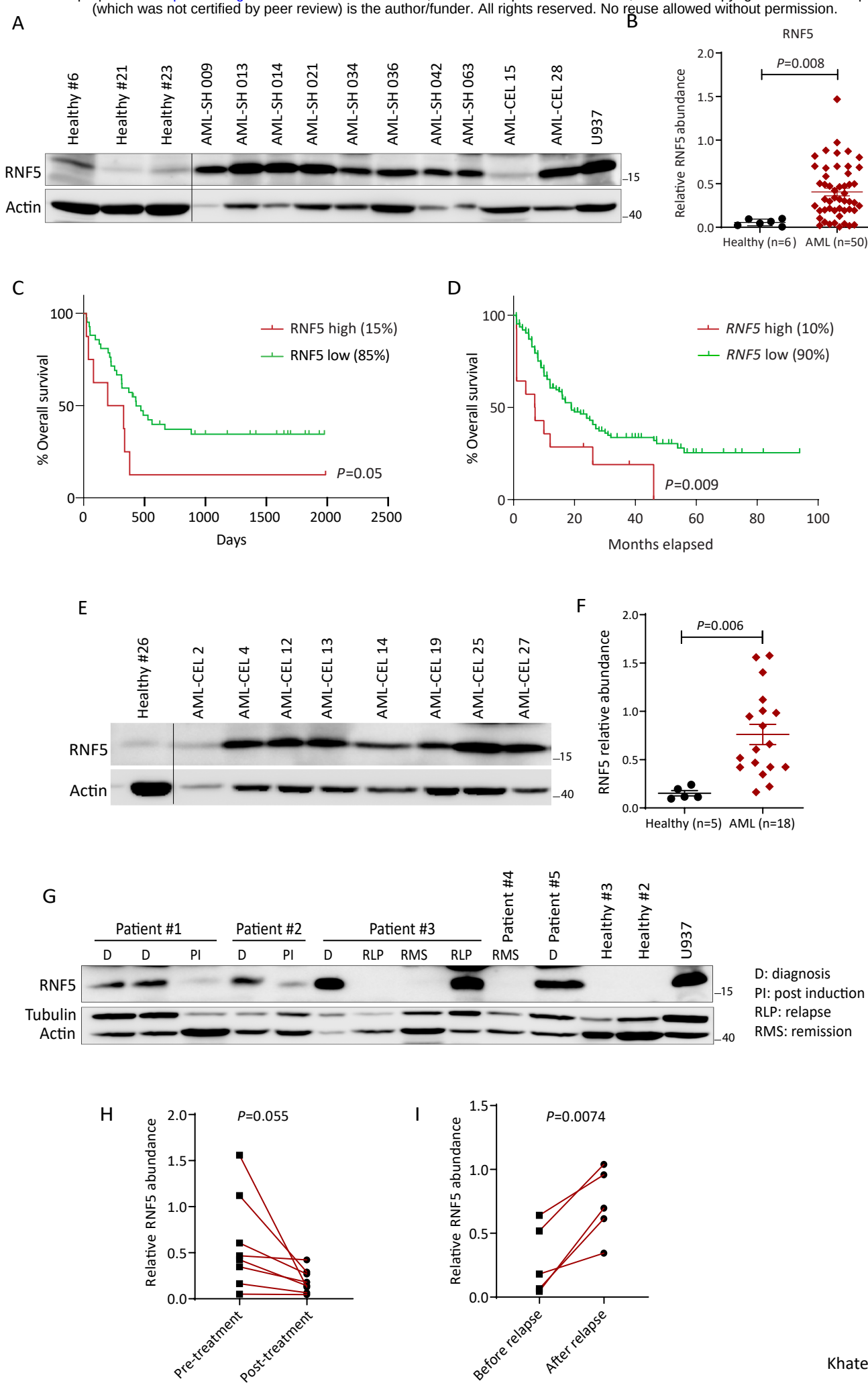

Khateb et al. Fig. 1

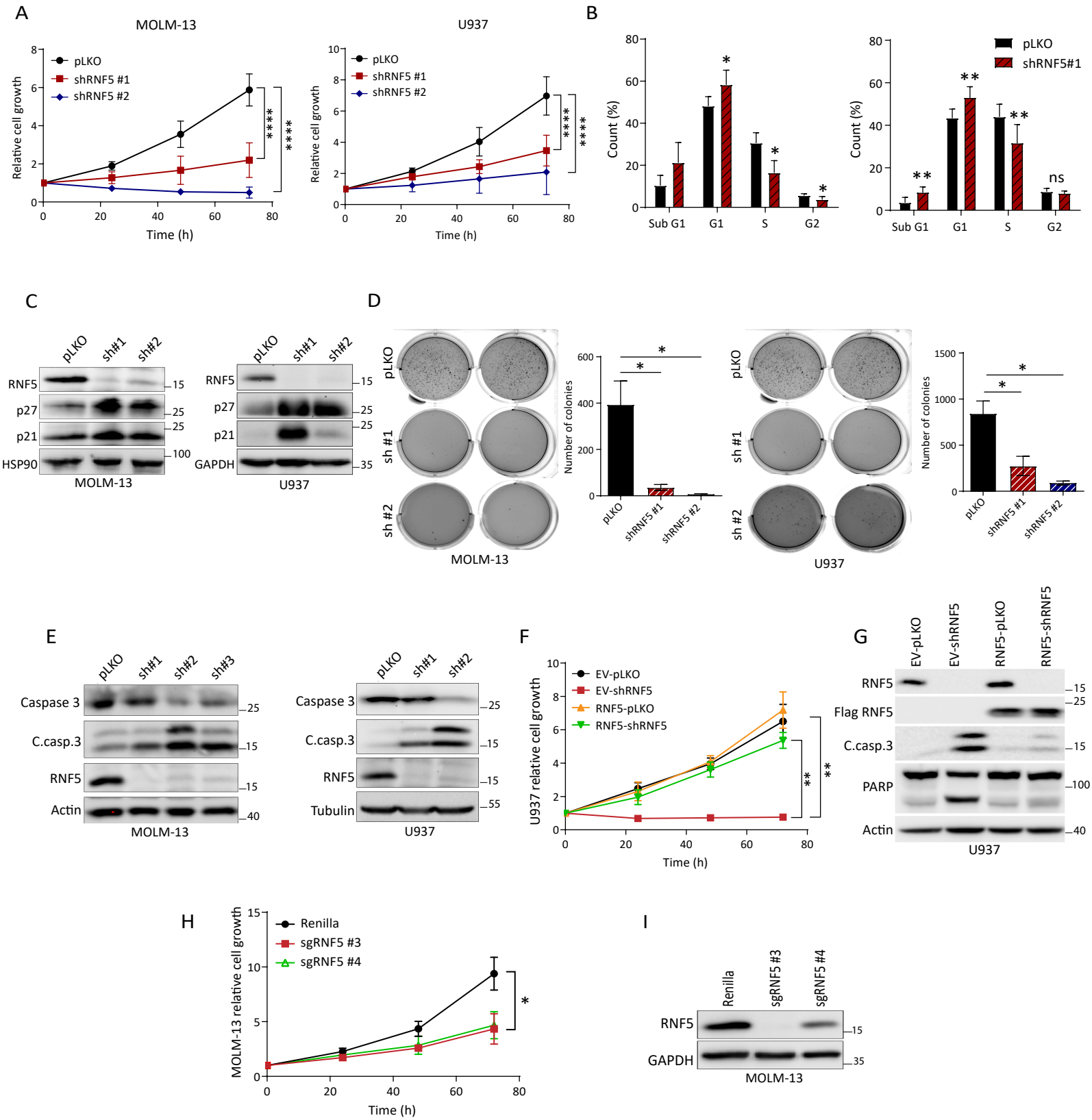

Khateb et al. Fig. 2

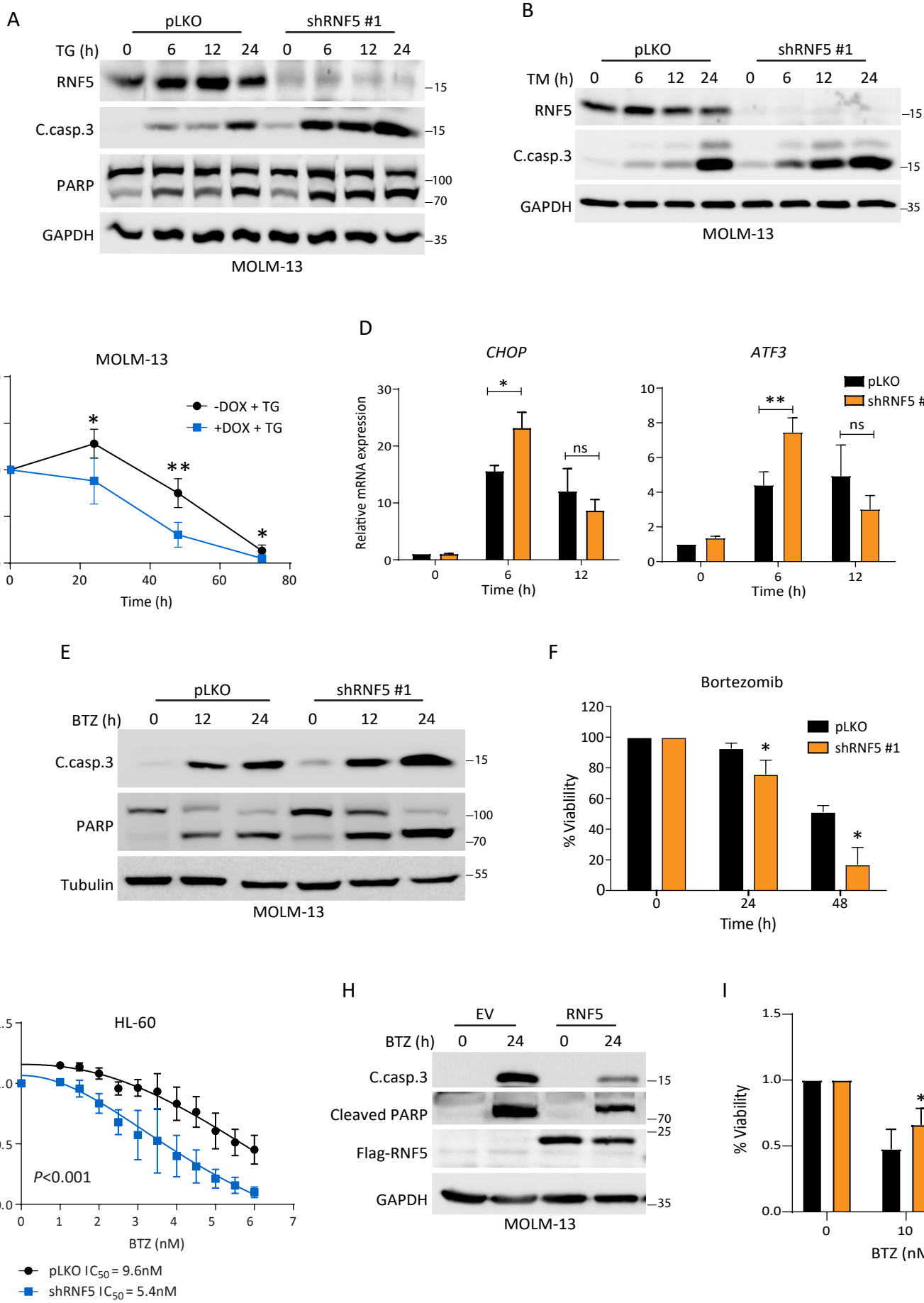

Khateb et al. Fig. 3

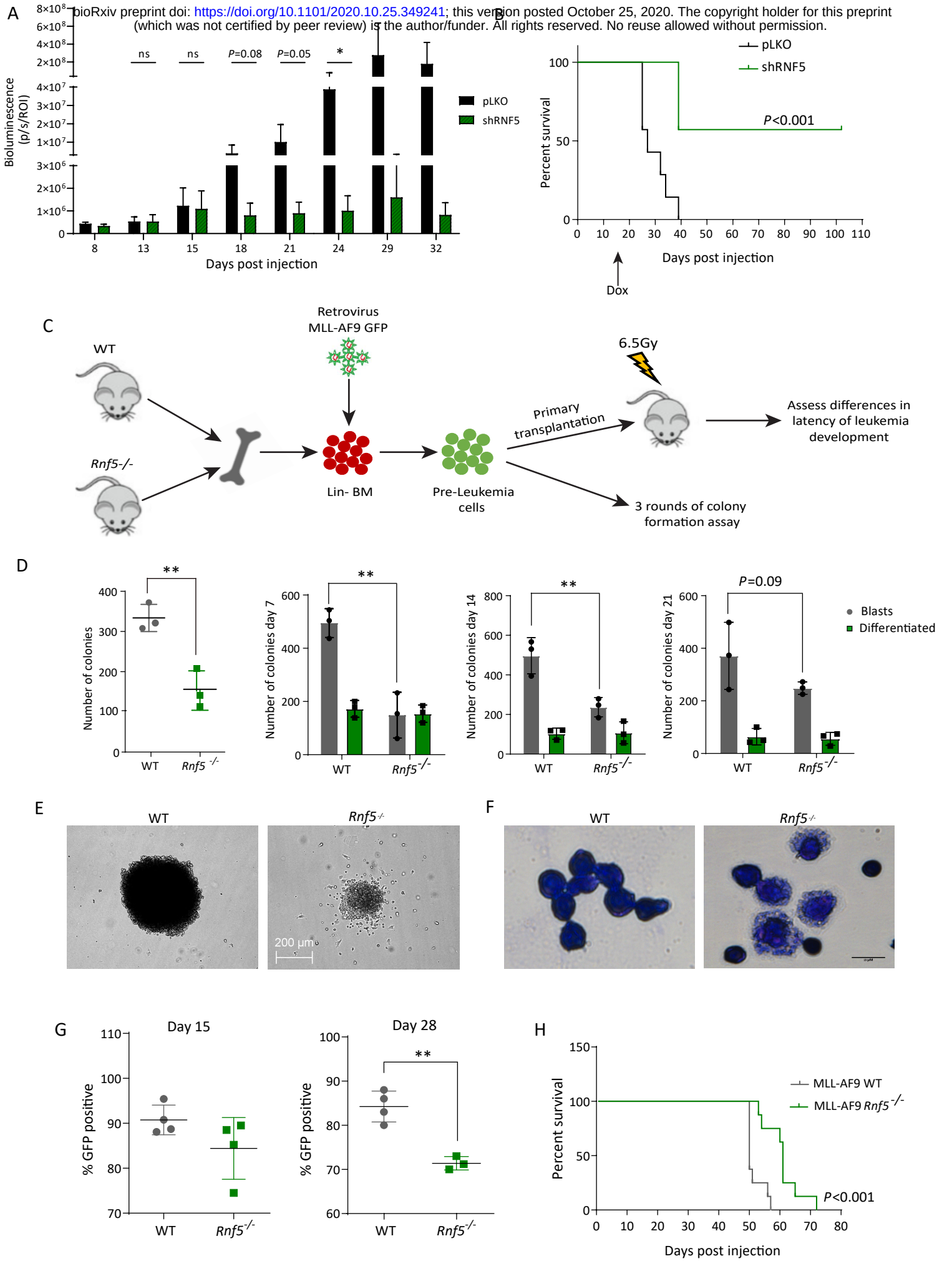

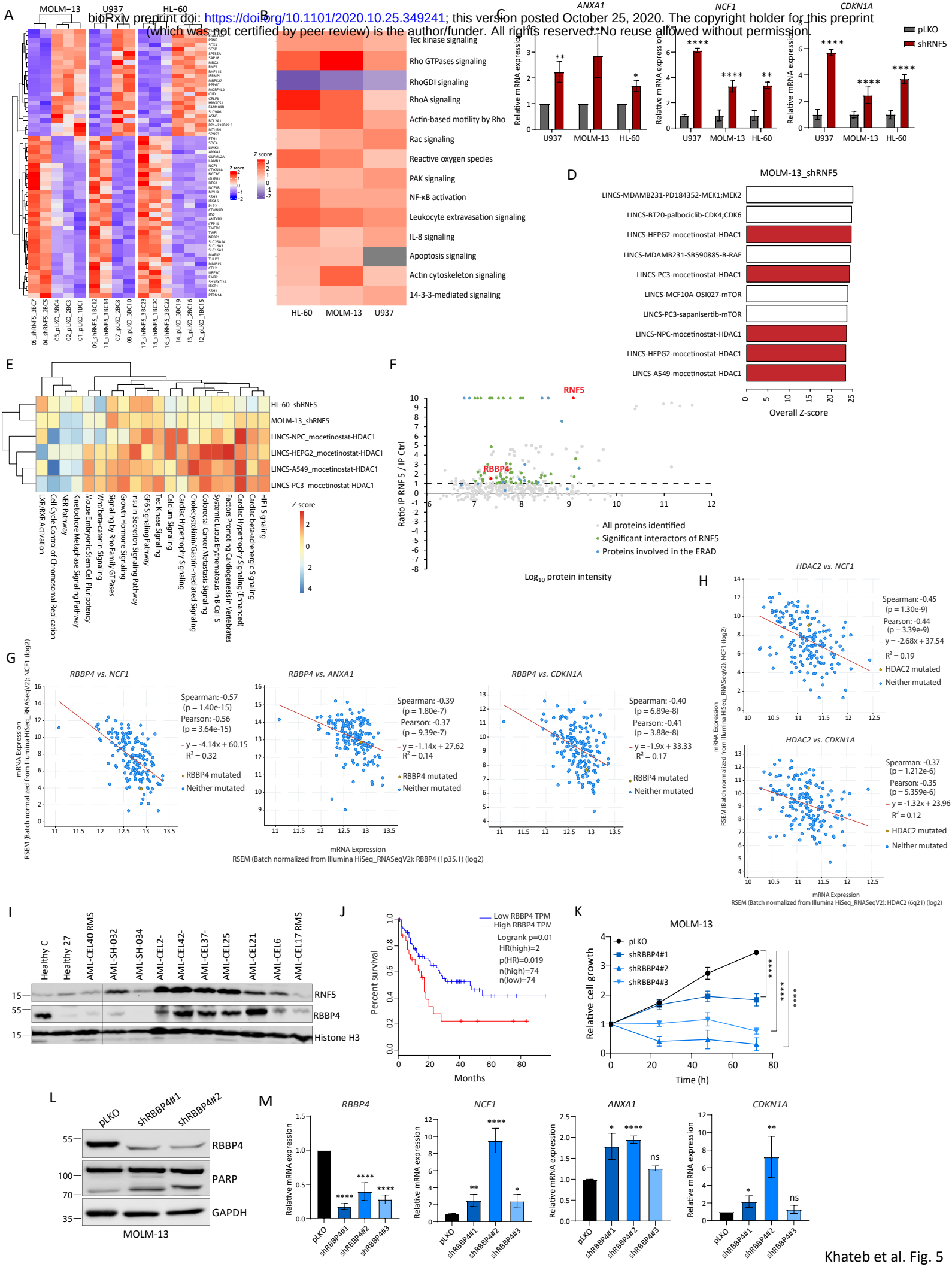

Khateb et al. Fig. 5

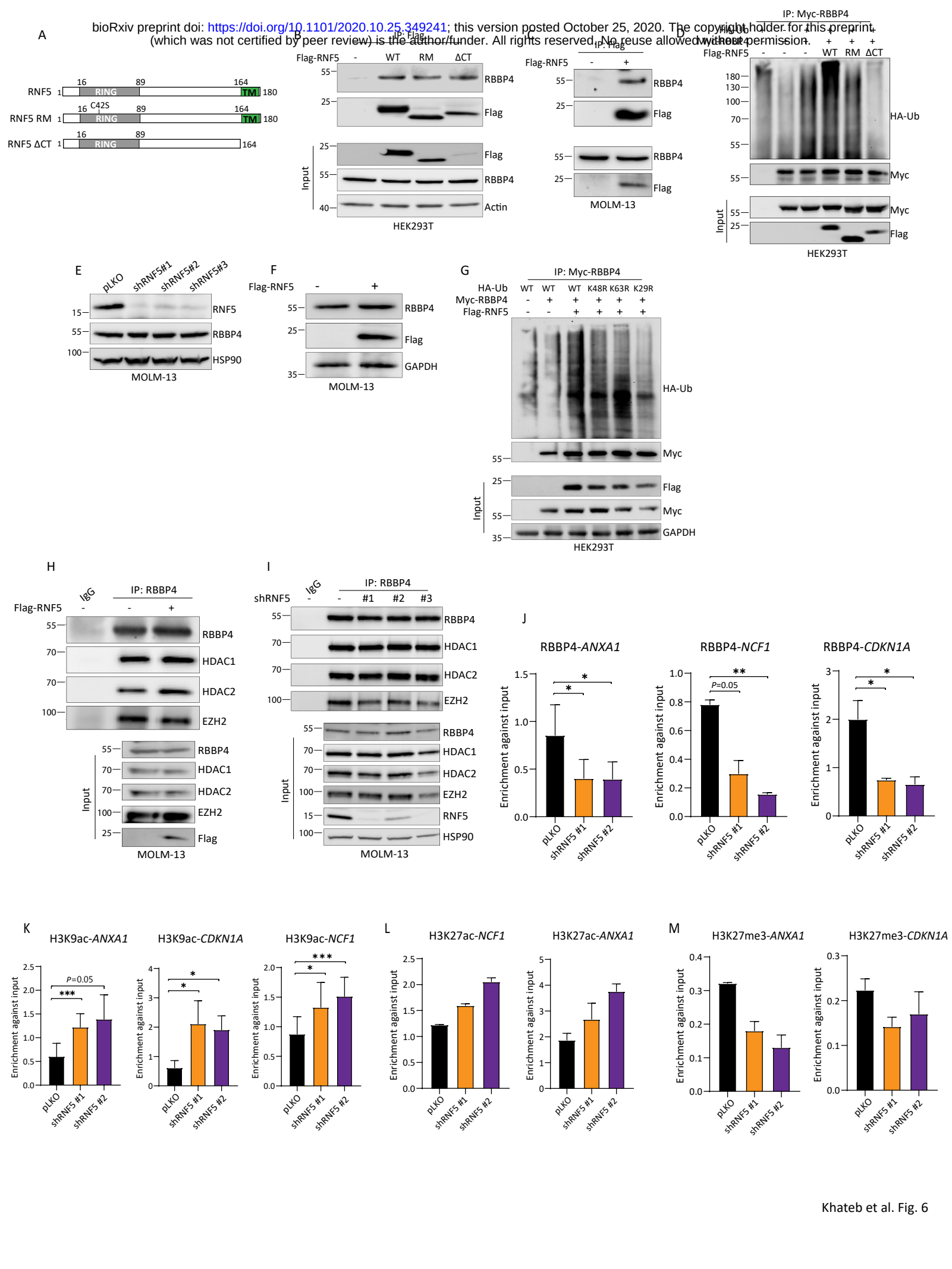

Khateb et al. Fig. 6

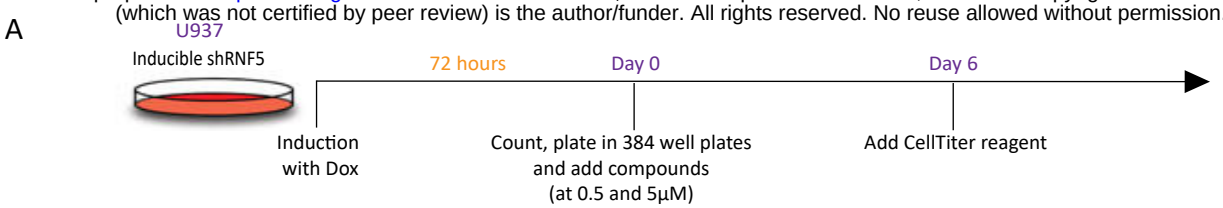

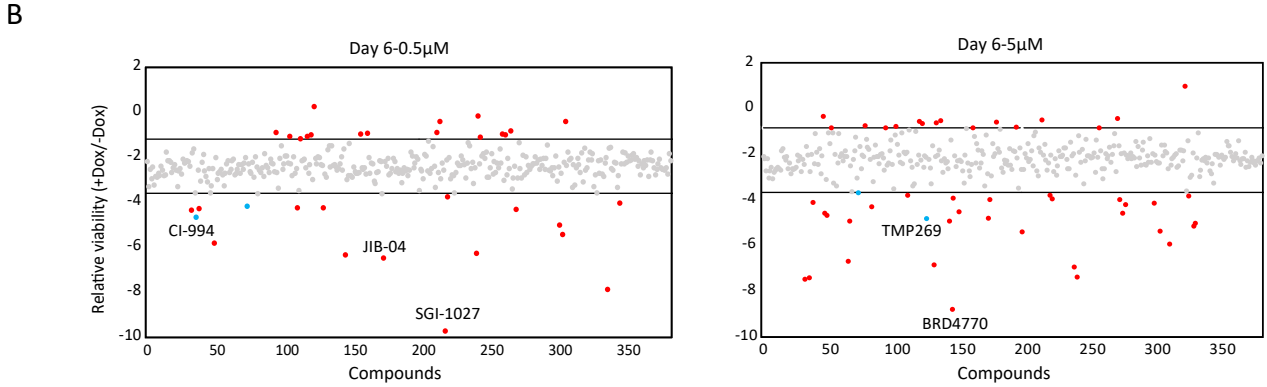

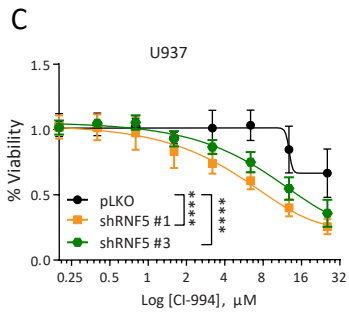

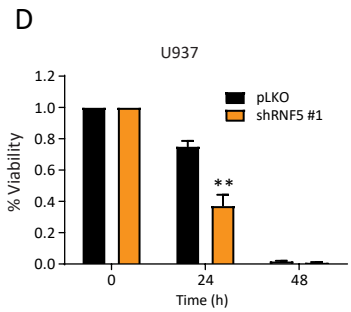

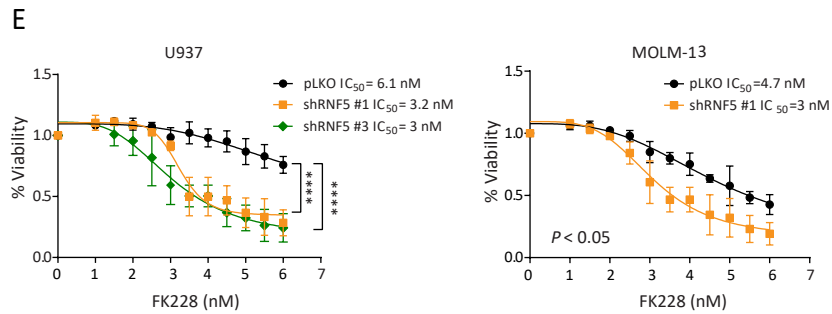

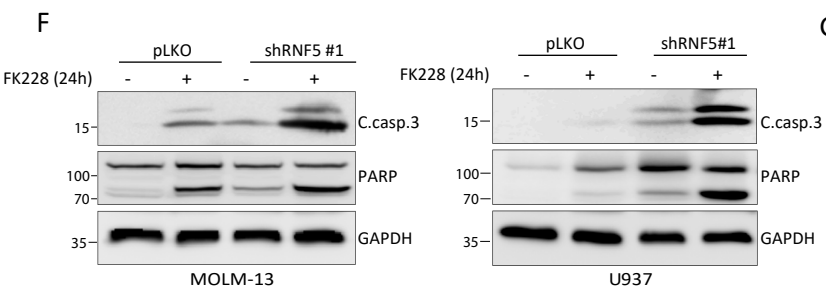

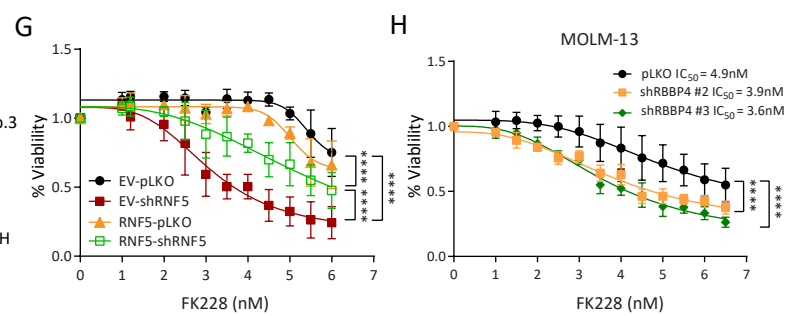

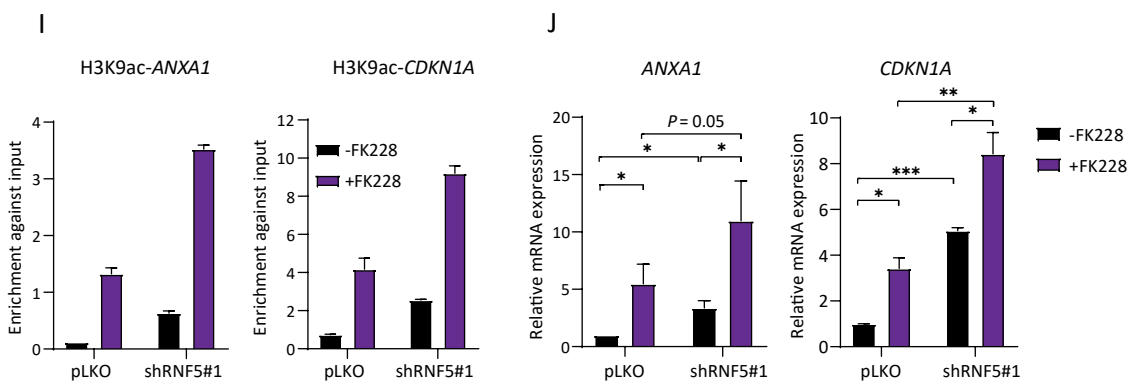

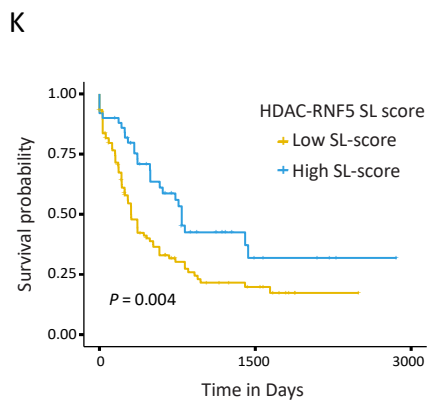

Khateb et al. Fig. 7

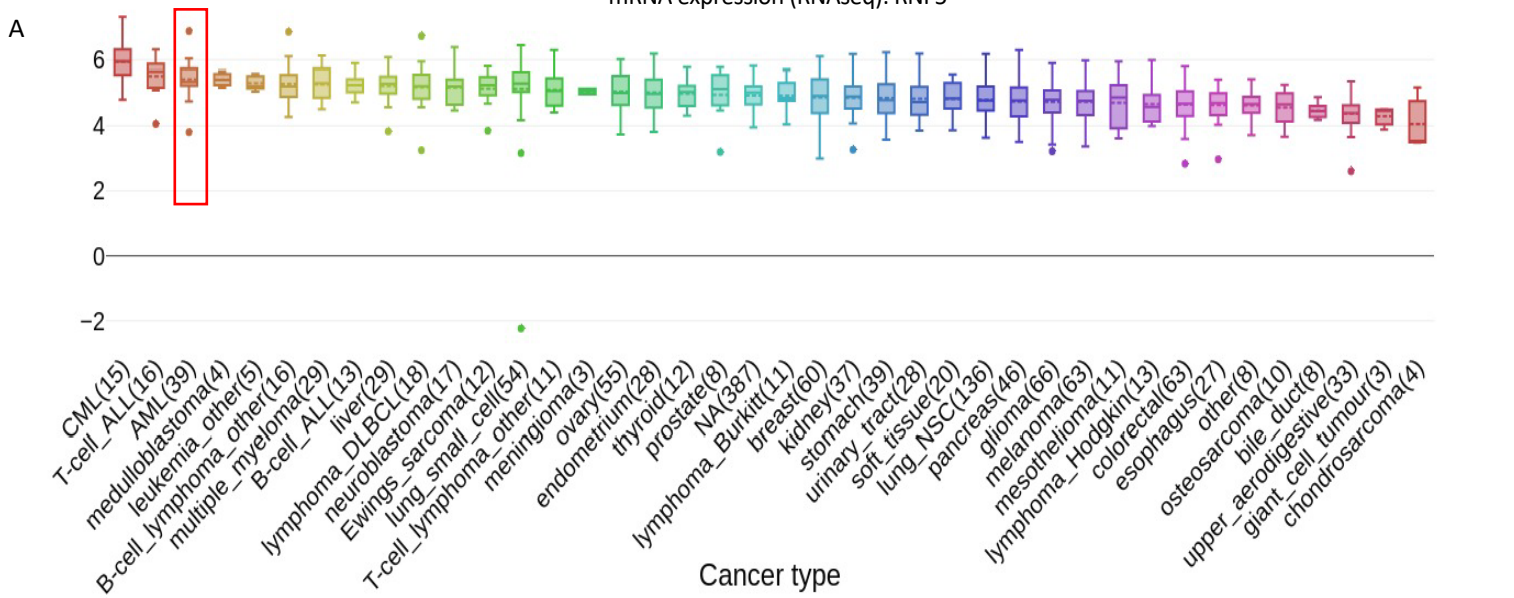

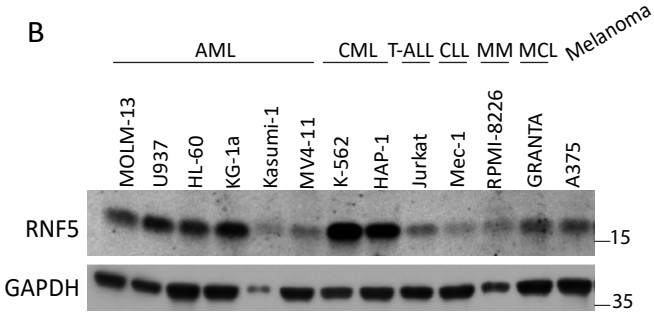

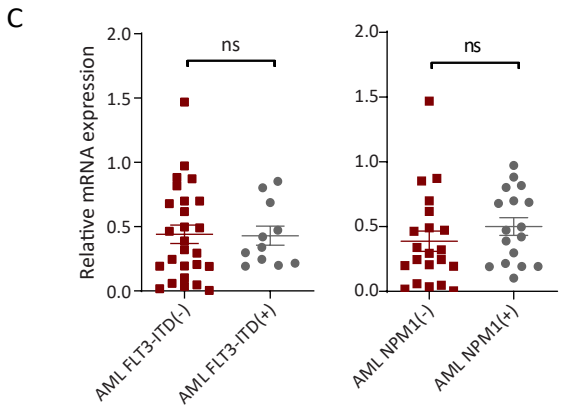

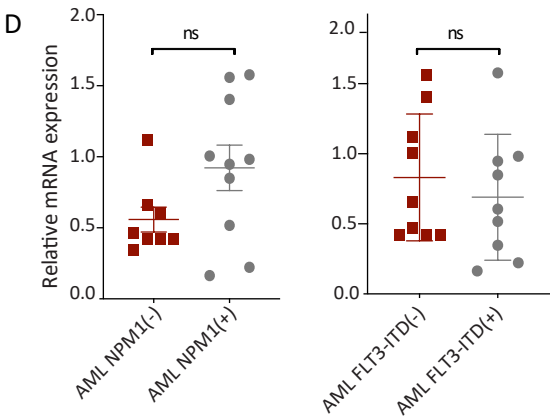

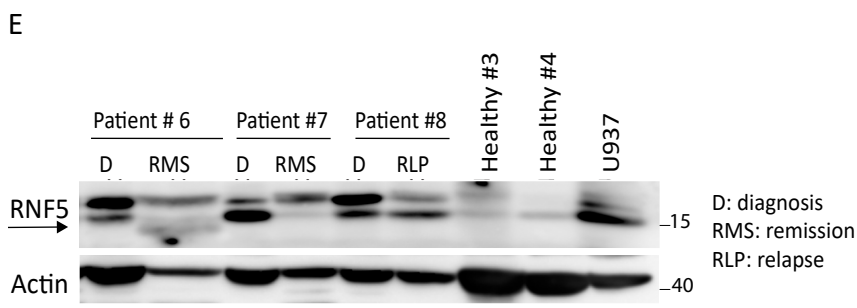

Khateb et al. Extended Data Fig. 1

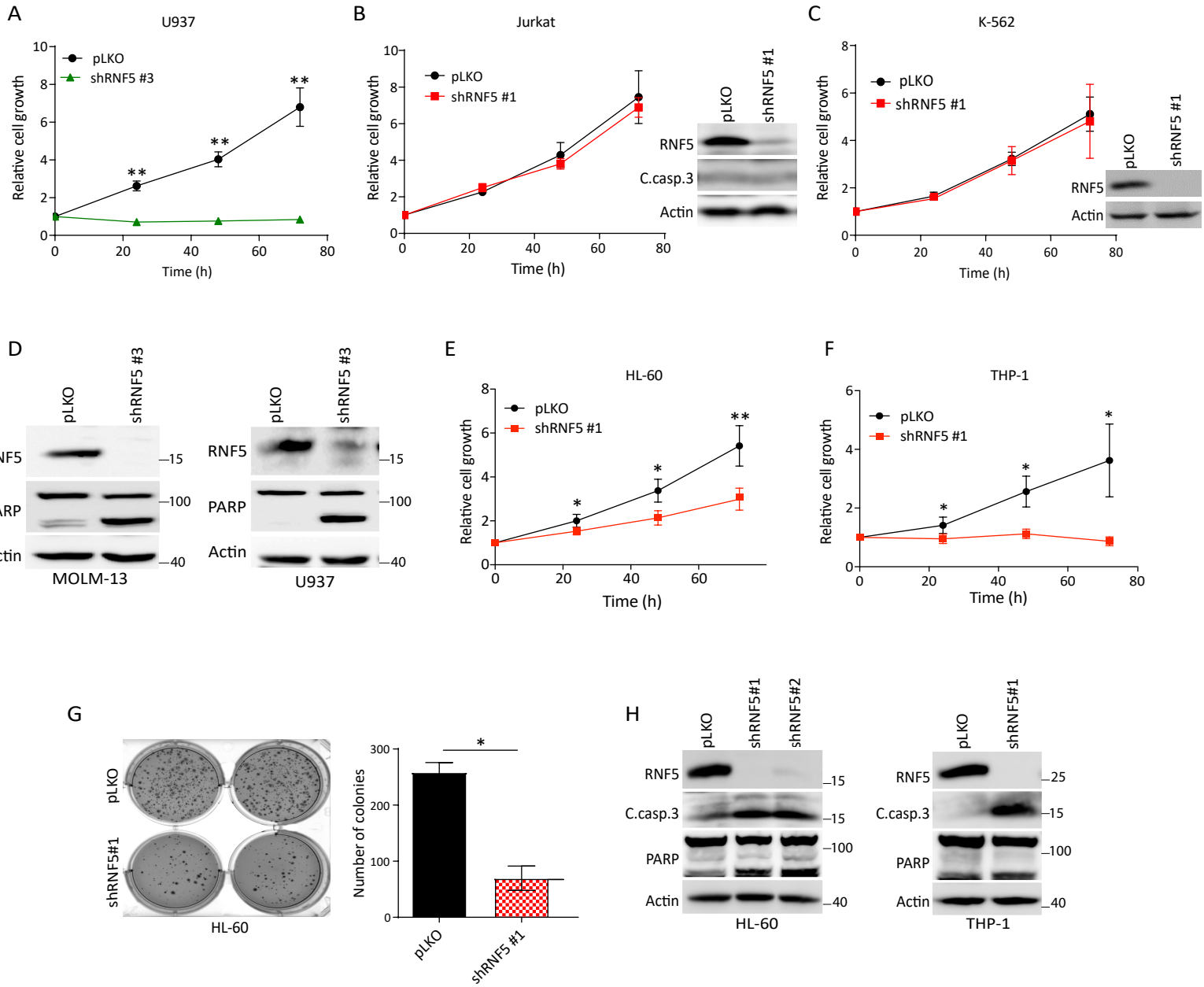

Khateb et al. Extended Data Fig. 2

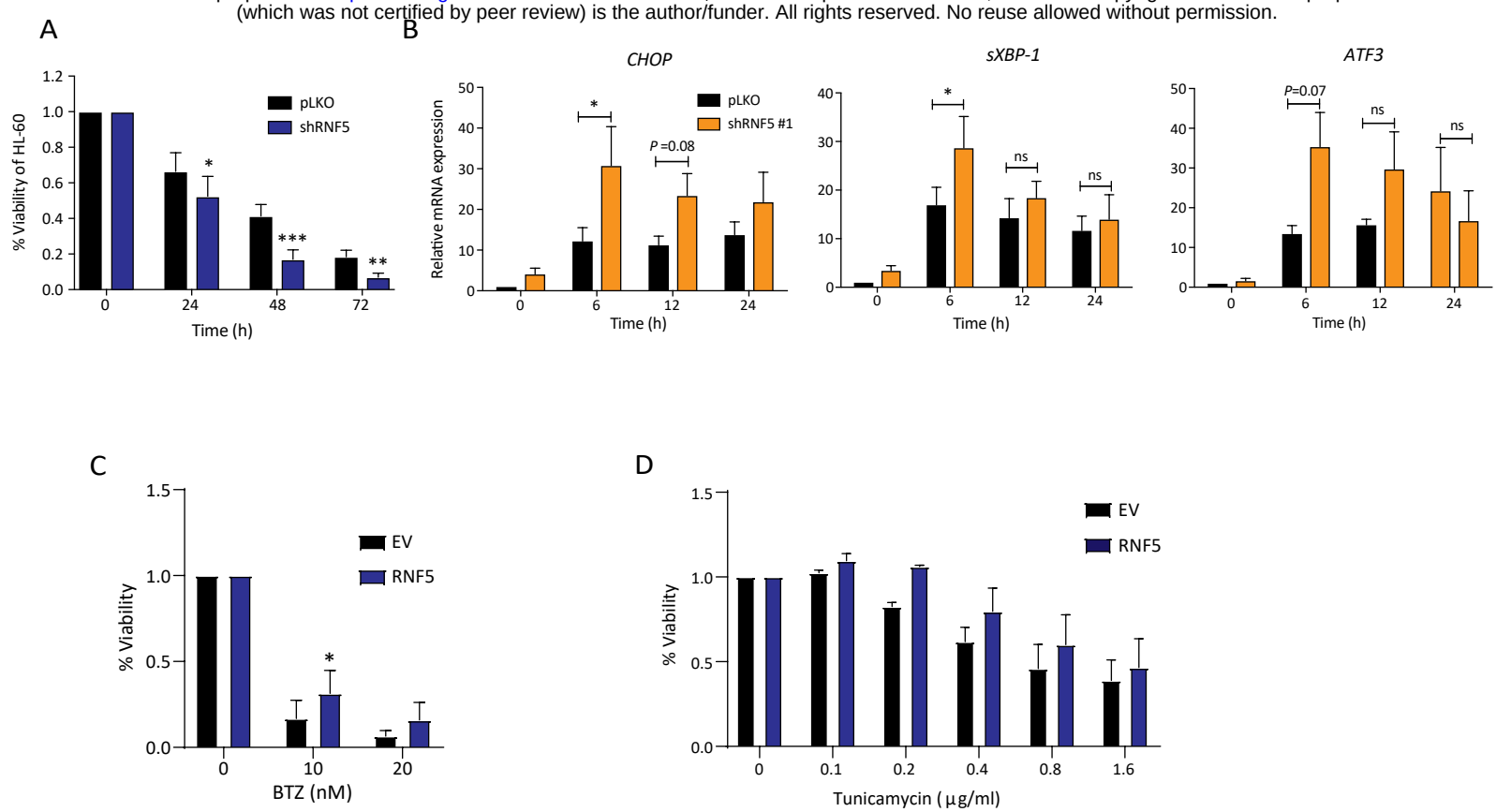

Khateb et al. Extended Data Fig. 3

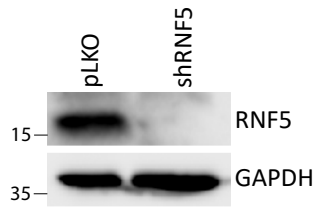

Khateb et al. Extended Data Fig. 4

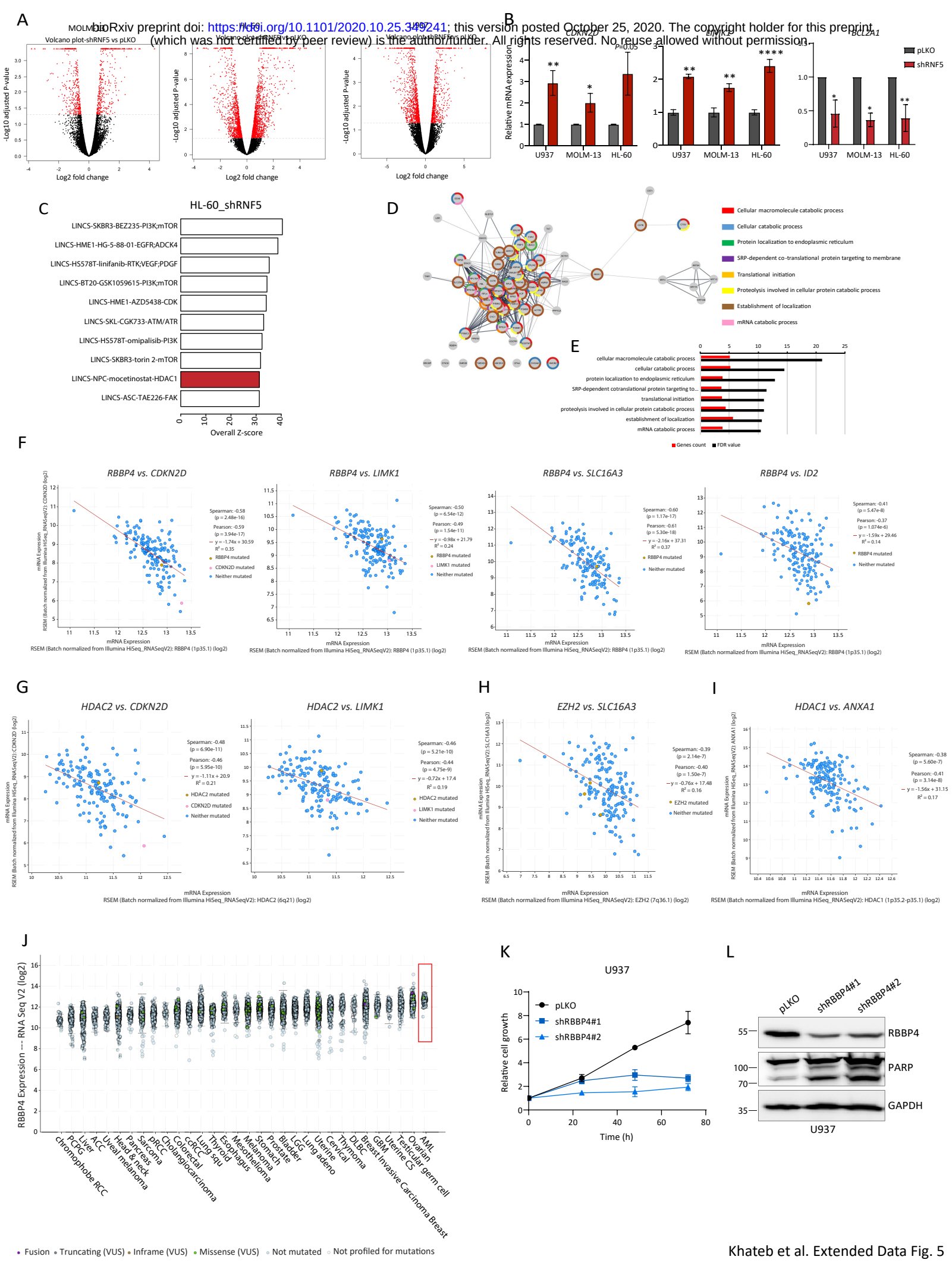

Khateb et al. Extended Data Fig. 5

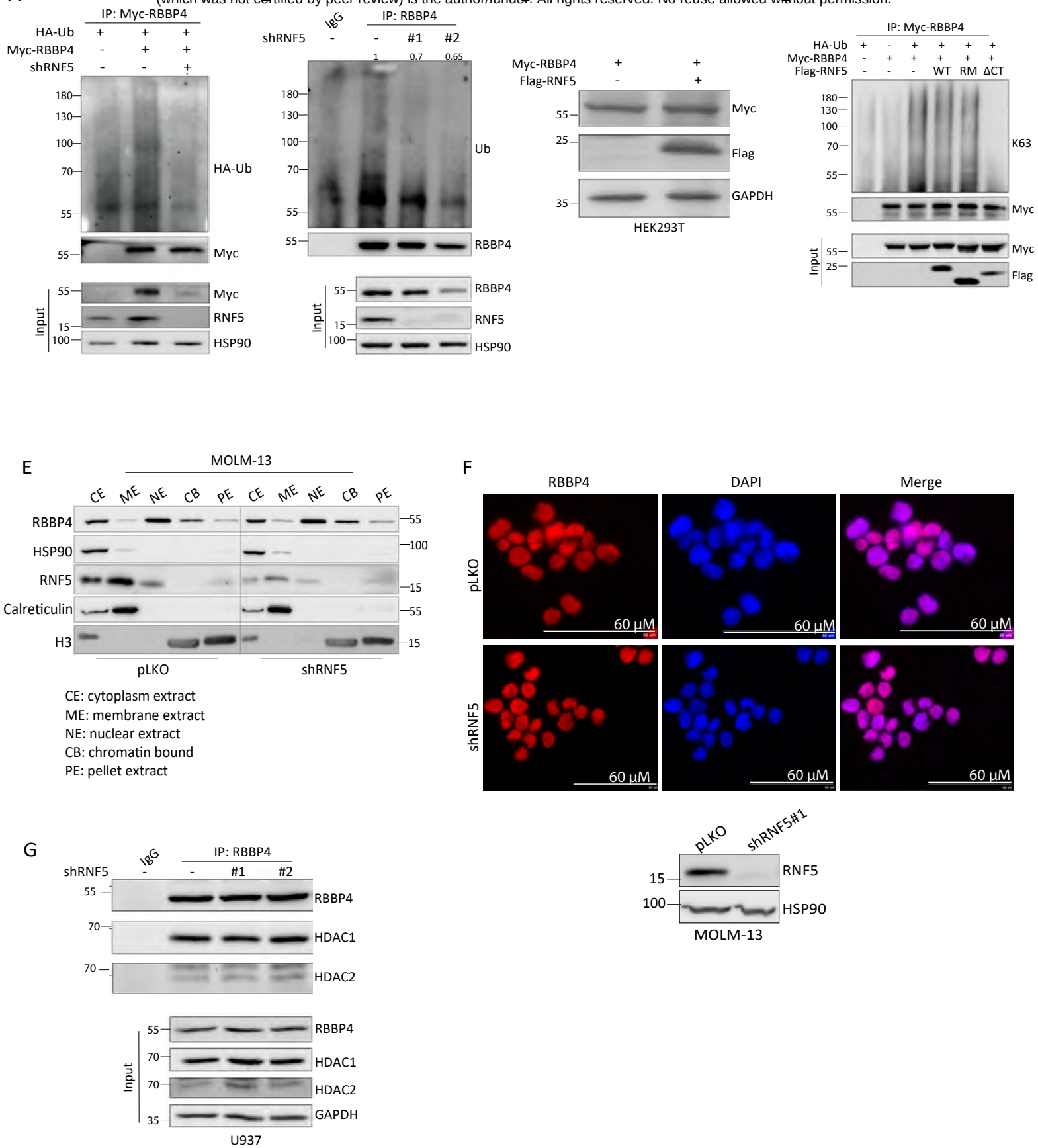

Khateb et al. Extended Data Fig. 6

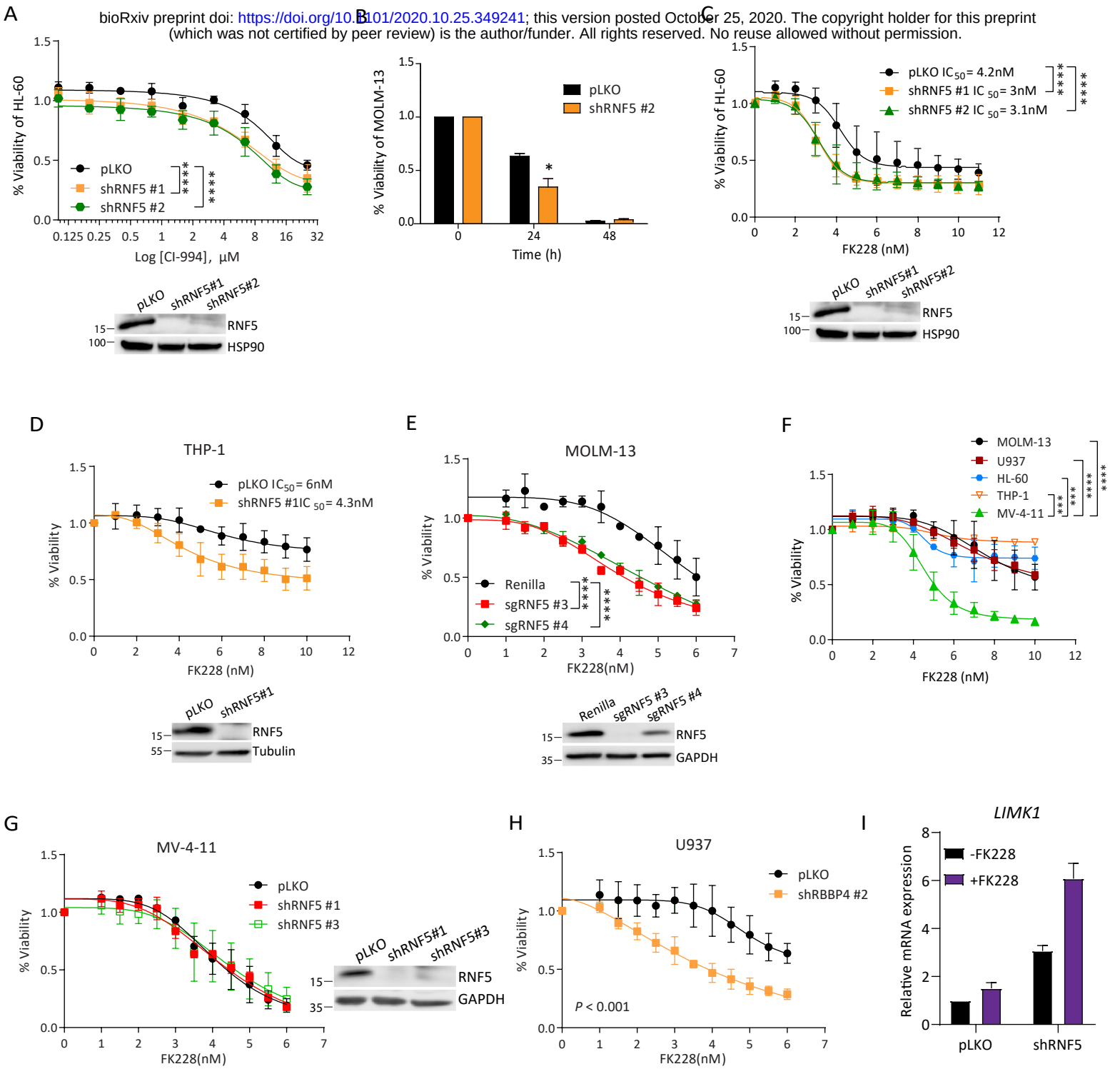

Khateb et al. Extended Data Fig. 7

SUPPLEMENTAL TABLES

Supplemental Table S1. Genes commonly deregulated upon RNF5 knockdown in AML cell lines (HL-60, MOLM-13, and U937)

Upregulated genes							
		Cell line					
		MOLM-13		U937		HL-60	
ID	Name	log2Fold Change	p.adj	log2Fold Change	p.adj	log2Fold Change	p.adj
ENSG00000102996.4	MMP15	2.516	2.35E-04	1.201	4.25E-02	0.912	1.17E-02
ENSG00000165178.8	NCF1C	1.729	3.79E-04	2.599	4.21E-04	1.901	3.08E-04
ENSG00000196878.8	LAMB3	1.676	1.08E-04	1.687	2.02E-02	2.877	1.09E-13
ENSG00000078246.11	TULP3	1.613	3.51E-05	1.073	6.31E-02	0.87	4.92E-03
ENSG00000159388.5	BTG2	1.473	1.28E-05	1.257	2.45E-02	1.842	2.35E-06
ENSG00000185585.15	OLFML2A	1.414	1.26E-03	2.136	6.75E-05	3.116	1.37E-05
ENSG00000182487.8	NCF1B	1.401	1.63E-03	3.021	1.18E-02	1.679	8.88E-04
ENSG00000124762.9	CDKN1A	1.297	4.63E-06	2.513	3.88E-08	1.892	1.74E-04
ENSG00000158517.9	NCF1	1.286	2.74E-02	2.636	6.99E-05	1.74	9.42E-07
ENSG00000135046.9	ANXA1	1.128	1.61E-05	2.133	2.16E-08	0.406	3.69E-02
ENSG00000129355.6	CDKN2D	1.103	4.47E-03	0.93	3.13E-02	1.849	1.86E-10
ENSG00000009335.13	UBE3C	1.067	3.15E-06	1.619	1.25E-05	0.515	1.86E-02
ENSG00000174007.7	CEP19	1.055	8.12E-02	1.542	3.49E-02	1.24	7.78E-05
ENSG00000107957.12	SH3PXD2A	0.955	2.82E-05	1.306	1.00E-02	0.478	1.29E-02
ENSG00000151239.9	TWF1	0.926	1.08E-04	1.248	1.22E-02	1.01	1.34E-04
ENSG00000084112.10	SSH1	0.838	2.01E-03	1.173	7.76E-03	0.561	3.69E-03
ENSG00000115216.9	NRBP1	0.823	2.87E-04	0.807	4.57E-02	1.108	4.35E-07
ENSG00000139278.5	GLIPR1	0.822	7.04E-03	3.01	3.25E-09	0.722	4.74E-04
ENSG00000106683.10	LIMK1	0.806	7.55E-03	1.069	3.77E-03	1.271	9.14E-09
ENSG00000085491.11	SLC25A24	0.791	3.57E-03	1.029	7.05E-03	1.35	8.75E-11
ENSG00000167996.11	FTH1	0.783	5.62E-02	1.343	2.18E-04	1.848	8.53E-15
ENSG00000115738.5	ID2	0.769	3.09E-02	1.495	3.07E-05	0.949	4.69E-05
ENSG00000161638.6	ITGA5	0.735	6.05E-03	1.002	8.49E-03	0.686	3.61E-04
ENSG00000163297.12	ANTXR2	0.721	3.68E-02	0.898	1.56E-02	1.014	1.93E-05
ENSG00000100345.16	MYH9	0.719	3.67E-03	0.812	5.04E-02	0.458	1.56E-02
ENSG00000150093.14	ITGB1	0.712	8.89E-03	1.189	9.87E-03	0.501	2.24E-02
ENSG00000141526.10	SLC16A3	0.696	3.86E-03	1.426	3.67E-05	0.535	1.66E-02
ENSG00000141526.10	SLC16A3	0.696	3.86E-03	1.426	3.67E-05	0.535	1.66E-02
ENSG00000124145.5	SDC4	0.688	9.72E-02	1.3	2.26E-03	1.356	7.10E-04
ENSG00000127507.13	EMR2	0.656	6.69E-03	1.933	5.13E-07	0.898	1.49E-07
ENSG00000165410.10	CFL2	0.61	7.53E-02	0.952	5.86E-02	1.18	6.67E-06

ENSG00000069956.7	MAPK6	0.605	1.59E-02	1.225	3.89E-04	0.544	6.08E-03
ENSG00000172830.8	SSH3	0.584	4.82E-02	1.869	1.50E-02	1.243	3.42E-04
ENSG00000102007.6	PLP2	0.576	4.33E-02	1.137	1.81E-03	0.587	5.57E-03
ENSG00000117500.8	TMED5	0.539	6.79E-02	0.87	2.80E-02	0.705	2.01E-04
ENSG00000152104.7	PTPN14	0.524	8.03E-02	1.818	6.64E-05	0.78	4.93E-03

Downregulated genes							
		Cell line					
		MOLM-13		**U937**		**HL-60**	
ID	**Name**	**log2Fold Change**	**p.adj**	**log2Fold Change**	**p.adj**	**log2Fold Change**	**p.adj**
ENSG00000146433.8	TMEM181	-0.481	8.74E-02	-0.934	1.47E-02	-0.973	9.99E-05
ENSG00000257093.2	KIAA1147	-0.625	3.68E-02	-1.362	1.44E-04	-1.105	3.96E-07
ENSG00000124766.4	SOX4	-0.639	1.36E-02	-1.063	3.92E-03	-0.468	3.20E-02
ENSG00000123562.12	MORF4L2	-0.655	8.10E-03	-0.982	1.10E-02	-0.431	3.91E-02
ENSG00000109929.5	SC5D	-0.675	1.83E-02	-0.805	5.38E-02	-0.609	2.35E-03
ENSG00000112972.10	HMGCS1	-0.695	1.54E-02	-2.068	3.59E-08	-1.023	9.78E-08
ENSG00000198689.5	SLC9A6	-0.801	6.61E-03	-0.894	4.04E-02	-0.564	2.02E-02
ENSG00000180354.11	MTURN	-0.863	3.27E-02	-0.903	3.53E-02	-1.716	1.82E-13
ENSG00000160767.16	FAM189B	-0.894	4.38E-03	-1.461	8.54E-03	-1.246	1.24E-04
ENSG00000176390.10	CRLF3	-0.971	5.12E-03	-1.213	5.31E-03	-0.642	1.54E-02
ENSG00000260196.1	RP1-239B22.5	-1.045	7.34E-03	-1.159	1.10E-02	-0.627	6.19E-03
ENSG00000165389.6	SPTSSA	-1.098	3.02E-06	-1.062	1.17E-02	-0.967	2.47E-06
ENSG00000150459.8	SAP18	-1.239	4.98E-09	-1.02	6.39E-03	-0.917	2.72E-05
ENSG00000171867.12	PRNP	-1.255	2.93E-07	-0.902	1.35E-02	-1.254	1.72E-09
ENSG00000182557.3	SPNS3	-1.296	5.85E-06	-1.577	3.18E-03	-1.085	5.98E-05
ENSG00000070669.12	ASNS	-1.325	1.45E-02	-1.161	1.14E-02	-0.644	4.77E-04
ENSG00000121848.9	RNF115	-1.388	3.81E-09	-1.644	1.51E-05	-1.341	6.49E-11
ENSG00000119414.7	PPP6C	-1.392	8.66E-10	-0.963	1.03E-02	-1.164	1.70E-06
ENSG00000113048.12	MRPS27	-1.398	2.07E-09	-1.003	9.40E-03	-1.64	5.78E-15
ENSG00000140379.7	BCL2A1	-1.45	2.27E-02	-1.124	2.71E-02	-1.351	5.10E-03
ENSG00000197223.7	C1D	-1.515	1.27E-05	-1.133	1.73E-02	-0.545	3.05E-02
ENSG00000134049.3	IER3IP1	-1.517	6.06E-08	-0.848	3.83E-02	-1.068	5.21E-09
ENSG00000011028.9	MRC2	-1.551	6.19E-13	-1.693	1.30E-03	-1.135	2.53E-04
ENSG00000204308.6	RNF5	-3.798	5.26E-45	-3.647	1.51E-15	-3.04	6.51E-14

Supplemental Table S2. List of RNF5 interacting proteins identified by LC-MS/MS

Protein name	Gene name	Number of Peptides	ratio IP RNF5 / IP Ctrl	p-value
E3 ubiquitin-protein ligase RNF5	RNF5	5	Found only in RNF5 IP	
BAG family molecular chaperone regulator 2	BAG2	11	Found only in RNF5 IP	
Transitional endoplasmic reticulum ATPase	VCP	20	Found only in RNF5 IP	
Large proline-rich protein BAG6	BAG6	9	Found only in RNF5 IP	
Erlin-2	ERLIN2	12	Found only in RNF5 IP	
FAS-associated factor 2	FAF2	9	Found only in RNF5 IP	
26S protease regulatory subunit 7	PSMC2	4	Found only in RNF5 IP	
26S protease regulatory subunit 6A	PSMC3	4	Found only in RNF5 IP	
26S protease regulatory subunit 10B	PSMC6	4	Found only in RNF5 IP	
26S proteasome non-ATPase regulatory subunit 11	PSMD11	3	Found only in RNF5 IP	
Erlin-1	ERLIN1	19	189.9	0.005
Proteasome subunit beta type-6	PSMB6	2	8.7	0.023
Heat shock 70 kDa protein 1A	HSPA1A	17	8.0	0.009
Heat shock cognate 71 kDa protein	HSPA8	36	6.1	0.013
Proteasome subunit alpha type-7	PSMA7	6	4.6	0.038
Proteasome subunit alpha type	PSMA6	8	4.3	0.004
Proteasome subunit alpha type	PSMA1	4	4.1	0.014
Proteasome subunit alpha type-2	PSMA2	4	3.1	0.016
Proteasome subunit alpha type-5	PSMA5	3	2.8	0.039
Proteasome subunit beta type-1	PSMB1	4	2.8	0.006
Heat shock protein HSP 90-beta	HSP90AB1	11	2.5	0.002
Stress-70 protein, mitochondrial	HSPA9	7	2.2	0.014
78 kDa glucose-regulated protein	HSPA5	21	2.2	0.008
Heat shock protein beta-1	HSPB1	9	3.1	0.016
T-complex protein 1 subunit theta	CCT8	7	2.7	0.024
T-complex protein 1 subunit gamma	CCT3	6	2.1	0.002
Actin-related protein 2	ACTR2	4	Found only in RNF5 IP	
Tropomodulin-3	TMOD3	4	Found only in RNF5 IP	
Transmembrane protein 33	TMEM33	4	Found only in RNF5 IP	
Ubiquitin-associated domain-containing protein 2	UBAC2	6	Found only in RNF5 IP	
Sequestosome-1 (p62)	SQSTM1	5	29.1	
Ubiquitin-40S ribosomal protein S27a	UBB	11	12.2	0.008
BRI3-binding protein	BRI3BP	3	8.4	0.000
ADP/ATP translocase 3	SLC25A6	9	8.1	0.002

ADP/ATP translocase 2	SLC25A5	11	5.9	0.001
Voltage-dependent anion-selective channel protein 2	VDAC2	2	4.7	0.005
Splicing factor 3B subunit 2	SF3B2	3	4.4	
Gelsolin	GSN	5	4.4	0.038
Tubulin alpha-1B chain	TUBA1B	17	4.0	0.003
60S acidic ribosomal protein P1	RPLP1	4	3.7	0.049
Eukaryotic translation initiation factor 3 subunit C	EIF3C	3	3.7	0.049
Annexin A1	ANXA1	14	3.5	0.048
40S ribosomal protein S15a	RPS15A	4	3.4	0.026
Keratin, type I cytoskeletal 13	KRT13	30	3.3	0.017
40S ribosomal protein S3	RPS3	6	3.1	0.025
Histone-binding protein RBBP4	RBBP4	5	3.1	0.043
Carboxypeptidase A4	CPA4	3	2.9	0.047
Actin, alpha skeletal muscle	ACTA1	19	2.8	0.035
Keratin, type I cuticular Ha3-II	KRT33B	58	2.8	0.042
Keratin, type I cytoskeletal 19	KRT19	14	2.5	0.007
Pre-mRNA-splicing factor ATP-dependent RNA helicase DHX15	DHX15	3	2.4	0.001
Keratin, type II cuticular Hb4	KRT84	56	2.4	
60S ribosomal protein L30	RPL30	3	2.4	0.010
60S ribosomal protein L4	RPL4	17	2.3	0.022
Protein S100-A8	S100A8	4	2.3	0.038
ATP synthase subunit alpha, mitochondrial	ATP5A1	7	2.2	0.020
Serine/threonine-protein kinase 38	STK38	17	2.2	0.035
Elongation factor 1-delta	EEF1D	6	2.2	0.015
60S ribosomal protein L18a	RPL18A	8	2.1	0.040
Tubulin beta chain	TUBB	13	2.1	0.037
40S ribosomal protein S24	RPS24	5	2.1	0.033
Protein phosphatase 1B	PPM1B	16	2.1	0.034
60S ribosomal protein L10	RPL10	7	2.1	0.003
40S ribosomal protein S8	RPS8	11	2.0	0.021

Supplemental Table S3. List of small molecule epigenetic modulators used to identify possible synergy with RNF5 knockdown AML cells.

Molecule Name	Bio-Activity	CAS Number
B2	SIRT2 inhibitor	115687-05-3
Valproic acid	HDAC inhibitor	99-66-1
Piceatannol	SIRT activator	10083-24-6
Resveratrol	SIRT1 activator	501-36-0
Suramin·6Na	SIRT1 inhibitor	129-46-4
Triacetylresveratrol	SIRT1 activator	42206-94-0
Phenylbutyrate·Na	HDAC inhibitor	1716-12-7
NSC-3852	HDAC inhibitor	3565-26-2
Nicotinamide	SIRT inhibitor	98-92-0
BML-266	SIRT2 inhibitor	96969-83-4
AGK2	SIRT2 inhibitor	304896-28-4
BIX-01294	Histone methyl transferase inhibitor	935693-62-2
SAHA	HDAC inhibitor	149647-78-9
Anacardic acid	HAT inhibitor	16611-84-0
5-Aza-2'-deoxycytidine	DNA Me transferase inhibitor	2353-33-5
M-344	HDAC inhibitor	251456-60-7
ITSA-1	Inhibitor of TSA activity	200626-61-5
Scriptaid	HDAC inhibitor	287383-59-9
EX-527	SIRT1 inhibitor	49843-98-3
Salermide	SIRT inhibitor	1105698-15-4
CI-994	HDAC inhibitor	112522-64-2
BML-210	HDAC inhibitor	537034-17-6
Tranylcypromine hemisulfate	Lysine demethylase inhibitor	13492-01-8 (H2SO4)
Trichostatin A	HDAC inhibitor	58880-19-6
2,4-Pyridinedicarboxylic Acid	Histone demethylase inhibitor	499-80-9
Garcinol	HAT inhibitor	78824-30-3
Splitomicin	SIRT-2 inhibitor	3/9/5690
Apicidin	HDAC inhibitor	183506-66-3
Suberoyl bis-hydroxamic acid	HDAC inhibitor	38937-66-5

Nullscript	Scriptaid Neg control	300816-11-9
Zebularine	DNA Me transferase inhibitor	10/6/3690
Isonicotinamide	nicotinamide antagonist	1453-82-3
Fluoro-SAHA	HDAC inhibitor	149648-08-8
Valproic acid hydroxamate	HDAC inhibitor	106132-78-9
MC-1293	HDAC inhibitor	117378-93-5
Butyrolactone 3	HAT inhibitor	778649-18-6
CTPB	HAT inhibitor	586976-24-1
Oxamflatin	HDAC inhibitor	151720-43-3
Sirtinol	SIRT inhibitor	410536-97-9
BML-278	SIRT1 actvator	120533-76-8
NCH-51	HDAC inhibitor	848354-66-5
Aminoresveratrol sulfate	SIRT1 activator	1224713-76-1
BML-281	HDAC-6 inhibitor	1045792-66-2
Droxinostat	Droxinostat (CMH, 5809354) is a selective inhibitor of HDAC, mostly for HDACs 6 and 8 with IC50 of 2.47uM and 1.46 uM, greater than 8-fold selective against HDAC3 and no inhibition to HDAC1, 2, 4, 5, 7, 9, and 10.	99873-43-5
Azacitidine	Azacitidine is a nucleoside analogue of cytidine that specifically inhibits DNA methylation by trapping DNA methyltransferases.	320-67-2
INO-1001 (3-Aminobenzamide)	INO-1001 is a potent inhibitor of PARP with IC50 of <50 nM in CHO cells and a mediator of oxidant-induced myocyte dysfunction during reperfusion. Phase 2.	3544-24-9
2-Methoxyestradiol (2-MeOE2)	2-Methoxyestradiol depolymerizes microtubules and blocks HIF-1alpha nuclear accumulation and HIF-transcriptional activity. Phase 2.	362-07-2
Procainamide HCl	Procainamide HCl is a sodium channel blocker, and also a DNA methyltransferase inhibitor, used in the treatment of cardiac arrhythmias.	614-39-1
Quercetin	Quercetin is a natural flavonoid present in vegetables, fruit and wine and is a PI3K inhibitor with IC50 of 2.4 ? 5.4 uM.	117-39-5
AG-490 (Tyrphostin B42)	AG-490 (Tyrphostin B42) is an inhibitor of EGFR with IC50 of 0.1 uM, 135-fold more selective for EGFR versus ErbB2, also inhibits JAK2 with no activity to Lck, Lyn, Btk, Syk and Src.	133550-30-8
RG108	RG108 is an inhibitor of DNA methyltransferase with IC50 of 115 nM, does not cause trapping of covalent enzymes.	48208-26-0

WHI-P154	WHI-P154 is a potent JAK3 inhibitor with IC50 of 1.8 uM, no activity against JAK1 or JAK2, also inhibits EGFR, Src, Abl, VEGFR and MAPK, prevents Stat3, but not Stat5 phosphorylation.	211555-04-3
JNJ-7706621	JNJ-7706621 is pan-CDK inhibitor with the highest potency on CDK1/2 with IC50 of 9 nM/4 nM and showing >6-fold selectivity for CDK1/2 than CDK3/4/6. It also potently inhibits Aurora A/B and has no activity on Plk1 and Wee1.	443797-96-4
PJ34	PJ-34 is a PARP inhibitor with EC50 of 20 nM and is equally potent to PARP1/2.	344458-19-1
WP1066	WP1066 is a novel inhibitor of JAK2 and STAT3 with IC50 of 2.30 uM and 2.43 uM in HEL cells; shows activity to JAK2, STAT3, STAT5, and ERK1/2 not JAK1 and JAK3.	857064-38-1
Entinostat (MS-275)	Entinostat (MS-275) strongly inhibits HDAC1 and HDAC3 with IC50 of 0.51 uM and 1.7 uM, compared with HDACs 4, 6, 8, and 10. Phase 1/2.	209783-80-2
Mocetinostat (MGCD0103)	Mocetinostat (MGCD0103) is a potent HDAC inhibitor with most potency for HDAC1 with IC50 of 0.15 ?M, 2- to 10- fold selectivity against HDAC2, 3, and 11, and no activity to HDAC4, 5, 6, 7, and 8. Phase 1/2.	726169-73-9
Belinostat (PXD101)	Belinostat (PXD101) is a novel HDAC inhibitor with IC50 of 27 nM, with activity demonstrated in cisplatin-resistant tumors. Phase 1/2.	414864-00-9
Panobinostat (LBH589)	Panobinostat (LBH589) is a novel broad-spectrum HDAC inhibitor with IC50 of 5 nM. Phase 3.	404950-80-7
Entacapone	Entacapone inhibits catechol-O-methyltransferase(COMT) with IC50 of 151 nM.	130929-57-6
Alisertib (MLN8237)	Alisertib (MLN8237) is a selective Aurora A inhibitor with IC50 of 1.2 nM. It has >200-fold higher selectivity for Aurora A than Aurora B. Phase 3.	1028486-01-2
Romidepsin (FK228, Depsipeptide)	Romidepsin (FK228, depsipeptide) is a potent HDAC1 and HDAC2 inhibitor with IC50 of 36 nM and 47 nM, respectively.	128517-07-7
S-Ruxolitinib (INCB018424)	S-Ruxolitinib is the chirality of INCB018424, which is the first potent, selective, JAK1/2 inhibitor to enter the clinic with IC50 of 3.3 nM/2.8 nM, >130-fold selectivity for JAK1/2 versus JAK3. Phase 3.	941678-49-5
ZM 447439	ZM 447439 is a selective and ATP-competitive inhibitor for Aurora A and Aurora B with IC50 of 110 nM and 130 nM, respectively. It is more than 8-fold selective for Aurora A/B than MEK1, Src, Lck and has little effect againstCDK1/2/4, Plk1, Chk1, etc.	331771-20-1
VX-680 (Tozasertib, MK-0457)	VX-680 (Tozasertib, MK-0457) is a pan-Aurora inhibitor, mostly against Aurora A with Kiapp of 0.6 nM, less potent towards Aurora B/Aurora C and 100-fold more selective for Aurora A than 55 other kinases. Phase 2.	639089-54-6
Danusertib (PHA-739358)	Danusertib (PHA-739358) is an Aurora kinase inhibitor for Aurora A/B/C with IC50 of 13 nM/79 nM/61 nM, modestly potent to Abl, TrkA, c-RET and FGFR1, and less potent to Lck, VEGFR2/3, c-Kit, CDK2, etc. Phase 2.	827318-97-8

AT9283	AT9283 is a potent JAK2/3 inhibitor with IC50 of 1.2 nM/1.1 nM; also potent to Aurora A/B, Abl(T315I). Phase 1/2.	896466-04-9
Barasertib (AZD1152-HQPA)	AZD1152-HQPA (Barasertib) is a highly selective Aurora B inhibitor with IC50 of 0.37 nM, ~100 fold more selective for Aurora B over Aurora A.	722544-51-6
SNS-314 Mesylate	SNS-314 Mesylate is a potent and selective inhibitor of Aurora A, Aurora B and Aurora C with IC50 of 9 nM, 31 nM, and 3 nM, respectively. It is less potent to Trk A/B, Flt4, Fms, Axl, c-Raf and DDR2. Phase 1.	1146618-41-8
CYC116	CYC116 is a potent inhibitor of Aurora A/B with Ki of 8.0 nM/9.2 nM, is less potent to VEGFR2 (Ki of 44 nM), with 50-fold greater potency than CDKs, not active against PKA, Akt/PKB, PKC, no effect on GSK-3alpha/beta, CK2, Plk1 and SAPK2A. Phase 1.	693228-63-6
ENMD-2076	ENMD-2076 has selective activity against Aurora A and Flt3 with IC50 of 14 nM and 1.86 nM, 25-fold selective for Aurora A than over Aurora B and less potent to VEGFR2/KDR and VEGFR3, FGFR1 and FGFR2 and PDGFRalpha. Phase 2.	1291074-87-7
Aurora A Inhibitor I	Aurora A Inhibitor I is a novel, potent, and selective inhibitor of Aurora A with IC50 of 3.4 nM. It is 1000-fold more selective for Aurora A than Aurora B.	1158838-45-9
PHA-680632	PHA-680632 is potent inhibitor of Aurora A, Aurora B and Aurora C with IC50 of 27 nM, 135 nM and 120 nM, respectively. It has 10- to 200-fold higher IC50 for FGFR1, FLT3, LCK, PLK1, STLK2, and VEGFR2/3.	398493-79-3
CCT129202	CCT129202 is an ATP-competitive pan-Aurora inhibitor for Aurora A, Aurora B and Aurora C with IC50 of 0.042 uM, 0.198 uM and 0.227 uM, respectively. It is less potent to FGFR3, GSK3beta, PDGFRbeta, etc.	942947-93-5
Hesperadin	Hesperadin potently inhibits Aurora B with IC50 of 250 nM. It markedly reduces the activity of AMPK, Lck, MKK1, MAPKAP-K1, CHK1 and PHK while it does not inhibit MKK1 activity in vivo.	422513-13-1
NVP-BSK805 2HCl	NVP-BSK805 is a potent and selective ATP-competitive JAK2 inhibitor with IC50 of 0.5 nM,>20-fold selectivity towards JAK1, JAK3 and TYK2.	1092499-93-8 (free base)
KW-2449	KW-2449 is a multiple-targeted inhibitor, mostly for Flt3 with IC50 of 6.6 nM, modestly potent to FGFR1, Bcr-Abl and Aurora A; little effect on PDGFR?, IGF-1R, EGFR. Phase 1.	1000669-72-6
LY2784544	LY2784544 is a potent JAK2 inhibitor with IC50 of 3 nM, effective in JAK2V617F, 8- and 20-fold selective versus JAK1 and JAK3. Phase 2.	1229236-86-5
AZ 960	AZ 960 is a novel ATP competitive JAK2 inhibitor with IC50 and Ki of <3 nM and 0.45 nM, 3-fold selectivity of AZ960 for JAK2 over JAK3.	905586-69-8
CYT387	CYT387 is an ATP-competitive inhibitor of JAK1/JAK2 with IC50 of 11 nM/18 nM, ~10-fold selectivity versus JAK3. Phase 1/2.	1056634-68-4
Tofacitinib (CP-690550,Tasocitinib)	Tofacitinib citrate (CP-690550 citrate) is a novel inhibitor of JAK3 with IC50 of 1 nM, 20- to 100-fold less potent against JAK2 and JAK1.	540737-29-9

TAK-901	TAK-901 is a novel inhibitor of Aurora A/B with IC50 of 21 nM/15 nM. It is not a potent inhibitor of cellular JAK2, c-Src or Abl. Phase 1.	934541-31-8
TG101209	TG101209 is a selective JAK2 inhibitor with IC50 of 6 nM, less potent to Flt3 and RET with IC50 of 25 nM and 17 nM, ~30-fold selective for JAK2 than JAK3, sensitive to JAK2V617F and MPLW515L/K mutations.	936091-14-4
AMG-900	AMG 900 is a potent and highly selective pan-Aurora kinases inhibitor for Aurora A/B/C with IC50 of 5 nM/4 nM /1 nM. It is >10-fold selective for Aurora kinases > p38>Tyk2>JNK2>Met>Tie2. Phase 1.	945595-80-2
MLN8054	MLN8054 is a potent and selective inhibitor of Aurora A with IC50 of 4 nM. It is more than 40-fold selective for Aurora A than Aurora B. Phase 1.	869363-13-3
Baricitinib (LY3009104, INCB028050)	Baricitinib is a selective JAK1 and JAK2 inhibitor with IC50 of 5.9 nM and 5.7 nM, ~70 and ~10-fold selective versus JAK3 and Tyk2, no inhibition to c-Met and Chk2. Phase 3.	1187594-09-7
TG101348 (SAR302503)	TG-101348 (SAR302503) is a selective inhibitor of JAK2 with IC50 of 3 nM, 35- and 334-fold more selective for JAK2 versus JAK1 and JAK3. Phase 1/2.	936091-26-8
MK-5108 (VX-689)	MK-5108 (VX-689) is a highly selective Aurora A inhibitor with IC50 of 0.064 nM and is 220- and 190-fold more selective for Aurora A than Aurora B/C, while it inhibits TrkA with less than 100-fold selectivity. Phase 1.	1010085-13-8
CCT137690	CCT137690 is a highly selective inhibitor of Aurora A, Aurora B and Aurora C with IC50 of 15 nM, 25 nM and 19 nM. It has little effect on hERG ion-channel.	1095382-05-0
CEP-33779	CEP33779 is a selective JAK2 inhibitor with IC50 of 1.8 nM, >40- and >800-fold versus JAK1 and TYK2.	1257704-57-6
FG-4592	FG-4592 is an HIF alpha prolyl hydroxylase inhibitor, stabilizes HIF-2 and induces EPO production. Phase 2/3.	808118-40-3
CUDC-907	CUDC-907 is a dual PI3K and HDAC inhibitor for PI3K? and HDAC1/2/3/10 with IC50 of 19 nM and 1.7 nM/5 nM/1.8 nM/2.8 nM, respectively. Phase 1.	1339928-25-4
Olaparib (AZD2281, Ku-0059436)	Olaparib (AZD2281, KU0059436) is a selective inhibitor of PARP1/2 with IC50 of 5 nM/1 nM, 300-times less effective against tankyrase-1. Phase 1/2.	763113-22-0
IOX2	IOX2 is a potent inhibitor of HIF-1alpha prolyl hydroxylase-2 (PHD2) with IC50 of 21 nM, >100-fold selectivity over JMJD2A, JMJD2C, JMJD2E, JMJD3, or the 2OG oxygenase FIH.	931398-72-0
Veliparib (ABT-888)	Veliparib (ABT-888) is a potent inhibitor of PARP1 and PARP2 with Ki of 5.2 nM and 2.9 nM, respectively. It is inactive to SIRT2. Phase 1/2.	912444-00-9
AR-42	AR-42 is an HDAC inhibitor with IC50 30 nM.	935881-37-1
Iniparib (BSI-201)	BSI-201 (Iniparib, SAR240550) is a PARP1 inhibitor with demonstrated effectiveness in triple-negative breast cancer (TNBC). Phase 3.	160003-66-7

PCI-24781 (Abexinostat)	PCI-24781 is a novel pan-HDAC inhibitor mostly targeting HDAC1 with Ki of 7 nM, modest potent to HDACs 2, 3, 6, and 10 and greater than 40-fold selectivity against HDAC8. Phase 1/2.	783355-60-2
LAQ824 (Dacinostat)	LAQ824 (Dacinostat) is a novel HDAC inhibitor with IC50 of 32 nM and is known to activate the p21 promoter.	404951-53-7
Quisinostat (JNJ-26481585)	JNJ-26481585 is a novel second-generation HDAC inhibitor with highest potency for HDAC1 with IC50 of 0.11 nM, modest potent to HDACs 2, 4, 10, and 11; greater than 30-fold selectivity against HDACs 3, 5, 8, and 9 and lowest potency to HDACs 6 and 7. Phase 2.	875320-29-9
Rucaparib (AG-014699,PF-01367338)	Rucaparib (AG-014699, PF-01367338) is an inhibitor of PARP with Ki of 1.4 nM for PARP1, also showing binding affinity to eight other PARP domains. Phase 1/2.	459868-92-9
SRT1720	SRT1720 is a selective SIRT1 activator with EC50 of 0.16 uM, but is >230-fold less potent for SIRT2 and SIRT3.	1001645-58-4
CUDC-101	CUDC-101 is a potent multi-targeted inhibitor against HDAC, EGFR and HER2 with IC50 of 4.4 nM, 2.4 nM, and 15.7 nM, and inhibits class I/II HDACs, but not class III, Sir-type HDACs. Phase 1.	1012054-59-9
MC1568	MC1568 is a selective HDAC inhibitor for maize HD1-A with IC50 of 100 nM. It is 34-fold more selective for HD1-A than HD1-B.	852475-26-4
Pracinostat (SB939)	SB939 is a potent pan-HDAC inhibitor with IC50 of 40-140 nM with exception for HDAC6. It has no activity against the class III isoenzyme SIRT I. Phase 2.	929016-96-6
Givinostat (ITF2357)	Givinostat (ITF2357) is a potent HDAC inhibitor for HDAC2, HDAC1B and HDAC1A with IC50 of 10 nM, 7.5 nM and 16 nM. Phase 1/2.	732302-99-7
AG-14361	AG14361 is a potent inhibitor of PARP1 with Ki of <5 nM. It is at least 1000-fold more potent than the benzamides.	328543-09-5
SGI-1776 free base	SGI-1776 is a novel ATP competitive inhibitor of Pim1 with IC50 of 7 nM, 50- and 10-fold selective versus Pim2 and Pim3, also potent to Flt3 and haspin. Phase 1.	1025065-69-3
Tubastatin A HCl	Tubastatin A is a potent and selective HDAC6 inhibitor with IC50 of 15 nM. It is selective (1000-fold more) against all other isozymes except HDAC8 (57-fold more).	1310693-92-5
PCI-34051	PCI-34051 is a potent and specific HDAC8 inhibitor with IC50 of 10 nM. It has greater than 200-fold selectivity over HDAC1 and 6, more than 1000-fold selectivity over HDAC2, 3, and 10.	950762-95-5
PFI-1 (PF-6405761)	PFI-1 is a selective BET (bromodomain-containing protein) inhibitor for BRD4 with IC50 of 0.22 uM.	1403764-72-6
Sodium Phenylbutyrate	Sodium Phenylbutyrate is a transcriptional regulators that act by altering chromatin structure via the modulation of HDAC activity.	1716-12-7
AZD2461	AZD2461 is a novel PARP inhibitor with low affinity for Pgp than Olaparib. Phase 1.	1174043-16-3
Resminostat	Resminostat dose-dependently and selectively inhibits HDAC1/3/6 with IC50 of 42.5 nM/50.1 nM/71.8 nM, less potent to HDAC8 with IC50 of 877 nM.	864814-88-0

I-BET151 (GSK1210151A)	I-BET151 (GSK1210151A) is a novel selective BET inhibitor for BRD2, BRD3 and BRD4 with IC50 of 0.5 uM, 0.25 uM, and 0.79 uM, respectively.	1300031-49-5
AZD1480	AZD1480 is a novel ATP-competitive JAK2 inhibitor with IC50 of 0.26 nM, selectivity against JAK3 and Tyk2, and to a smaller extent against JAK1. Phase 1.	935666-88-9
XL019	XL019 is a potent and selective JAK2 inhibitor with IC50 of 2.2 nM, exhibiting >50-fold selectivity over JAK1, JAK3 and TYK2. Phase 1.	945755-56-6
Tubacin	Tubacin is a highly potent and selective, reversible, cell-permeable HDAC6 inhibitor with an IC50 of 4 nM, approximately 350-fold selectivity over HDAC1.	537049-40-4
ZM 39923 HCl	ZM 39923 is an JAK1/3 inhibitor with pIC50 of 4.4/7.1, almost no activity to JAK2 and modestly potent to EGFR; also found to be sensitive to transglutaminase.	1021868-92-7
3-Deazaneplanocin A (DZNeP)	3-deazaneplanocin A (DZNeP), an analog of adenosine, is a competitive inhibitor of S-adenosylhomocysteine hydrolase with Ki of 50 pM.	120964-45-6
SMI-4a	SMI-4a is a potent inhibitor of Pim1 with IC50 of 17 nM, modest potent to Pim-2, does not significantly inhibit other serine/threonine- or tyrosine-kinases.	438190-29-5
(+)-JQ1	(+)-JQ1 is a BET bromodomain inhibitor, with IC50 of 77 nM/33 nM for BRD4(1/2), binding to all bromodomains of the BET family, but not to bromodomains outside the BET family.	1268524-70-4
BMN 673	BMN 673 is a novel PARP inhibitor with IC50 of 0.58 nM. It is also a potent inhibitor of PARP-2, but does not inhibit PARG and is highly sensitive to PTEN mutation. Phase 1.	1207456-01-6
Pacritinib (SB1518)	Pacritinib (SB1518) is a potent and selective inhibitor of Janus Kinase 2 (JAK2) and Fms-Like Tyrosine Kinase-3 (FLT3) with IC50s of 23 and 22 nM, respectively.	937272-79-2
Rocilinostat (ACY-1215)	Rocilinostat (ACY-1215) is a selective HDAC6 inhibitor with IC50 of 5 nM. It is >10-fold more selective for HDAC6 than HDAC1/2/3 (class I HDACs) with slight activity against HDAC8, minimal activity against HDAC4/5/7/9/11, Sirtuin1, and Sirtuin2.	1316214-52-4
UPF 1069	UPF 1069 is a selective PARP2 inhibitor with IC50 of 0.3 ?M. It is ~27-fold selective against PARP1.	1048371-03-4
EPZ5676	EPZ-5676 is an S-adenosyl methionine (SAM) competitive inhibitor of protein methyltransferase DOT1L with Ki of 80 pM, demonstrating >37,000-fold selectivity against all other PMTs tested, inhibits H3K79 methylation in tumor. Phase 1.	1380288-87-8
GSK J4 HCl	GSK J4 HCl is a cell permeable prodrug of GSK J1, which is the first selective inhibitor of the H3K27 histone demethylase JMJD3 and UTX with IC50 of 60 nM and inactive against a panel of demethylases of the JMJ family.	1797983-09-5
EPZ004777	EPZ004777 is a potent, selective DOT1L inhibitor with IC50 of 0.4 nM.	1338466-77-5

Bromosporine	Bromosporine is a broad spectrum inhibitor for bromodomains with IC50 of 0.41 uM, 0.29 uM, 0.122 uM and 0.017 uM for BRD2, BRD4, BRD9 and CECR2, respectively.	1619994-69-2
Lomeguatrib	Lomeguatrib is a potent inhibitor of O6-alkylguanine-DNA-alkyltransferase with IC50 of 5 nM.	192441-08-0
I-BET-762	I-BET-762 is an inhibitor for BET proteins with IC50 of ~35 nM, suppresses the production of proinflammatory proteins by macrophages and blocks acute inflammation, highly selective over other bromodomain-containing proteins.	1260907-17-2
RGFP966	RGFP966 is an HDAC3 inhibitor with IC50 of 0.08 uM, exhibits > 200-fold selectivity over other HDAC.	1396841-57-8
SGC 0946	SGC 0946 is a highly potent and selective DOT1L methyltransferase inhibitor with IC50 of 0.3 nM, is inactive against a panel of 12 PMTs and DNMT1.	1561178-17-3
SGI-1027	SGI-1027 is a DNMT inhibitor with IC50 of 6, 8, 7.5 uM for DNMT1, DNMT3A, and DNMT3B	1020149-73-8
EPZ-6438	EPZ-6438 is a potent, and selective EZH2 inhibitor with Ki and IC50 of 2.5 nM and 11 nM, exhibiting a 35-fold selectivity versus EZH1 and >4,500-fold selectivity relative to 14 other HMTs.	1403254-99-8
RVX-208	RVX-208 is a potent BET bromodomain inhibitor with IC50 of 0.510 ?M for BD2, about 170-fold selectivity over BD1. Phase 2.	1044870-39-4
MM-102	MM-102 is a high-affinity peptidomimetic MLL1 inhibitor with IC50 of 0.4 uM.	1417329-24-8
RG2833 (RGFP109)	RG2833 (RGFP109) is a brain-penetrant HDAC inhibitor with IC50 of 60 nM and 50 nM for HDAC1 and HDAC3, respectively.	1215493-56-3
SGC-CBP30	SGC-CBP30 is a potent CREBBP/EP300 inhibitor with IC50 of 21 nM and 38 nM, respectively.	1613695-14-9
ME0328	ME0328 is a potent and selective PARP inhibitor with IC50 of 0.89 uM for PARP3, about 7-fold selectivity over PARP1.	1445251-22-8
UNC669	UNC669 is a potent and selective MBT (malignant brain tumor) inhibitor with IC50 of 6 uM for L3MBTL1, 5- and 11-fold selective over L3MBTL3 and L3MBTL4.	1314241-44-5
OTX015	OTX015 is a potent BET bromodomain inhibitor with EC50 ranging from 10 to 19 nM for BRD2, BRD3, and BRD4. Phase 1.	202590-98-5
Nexturastat A	Nexturastat A is a potent and selective HDAC6 inhibitor with IC50 of 5 nM, >190-fold selectivity over other HDACs.	1403783-31-2
OG-L002	OG-L002 is a potent and specific LSD1 inhibitor with IC50 of 20 nM, exhibiting 36- and 69-fold selectivity over MAO-B and MAO-A, respectively.	1357302-64-7
C646	C646 is an inhibitor for histone acetyltransferase, and inhibits p300 with a Ki of 400 nM. Preferentially selective for p300 versus other acetyltransferases.	328968-36-1

UNC1215	UNC1215 is a potent and selective MBT (malignant brain tumor) antagonist, which binds L3MBTL3 with IC50 of 40 nM and Kd of 120 nM, 50-fold selective versus other members of the human MBT family.	1415800-43-9
IOX1	IOX1 is a potent and broad-spectrum inhibitor of 2OG oxygenases, including the JmjC demethylases.	5852-78-8
AZD1208	AZD1208 is a potent, and orally available Pim kinase inhibitor with IC50 of 0.4 nM, 5 nM, and 1.9 nM for Pim1, Pim2, and Pim3, respectively. Phase 1.	1204144-28-4
CX-6258 HCl	CX-6258 HCl is a potent, orally efficacious pan-Pim kinase inhibitor with IC50 of 5 nM, 25 nM and 16 nM for Pim1, Pim2, and Pim3, respectively.	1353859-00-3
CPI-203	CPI-203 is a potent BET bromodomain inhibitor with IC50 of 37 nM for BRD4.	1446144-04-2
TMP269	TMP269 is a potent, selective class IIa HDAC inhibitor with IC50 of 157 nM, 97 nM, 43 nM and 23 nM for HDAC4, HDAC5, HDAC7 and HDAC9, respectively.	1314890-29-3
Filgotinib (GLPG0634)	Filgotinib (GLPG0634) is a selective JAK1 inhibitor with IC50 of 10 nM, 28 nM, 810 nM, and 116 nM for JAK1, JAK2, JAK3, and TYK2, respectively. Phase 2.	1206161-97-8
Isoliquiritigenin	A flavonoid found in licorice root that displays antioxidant, anti-inflammatory, and antitumor activities; induces quinone reductase-1 with a concentration required to double activity of 1.8 µM in mouse hepatoma cells	961-29-5
Ellagic Acid	A polyphenolic antioxidant that is abundant in many fruits, vegetables, plant bark, and peels; has anti-carcinogenic, anti-mutagenic, anti-inflammatory, and organ-preserving properties; blocks methylation of H3R17 by CARM1 without significantly altering histone acetylase or DNA methyltransferase activity	476-66-4
Sodium Butyrate	A short chain fatty acid that inhibits HDACs, induces growth arrest, differentiation and apoptosis in cancer cells, and suppresses inflammation by reducing the expression of pro-inflammatory cytokines	156-54-7
Etoposide	An inhibitor of topoisomerase II (IC50 = 60.3 µM); can have much greater potencies when evaluated in cell-based cytotoxicity assays (e.g., IC50 = 5.14 nM for MCF-7 cells); can also inhibit nuclear receptor coactivator 3 (IC50 of 2.48 µM)	33419-42-0
Tenovin-1	A small molecule activator of p53 that decreases the growth of BL2 Burkitt's lymphoma and ARN8 melanoma cells; inhibits the deacetylase activity of purified human SIRT1 and SIRT2	380315-80-0
Gemcitabine	A nucleoside analog that arrests tumor growth and induces apoptosis by inhibiting DNA replication and repair; inhibits repair-mediated DNA demethylation inducing epigenetic gene silencing and has broad antiretroviral activity	95058-81-4

CPTH2 (hydrochloride)	Specifically inhibits Gcn5-dependent acetylation of histone H3K14 at a concentration of 0.8 mM both in vitro and in vivo	357649-93-5
UNC0638	A potent, selective G9a and GLP HMTase inhibitor (IC50s = <15 and 19 nM, respectively); inhibits H3K9 dimethylation in MDA-MB231 cells (IC50 = 81 nM) and demonstrates favorable separation of functional and toxic effects	1255580-76-7
Phthalazinone pyrazole	A potent inhibitor of Aurora A kinase (IC50 = 31 nM); does not inhibit Aurora B kinase at doses up to 100 µM; inhibits the proliferation of HCT116, Colo205, and MCF-7 cells (IC50 = 7.8, 2.9, and 1.6 µM, respectively)	88048-62-7
4-iodo-SAHA	A hydrophobic derivative of the class I and class II HDAC inhibitor SAHA that demonstrates >60% inhibition of HDAC1 and HDAC6 activity in a deacetylase activity assay; inhibits proliferation of SK-BR-3 breast-derived, HT29 colon-derived, and U937 leukemia cell lines with EC50 values of 1.1, 0.95, and 0.12 µM, respectively	1219807-87-0
UNC0321 (trifluoroacetate salt)	A potent and selective G9a HMTase inhibitor (IC50 = 6 nM; Ki = 63 pM); more than 40,000-fold selective for G9a over SET7/9, SET8, PRMT3, and JMJD2E	1238673-32-9
(-)-Neplanocin A	Potently and irreversibly inactivates SAH hydrolase (Ki = 8.39 nM); has antitumor activity against mouse leukemia L1210 cells and broad-spectrum antiviral activity	72877-50-0
Cl-Amidine (trifluoroacetate)	An inhibitor of PAD4 deimination activity (IC50 = 5.9 µM) that also inhibits PAD1 and PAD3 (IC50 = 0.8 and 6.2 µM, respectively); dose dependently decreases the citrulline content in serum and joints and reduces the development of IgG autoantibodies in a CIA mouse model of inflammatory arthritis	913723-61-2
F-Amidine (trifluoroacetate salt)	Inhibits PAD4 activity (IC50 = 21.6 µM) as well as PAD1 and PAD3 activity (IC50s = 29.5 and 350 µM, respectively); cytotoxic to HL-60, MCF-7, and HT-29 cancer cell lines (IC50s = 0.5, 0.5 and 1 µM, respectively)	877617-46-4
JGB1741	A SIRT1-specific inhibitor (IC50 = 15 µM); inhibits metastatic breast cancer MDA-MB 231 cell proliferation (IC50 = 512 nM), dose-dependently increasing p53 acetylation and p53-mediated apoptosis in these cells	1256375-38-8
CCG-100602	Inhibits RhoA/C-mediated, SRF-driven luciferase expression in PC3 prostate cancer cells with an IC50 value of 9.8 µM	1207113-88-9
CAY10669	An inhibitor of the HAT PCAF (p300/CREB-binding protein-associated factor; IC50 = 662 µM), displaying a 2-fold improvement in inhibitory potency over anacardic acid; dose dependently inhibits histone H4 acetylation in HepG2 cells in vitro at 30-60 µM	1243583-88-1
Delphinidin (chloride)	A natural plant pigment which induces the release of nitric oxide by vascular endothelium, causing vasorelaxation; inhibits signaling through EGFRs, suppressing the expression of ERa and inducing both apoptosis and autophagy at a dose of 1-40 µM; inhibits the HAT activities of p300/CBP (IC50 = ~ 30 µM)	528-53-0

MI-2 (hydrochloride)	Potently binds menin, blocks the menin-MLL fusion protein interaction (IC50 = 0.45 µM), and induces apoptosis in cells expressing MLL fusion proteins	1271738-62-5
MI-nc (hydrochloride)	A weak inhibitor of the menin-MLL fusion protein interaction (IC50 = 193 µM), intended as a negative control compound for tests involving MI-2	1359873-45-2
Octyl-.alpha.-ketoglutarate	A stable, cell-permeable form of a-ketoglutarate which accumulates rapidly and preferentially in cells with a dysfunctional TCA cycle; stimulates PHD activity and increases HIF-1a turnover when used at 1 mM; competitively blocks succinate- or fumarate-mediated inhibition of PHD	876150-14-0
Daminozide	A selective inhibitor of the human 2-oxoglutarate (JmjC) histone demethylases KDM2A, PHF8, and KDM7A (IC50s = 1.5, 0.55, and 2.1 µM, respectively)	1596-84-5
GSK-J1 (sodium salt)	A potent, cell impermeable inhibitor of the H3K27 histone demethylases JMJD3 and UTX (IC50s = 18 and 56 µM, respectively as measured by mass spectrometry; IC50 = 60 nM in JMJD3 antibody-based assays)	1373422-53-7
GSK-J2 (sodium salt)	A pyridine regio-isomer of GSK-J1 which poorly inhibits JMJD3 (IC50 > 100 µM), making it an appropriate negative control for in vitro studies involving GSK-J1	1394854-52-4
GSK-J5 (hydrochloride)	A pyridine regio-isomer of the JMJD3 inhibitor GSK-J4; cell-permeable and hydrolyzed to a free base, which is a weak inhibitor of JMJD3 (IC50 > 100 µM), making it an ideal negative control molecule	1797983-32-4
HC Toxin	A cell-permeable, reversible inhibitor of HDACs (IC50 = 30 nM)	83209-65-8
(+)-Abscisic Acid	A plant hormone with diverse roles in disease resistance, plant development, and response to stresses; regulates gene expression and may contribute to epigenetic changes at the chromatin level	21293-29-8
4-pentynoyl-Coenzyme A (trifluoroacetate salt)	An acyl-CoA donor that can be metabolically transferred onto lysine residues of proteins by lysine acetyltransferases; an azide-alkyne bioconjugation reaction, known as click chemistry, can then be used to tag the acetylated proteins with fluorescent or biotinylated labels for subsequent analysis	50347-32-5
coumarin-SAHA	A fluorescent probe that competitively binds HDAC; demonstrates fluorescence excitation and emission maxima of 325 and 400 nm, respectively, which is quenched by 50% when bound to HDAC	1260635-77-5
SAHA-BPyne	A SAHA derivative with a benzophenone crosslinker and an alkyne tag to be used for profiling HDAC activities in proteomes and live cells; labels HDAC complex proteins both in proteomes at 100 nM and in live cells at 500 nM; IC50 = ~3 µM for inhibition of HDAC activity in HeLa cell nuclear lysates in an HDAC activity assay	930772-88-6
UNC0631	A potent and selective inhibitor of G9a activity in vitro (IC50 = 4 nM) and G9a/GLP-mediated dimethylation of histone 3 on lysine 9 in MDA-MB-231 cells (IC50 = 25 nM)	1320288-19-4

UNC0646	A potent and selective inhibitor of G9a and GLP activities in vitro (IC50s = 6 and 15 nM, respectively) and G9a/GLP-mediated dimethylation of histone 3 on lysine 9 in MDA-MB-231 cells (IC50 = 26 nM)	1320288-17-2
GSK4112?	A synthetic agonist for REV-ERBa (EC50 = 0.4 μM) that mimics the action of heme; at 10 μM inhibits the expression of the circadian target gene bmal1 and reduces glucose output by 30% in mouse primary hepatocytes by repressing the expression of several gluconeogenic genes	1216744-19-2
Lestaurtinib	A staurosporine analog that potently inhibits JAK2 kinase (IC50 = 1 nM) and downstream targets STAT5 (IC50 = 10-30 nM) and STAT3 in a human erythroleukemic cell line expressing the JAK2V617F mutation; potently inhibits the epigenetic kinase PRK1 (PKN1) in vitro (IC50 = 8.6 nM)	111358-88-4
Tenovin-6	A analog of tenovin-1; elevates p53 activity in MCF-7 cells at 10 μM and reduces growth of ARN8 melanoma xenograft tumors in SCID mice at a dose of 50 mg/kg	1011557-82-6
Chaetocin	A fungal mycotoxin that inhibits the Lys9-specific histone methyltransferases SU(VAR)3-9 (IC50 = 0.8 μM), G9a (IC50 = 2.5 μM), and DIM5 (IC50 = 3 μM)	28097-03-2
CBHA	HDAC1 and HDAC3 inhibitor (ID50 = 0.01 and 0.07 μM, respectively, in vitro); induces apoptosis in nine different neuroblastoma cell lines in culture (0.5-4.0 μM) and completely suppresses neuroblastoma tumor growth in SCID mice at 200 mg/kg	174664-65-4
Mirin	An inhibitor of the DNA damage sensor MRN, inhibiting MRN-dependent phosphorylation of histone H2AX (IC50 = 66 μM); prevents activation of ATM by blocking the nuclease activity of Mre11; induces G2 arrest, abolishes the radiation-induced G2/M checkpoint, and prevents homology-directed repair of DNA damage	299953-00-7
6-Thioguanine	A thio analog of the purine base guanine that incorporates into DNA during replication, inducing double-strand breaks that destabilize its structure and result in cytotoxicity; used as a chemotherapeutic for acute leukemia and other types of cancer, including BRCA2-mutated tumors	154-42-7
SIRT1/2 Inhibitor IV	A cell-permeable inhibitor of SIRT1 (IC50 = 56 μM) and SIRT2 (IC50 = 59 μM); less effectively inhibits SIRT5 (IC50 >300 μM) and has no effect on class I and II HDACs; sensitizes H460 lung cancer cells to etoposide and paclitaxel; blocks a SIRT1-dependent hypoxic response in vivo	14513-15-6
CAY10591	An activator of SIRT1 that decreases TNF-a levels from 325 pg/ml (control) to 104 and 53 pg/ml at 20 and 60 μM, respectively; exhibits a significant dose-dependent effect on fat mobilization in differentiated adipocytes	839699-72-8
S-Adenosylhomocysteine	An amino acid derivative and an intermediate, by-product, or modulator of several metabolic pathways, including the activated methyl cycle and cysteine biosynthesis; also a product of SAM-	979-92-0

	dependent methylation of biological molecules, including DNA, RNA, and histones, and other proteins	
HNHA	A cell-permeable inhibitor of HDAC activity (IC50 = 100 nM)	926908-04-5
2-Hydroxyglutaric Acid (sodium salt)	An a-hydroxy acid, overproduced in 2-hydroxyglutaric aciduria; mutations in IDH1 and IDH2 cause these enzymes to convert isocitrate to 2-hydroxyglutarate; competitively inhibits a-ketoglutarate-dependent dioxygenases, including lysine demethylases and DNA hydroxylases	40951-21-1
3,3'-Diindolylmethane	Phytochemical from cruciferous vegetables that demonstrates anticancer and chemopreventative effects (10-30 µM) involving the induction of Phase 2 enzymes, promotion of apoptosis, induction of cell cycle arrest, inhibition of cell proliferation, and inhibition of histone deacetylases and DNA methylation activities	5/4/1968
S-(5'-Adenosyl)-L-methionine chloride (hydrochloride)	A ubiquitous methyl donor involved in a wide variety of biological reactions, including those mediated by DNA and protein methyltransferases A stable salt of SAM that is included in nutritional supplements for oral use; reportedly ameliorates depression, pain associated with osteoarthritis and fibromyalgia, and liver toxicity	86867-01-8
Pimelic Diphenylamide 106	A slow, tight-binding inhibitor of class I HDACs, progressively binding HDACs and remaining bound after wash-out; inhibits class I HDACs (IC50 = 150, 760, 370, and 5,000 nM for HDAC1, 2, 3, and 8, respectively) but not class II HDACs (IC50 > 180 µM for HDAC4, 5, and 7)	937039-45-7
2',3',5'-triacetyl-5-Azacytidine	A prodrug form of 5-azacytidine, an inhibitor of DNA methyltransferaes, that may reverse epigenetic changes	10302-78-0
UNC0224	A potent and selective G9a HMTase inhibitor (IC50 = 15 nM, Kd = 23 mM); more than 1,000-fold selective for G9a over SET7/9 and SET8	1197196-48-7
Sinefungin	A nucleoside structurally related to SAH and SAM that inhibits SET domain-containing methyltransferases (IC50 values range from 0.1-20 µM)	58944-73-3
Pyroxamide	An inhibitor of HDAC, including HDAC1 (IC50 = 0.1-0.2 µM); induces growth suppression and cell death of certain types of cancer cells in culture	382180-17-8
WDR5-0103	A small molecule that binds a peptide-binding pocket on WDR5 (Kd = 450 nM), inhibiting the catalytic activity of the MLL core complex in vitro (IC50 = 39 µM)	890190-22-4
AMI-1 (sodium salt)	A cell permeable inhibitor of PRMTs; inhibits both yeast Hmt1p and human PRMT1 (IC50 = 3.0 and 8.8 µM, respectively); also effectively blocks the activity of PRMTs 3, 4, and 6 but not that of lysine methyltransferases; inhibits HIV-1 reverse transcriptase (IC50 = 5.0 µM)	20324-87-2

GSK343	A selective, cell-permeable EZH2 inhibitor (IC50 = 4 nM) that has been shown to inhibit the trimethylation of H3K27 in HCC1806 cells with an IC50 value of 174 nM	1346704-33-3
I-CBP112 (hydrochloride)	A selective inhibitor of CBP and EP300 which directly binds their bromodomains (Kds = 0.142 and 0.625 µM); shows only weak cross reactivity with the bromodomains of BET proteins and shows no interaction with other bromodomains	1640282-31-0
UNC1999	A selective, cell-permeable EZH2 inhibitor (IC50 = 2 nM) that has been shown to inhibit H3K27methylation in MCF10A cells with an IC50 value of 124 nM	1431612-23-5
PFI-3	Binds avidly and selectively to the structurally-similar bromodomains of SMARCA4 and PB1(domain 5) with Kd values of 89 and 48 nM, respectively; also interacts with the bromodomain of SMARCA2; does not interact with other bromodomains or with a panel of kinases	1819363-80-8
2,4-DPD	A cell permeable, competitive inhibitor of HIF-PH with effective concentrations in the low µM range	41438-38-4
DMOG	A cell permeable, competitive inhibitor of HIF-1a prolyl hydroxylase; stabilizes HIF-1a expression at normal oxygen tensions in cultured cells at concentrations between 0.1 and 1 mM	89464-63-1
CAY10398	An inhibitor of HDAC (IC50 = 10 µM)	193551-00-7
RSC-133	Promotes the reprogramming of human somatic cells to pluripotent stem cells; increases the number of human foreskin fibroblasts that express alkaline phosphatase when used at 10 µM with four standard reprogramming factors; down-regulates inducers of cellular senescence and inhibits Dnmt1 and HDAC1	1418131-46-0
N-Oxalylglycine	A cell permeable inhibitor of a-ketoglutarate-dependent enzymes, including JMJD2A, JMJD2C, and JMJD2E (IC50s = 250, 500, and 24 µM, respectively); inhibits the prolyl hydroxylase domain-containing proteins PHD1 and PHD2 with IC50 values of 2.1 and 5.6 µM, respectively	5262-39-5
Chidamide	An HDAC inhibitor that increases histone H3 acetylation levels in LoVo and HT-29 colon cancer cells at concentrations as low as 4 µM; dose-dependently decreases the activation of several oncogenic signaling kinases and induces cell cycle arrest in colon cancer cells	743420-02-2
EPZ005687	A potent, selective inhibitor of the lysine methyltranferase EZH2 (Ki = 24 nM), the enzymatic subunit of PRC2; blocks trimethylation of the PRC2 target H3K27 (IC50 = 80 nM), decreasing the proliferation of lymphoma cells carrying mutant, but not wild-type, EZH2	1396772-26-1
AK-7	A cell- and brain-permeable inhibitor of SIRT2 (IC50 = 15.5 µM); dimishes neuronal cell death induced by mutant huntingtin fragment in culture; down-regulates cholesterol biosynthetic gene expression and reduces total cholesterol levels in neurons in vivo	420831-40-9

UNC0642	A selective inhibitor of G9a and GLP methyltransferases that competitively inhibits binding of H3K9 substrates with a Ki = 3.7 nM; reduces H3K9 dimethylation levels in MDA-MB-231 and PANC-1 cells (IC50s = 110 and 40 nM, respectively); displays improved pharmacokinetic properties relative to UNC0638	1481677-78-4
(R)-PFI-2 (hydrochloride)	A potent, cell-permeable inhibitor of SET7/9 (IC50 = 2 nM) that demonstrates greater than 1,000-fold selectivity over a panel of 18 other methyltransferases	1627607-87-7
HPOB	A potent, selective inhibitor of HDAC6 (IC50 = 56 nM); induces acetylation of a-tubulin but not histones; enhances the cytotoxicity of the broad spectrum HDAC inhibitor SAHA against cancer cells in nude mice carrying an androgen-dependent CWR22 human prostate cancer xenograft	1429651-50-2
2-hexyl-4-Pentynoic Acid	Inhibits HDAC activity much more potently (IC50 = 13 µM) than valproic acid (IC50 = 398 µM); induces histone hyperacetylation in cerebellar granule cells significantly at 5 µM; induces the expression of Hsp70-1a and Hsp70-1b and protects cerebellar granule cells from glutamate-induced excitotoxicity	96017-59-3
JIB-04	A pyridine hydrazone that broadly inhibits Jumonji histone demethylases (IC50 values are 230, 340, 435, 445, 855, and 1100 nM for JARID1A, JMJD2E, JMJD2B, JMJD2A, JMJD3 and JMJD2C, respectively); inhibits Jumonji demethylase activity, alters gene expression, and blocks viability of cancer cells both in vitro and in vivo	199596-05-9
CAY10683	A potent HDAC inhibitor that inhibits HDAC2 and HDAC6 with IC50 values of 0.119 and 434 nM; ineffective against HDAC4 (IC50 = >1,000 nM); inhibits the growth of HCT-116 cells and HuT-78 cells (GI50 = 29.4 and 1.4 µM, respectively) more effectively than human dermal fibroblasts (GI50 = >100 µM)	1477949-42-0
GSK 126	A selective, SAM-competitive small molecule inhibitor of EZH2 methyltransferase activity (Ki = 0.57 nM; IC50 = 9.9 nM versus that of EZH1: Ki = 89 nM; IC50 = 680 nM); inhibits global H3K27me3 levels, inhibiting the proliferation of EZH2 mutant DLBCL cell lines (IC50 = 28-61 nM) as well as the growth of EZH2 mutant DLBCL xenografts in mice receiving a daily dose of 50 mg/kg	1346574-57-9
MS-436	A potent BRD4 bromodomain inhibitor that binds BD1 more avidly than BD2 (Ki values are 30-50 nM for BD1 and 340 nM for BD2); also binds BD1 and BD2 of BRD3 (Kis = 100 and 140 nM, respectively) as well as bromodomains of other BET and non-BET proteins with low micromolar affinities	1395084-25-9
5-Methylcytidine	A modified nucleoside derived from 5-methylcytosine and is a minor constituent of RNA as well as DNA for certain organisms; used in epigenetics research, especially in studies involving DNA methylation processes	2140-61-6
AGK7	An inactive control to be used in experiments with AGK2; has IC50 values greater than 50 µM on SIRT1 and SIRT2 and greater than 5 µM on SIRT3	304896-21-7

5-Methyl-2'-deoxycytidine	A pyrimidine nucleoside used in epigenetics research to investigate the dynamics of DNA methylation pattern in the control of gene expression	838-07-3
B32B3	A cell-permeable, ATP-competitive inhibitor of VprBP that blocks phosphorylation of histone 2A at Thr120 in DU-145 human prostate cancer cells (IC50 = 500 nM); strongly suppresses the proliferation of DU-145 cells, which overexpress VprBP, both in vitro and in xenograft tumors in mice	294193-86-5
GSK-LSD1 (hydrochloride)	An irreversible, mechanism-based inhibitor of LSD1 (IC50 = 16 nM); induces gene expression changes in various cancer cell lines, inhibiting their proliferation (EC50s <5 nM)	1431368-48-7
AZ 505	A potent inhibitor of SMYD2 (IC50 = 0.12 µM) that is without effect on a panel of other protein lysine methyltransferases	1035227-43-0
BRD73954	A small molecule inhibitor that potently and selectively inhibits both HDAC6 and HDAC8 (IC50s = 36 and 120 nM, respectively)	1440209-96-0
CPI-360	CPI-360 is a potent, selective,and SAM-competitive EZH1 inhibitor with IC50 of 102.3 nM, >100-fold selectivity over other methyltransferases.	1802175-06-9
Remodelin	Remodelin is a potent acetyl-transferase NAT10 inhibitor.	1622921-15-6
UNC0379	UNC0379 is a selective, substrate competitive inhibitor of N-lysine methyltransferase SETD8 with IC50 of 7.9 µM, high selectivity over 15 other methyltransferases.	1620401-82-2
GSK2801	GSK2801 is a selective bromodomains BAZ2A/B inhibitor with K_D of 257 nM and 136 nM, respectively.	1619994-68-1
CPI-169	CPI-169 is a potent, and selective EZH2 inhibitor with IC50 of 0.24 nM, 0.51 nM, and 6.1 nM for EZH2 WT, EZH2 Y641N, and EZH1, respectively.	1450655-76-1
ORY-1001 (RG-6016)	ORY-1001 (RG-6016) is an orally active and selective lysine-specific demethylase LSD1/KDM1A inhibitor with IC50 of <20 nM, with high selectivity against related FAD dependent aminoxidases. Phase 1.	1431326-61-2
SP2509	SP2509 is a selective histone demethylase LSD1 inhibitor with IC50 of 13?nM, showing no activity against MAO-A, MAO-B, lactate dehydrogenase and glucose oxidase.	1423715-09-6
EI1	EI1 is a potent and selective EZH2 inhibitor with IC50 of 15 nM and 13 nM for EZH2 (WT) and EZH2 (Y641F), respectively.	1418308-27-6
BRD4770	BRD4770 is a histone methyltransferase G9a inhibitor with IC50 of 6.3 µM, and induces cell senescence.	1374601-40-7
GSK503	GSK503 is a potent and specific EZH2 methyltransferase inhibitor.	1346572-63-1

GSK1324726A (I-BET726)	GSK1324726A (I-BET726) is a highly selective inhibitor of BET family proteins with IC50 of 41 nM, 31 nM, and 22 nM for BRD2, BRD3, and BRD4, respectively.	1300031-52-0
MI-3 (Menin-MLL Inhibitor)	MI-3 (Menin-MLL Inhibitor) is a potent menin-MLL interaction inhibitor with IC50 of 648 nM.	1271738-59-0
MG149	MG149 is a potent histone acetyltransferase inhibitor with IC50 of 74 µM and 47 µM for Tip60 and MOF,respectively.	1243583-85-8
ML324	ML324 is a selective inhibitor of jumonji histone demethylase (JMJD2) with IC50 of 920 nM.	1222800-79-4
OF-1	OF-1 is a potent inhibitor of BRPF1B and BRPF2 bromodomain with K_d of 100 nM and 500 nM, respectively.	919973-83-4
4SC-202	4SC-202 is a selective class I HDAC inhibitor with IC50 of 1.20 µM, 1.12 µM, and 0.57 µM for HDAC1, HDAC2, and HDAC3, respectively. Also displays inhibitory activity against Lysine specific demethylase 1 (LSD1). Phase 1.	910462-43-0
NI-57	NI-57 is a selective and potent inhibitor of BRPF (Bromodomain and PHD Finger) family of proteins (BRPF1/2/3). NI-57 shows accelerated FRAP recovery at 1 µM in the BRPF2 FRAP assay preventing binding of full-length BRPF2 to chromatin.	1883548-89-7
MS023 hydrochloride	MS023 is a potent and selective chemical probe for Type I protein arginine methyltransferases (PRMTs). MS023 is a potent inihbitor of PRMTs 1,3,4,6,and 8 (IC50 = 30, 119, 83, 8, and 8 nM, respectively), which are responsible for asymmetric dimethylation of arginine residues. MS023 is active in cells.	1831110-54-3
OICR-9429	OICR-9429 is a cell penetrant, potent and selective antagonist of the interaction of WDR5 (WD repeat domain 5) with peptide regions of MLL and Histone 3 that potently binds to WDR5. OICR-9429 inhibits the interaction of WDR5 with MLL1 and RbBP5 in cells.	1801787-56-3
LLY-507	LLY-507 is a potent and selective inhibitor of SMYD2 protein lysine methyltransferase (PKMT) with an in vitro IC50 <15 nM and >100-fold selectivity over other methyltransferases and other non-epigenetic targets. LY-507 has been shown to inhibit p53K370 monomethylation in cells with an IC50 ~600 nM.	1793053-37-8
I-BRD9	I-BRD9 is a selective cellular chemical probe for bromodomain-containing protein 9 (BRD9), thought to be a member of the chromatin remodelling SWI/SNF BAF complex, which plays a fundamental role in gene expression regulation. I-BRD9 has a pIC50 value of 7.3 with greater than 700-fold selectivity over the BET family and 200-fold over the highly homologous bromodomain-containing protein 7 (BRD7) and greater than 70-fold selectivity against a panel of 34 bromodomains.	1714146-59-4

SGC707	SGC707 is a potent allosteric inhibitor of protein arginine methyltransferase 3 (PRMT3). SGC707 has an IC50 value of 50 nM and >100-fold selectivity over other methyltransferases and non-epigenetic targets. SGC707 binds to PRMT3 with KD of 50 nM (ITC), and inhibits histone methylation in cells with an IC50 value below 1 µM.	1687736-54-4
BAZ2-ICR	BAZ2-ICR is a chemical probe for BAZ2A/B bromodomains with >100-fold selectivity over other bromodomains, with the exception of CECR2 (15-fold selectivity). BAZ2A is an essential component of the nucleolar remodeling complex (NoRC), which mediates recruitment of histone modifyine enzymes and DNA methylase involved in the silencing of ribosomal RNA transcription by RNA polymerase I. BAZ2B is believed to be involved in regulating nucleosome mobilization along linear DNA. BAZ2-ICR binds to BAZ2A with a KD of 109 nM (ITC) and to BAZ2B with a KD of 170 nM (ITC). BAZ2-ICR also shows accelerated Fluorescence recovery after photobleaching (FRAP) recovery at 1 µM in the BAZ2A FRAP assay.	1665195-94-7
A-366	A-366 is an SGC chemical probe for G9a/GLP, developed in collaboration with Abbvie. A-366 is a potent, selective inhibitor of the histone methyltransferase G9a. The IC50 values for G9a inhbition in enzymatic and cell based assays are 3.3 and approximately 3 µM, respectively. A-366 has little or no detectable activity against a panel of 21 other methyltransferases.	1527503-11-2
MS049 hydrochloride	MS049 is a potent and selective inhibitor of protein arginine methyltransferases (PRMTs) PRMT 4 and PRMT6. MS049 is active in cells.	1502816-23-0
PFI-4	PFI-4 is an SGC chemical probe for the bromodomains of the BRPF (BRomodomain and PHD Finger containing) scaffolding protein BRPF1B. The BRPF proteins (BRPF1/2/3) assemble histone acetyltransferase (HAT) complexes of the MYST transcriptional coactivator family members MOZ and MORF. The BRPF1 protein is the scaffold subunit of the MYST acetyltransferase complex, which plays a crucial roles in DNA repair, recombination and replication as well as transcription activation. Mutations in MOZ, MORF, and BRPF1 have all been associated with cancer. BRPF1 exists in 2 different isoforms: BRPF1A and BRPF1B. PFI-4 specifically binds to BRPF1B with a Kd =13 nM as determined by ITC. It reduces recovery time in triple BRD cell construct in FRAP and is potent in cells with IC50 250nM, while showing no effect on BRPF1A.	900305-37-5
A-196	A-196 is a potent and selective chemical inhibitor of SUV420H1 and SUV420H2 that inhibits the di- and trimethylation of H4K20me in multiple cell lines.	1982372-88-2

(+/-)-JQ1	The human BET family, which includes BRD2, BRD3, BRD4 and BRDT, play a role in regulation of gene transcription. (+/-)-JQ1 ((+/-)SGCBD01) is a selective BET bromodomain (BRD) inhibitor that inhibits Brd4 (Bromodomain-containing 4). Brd4 forms complexes with chromatin via two tandem bromodomains (BD1 and BD2) that bind to acetylated lysine residues in histones and Brd4 association with acetylated chromatin is believed to regulate the recruitment of elongation factor b and additional transcription factors to specific promoter regions. The nuclear protein in testis (NUT) gene is known to form fusions with Brd4 that create a potent oncogene, leading to rare, but highly lethal tumors referred to as NUT midline carcinomas (NMC). JQ1 inhibits recruitment and binding of Brd4 to TNFa and E-selectin promoter elements, and accelerates recovery time in FRAP (fluorescence recovery after photobleaching) assays using GFP-Brd4. Thus JQ1/SGCBD01 is a useful tool to study the role of Brd4 in transcriptional initiation.	1268524-69-1

Supplemental Table S4. List of primers used for RT-qPCR analysis.

Gene	Forward	Reverse
RNF5	AAAGCTGGGATCAGCAGAGA	ATCACCAAATGGCTGGAATC
ANXA1	ATACAGATGCCAGGGCTTTGTATGA	TGGGATGTCTAGTTTCCACCACACA
H3A	AAGCAGACTGCCCGCAAAT	GGCCTGTAACGATGAGGTTTC
sXBP1	GCTGGCAGGCTCTGGGGAAG	TGCTGAGTCCGCAGCAGGTG
CHOP	GGAAACAGAGTGGTCATTCCC	CTGCTTGAGCCGTTCATTCTC
ATF3	CCTCTGCGCTGGAATCAGTC	TTCTTTCTCGTCGCCTCTTTTT
LIMK1	CAAGGGACTGGTTATGGTGGC	CCCCGTCACCGATAAAGGTC
CDKN2D	AGTCCAGTCCATGACGCAG	ATCAGGCACGTTGACATCAGC
CDKN1A	TGTCCGTCAGAACCCATGC	AAAGTCGAAGTTCCATCGCTC
BCL2A1	CTGCACCTGACGCCCTTCACC	CACATGACCCCACCGAACTCAAAGA
NCF1	GGGGCGATCAATCCAGAGAAC	GTACTCGGTAAGTGTGCCCTG
YWHAZ	ACTTTTGGTACATTGTGGCTTCAA	CCGCCAGGACAAACCAGTAT

Supplemental Table S5. List of primers used for ChIP analysis.

Gene	Forward	Reverse
ANXA1	TCACTTTGTTTTTGGACATAGCTGA	CCACACCTAGCAACCAGAAGTTAG
NCF1	TCATGCCTGTAATCCCAACA	CTCTGCCTTCCAGGTTCAAG
CDKN1A	GGTGTCTAGGTGCTCCAGGT	GCACTCTCCAGGAGGACACA